Diabetic Microcirculatory Disturbances and Pathologic Erythropoiesis Provoked by Deposition of Amyloid-Forming Amylin in Red Blood Cells and Capillaries

Journal:	*Kidney International*
Manuscript ID	KI-01-19-0128.R2
Article Type:	Basic Research
Date Submitted by the Author:	23-Jul-2019
Complete List of Authors:	Verma, Nirmal Liu, Miao Ly, Han Loria, Analia Campbell, Kenneth Bush, Heather Kern, Philip Jose, Pedro; George Washington University, Division of Renal Diseases & Hypertension, Department of Medicine and Department of Pharmacology and Physiology Taegtmeyer, Heinrich; UT Medical School at Houston, Bers, Donald; Univ Calif Davis, Pharmacology Despa, Sanda Goldstein, Larry Murray, Andrew Despa, Florin; The Univesrity of Kentucky , Pharmacology
Subject Area:	Diabetic Nephropathy, Renal Pathology
Keywords:	cardiovascular disease, diabetes, erythropoietin, hypoxia, inflammation

INDEX OF THE CHANGES

1. Provided all figures as separate files in .tif format with resolution of 600 dpi.
2. Added scale bar in all photomicrographs.
3. Western blot analysis of VCAM-1 expression in brain capillary lysates is replaced by Western blot analysis and ELISA of VACM-1 expression in kidney capillaries in supplementary figure 8.
4. Protocol for isolation of capillaries from kidney tissue is provided in the supplementary methods.
5. Details of VACM-1 ELISA kit and VCAM-1 antibody are added in the Methods section.
6. All changes in response to the reviewers' comments are made in the manuscript (details are provided in 'ITEMIZED RESPONSES' sheet).

We thank the editors and reviewers for their careful and helpful comments. We revised the manuscript as suggested. Below are point-by-point responses.

Specific Comments Resulting from the Editorial Conference:

The manuscript was overall adequately revised. However, there remain some issues to be addressed. Please check the comments by the reviewers carefully and revise your manuscript. We will be glad to publish your MS afterwards.

Please make sure to upload a graphical abstract of your paper. Guidelines for content and a design template for this required graphical abstract are attached with this email. The Graphical Abstracts will be published as provided and will not be included with the proof.

Reviewer(s)' Comments to Author:

Reviewer: 1

Comments to the Author
There are a few minor issues that should be addressed.
1. Page 2 (Abstract): The first sentence of the abstract makes no sense to me. Please revise. Also, "whilst also reducING renal accumulation" (line 30).
Answer: The first sentence of the abstract was altered to read: "In type-2 diabetes, the oxygen-carrying capacity of red blood cells (RBCs) and the integrity and stability of the blood capillaries decline causing tissue hypoxia and end organ malfunction."

2. Page 5, line 15: "The upregulation of formation of epoxyeicosatrienoic acids (EETs) in endothelial cells (EC)".
Answer: We made the suggested change

3. Page 6, line 8: "or stroke (S) also had elevated RBC…".
Answer: We made the suggested change.

4. Page 6, line 13: "…and C groups tag heart failure or cancer…". I do not know what you mean by "tag" here.

Answer: We replaced "tag" by "indicate".

5. Page 9, line 30: "Something cannot be "non-significantly higher". You set a critical value of P to make a decision about rejecting or not rejecting the null hypothesis. You cannot have it both ways. I suggest something like, "…and tended to be higher in age-matched diabetic UCD rats (P = ??)".

Answer: We replaced "non-significantly higher" by "tended to be higher in age-matched diabetic UCD rats (P = 0.27)"."

6. Page 11, line 42: The word "arginase" is not a proper noun.

Answer: We replaced "Arginase" by "arginase"

7. Page 12, lines 1-6: "Impairment of tissue oxygen-sensing found in diabetic HIP rats was mirrored in control rats intravenously infused with amylin-coated RBCs and in diabetic UCD rats intravenously infused with human amylin." This sentence does not convey your intended meaning. If rats are to be intravenously infused you would somehow have to stuff them into a syringe.

Answer: We rephrased the statement to read "Impairment of tissue oxygen-sensing found in diabetic HIP rats was mirrored in control rats that were given amylin-coated RBCs intravenously and in diabetic UCD rats that were given human amylin intravenously."

8. Page 14, Lines 21-22: Please give the concentration of APAU in the drinking water. The stated "1 ml drug/L" is meaningless.

Answer: APAU was formulated in polypropylene glycol at a concentration of 10 mg/mL with 30 minutes sonication. The APAU aliquot was added to the drinking water at a final content of 1%.

Reviewer: 2

Comments to the Author

The authors have addressed most questions raised by the referees. However, there is still a few issues that should be addressed.

First, in the Result section, you should clearly state brain tissue was sampled for western blot analysis shown in Supplementary Figure 7.

Answer: In the meantime, we performed the VCAM-1 expression experiment on kidney capillary lysates and these data are now replacing the data on brain capillary lysates in Supplementary figure 8.

Second, if VCAM-1 expression is up-regulated at the protein level, what is the ligand on RBC? The referee wonders that the putative molecule is integrin to play a key role in firm adhesion as you evaluated in Figure 5A. Please mention whatever is a candidate ligand on RBC in the Discussion section.

Answer: The following sentence was added in the Discussion section "Future studies need to identify the ligand pairs for the amylin-mediated adhesive interaction between vascular ECs and RBCs. Candidate ligand pairs may include the VCAM-1-α4β1-integrin pair of proteins that appears to be involved in sickle cell disease[40]." A relevant reference paper was added in the bibliography list: White J, Lancelot M, Sarnaik S, et al. Increased erythrocyte adhesion to VCAM-1 during pulsatile flow: Application of a microfluidic flow adhesion bioassay. *Clin. Hemorheol. Microcirc*. 2015;60:201-13

Third, no asterisks in Figure 5A. Is there a significant difference between any pairs?

Answer: There is no difference between groups by one-way ANOVA. We revised the text describing the findings in Fig 5a to read: The adhesion of RBCs to cultured vascular endothelial cells (ECs) under flow condition tended to be greater for HIP rat RBCs than RBCs from UCD rats (P = 0.17) and from WT rats (P = 0.17) (Figure 5a).

Diabetic Microcirculatory Disturbances and Pathologic Erythropoiesis Provoked by Deposition of Amyloid-Forming Amylin in Red Blood Cells and Capillaries

Nirmal Verma, Ph.D[1#], Miao Liu, Ph.D[1#], Han Ly, BS[1], Analia Loria, Ph.D[1], Kenneth S. Campbell, Ph.D[2], Heather Bush, Ph.D[3], Philip A. Kern, M.D.[4], Pedro A. Jose, M.D., Ph.D.[5], Heinrich Taegtmeyer, M.D., D.Phil.[6], Donald M. Bers, Ph.D[7], Sanda Despa, Ph.D[1], Larry B. Goldstein, M.D.[8], Andrew J. Murray, Ph.D.[9] and Florin Despa, Ph.D[1,8]

[1]Department of Pharmacology and Nutritional Sciences, University of Kentucky, Lexington, KY, USA.

[2]Department of Physiology, University of Kentucky, Lexington, KY, USA.

[3]Department of Biostatistics, College of Public Health, University of Kentucky, Lexington, KY, USA.

[4]Division of Endocrinology, Department of Medicine, University of Kentucky, Lexington, KY, USA.

[5]Department of Medicine, Division of Renal Diseases & Hypertension, The George Washington University School of Medicine & Health Sciences, Washington, DC, USA.

[6]Department of Internal Medicine, McGovern Medical School at UT Health, Houston, TX, USA

[7]Department of Pharmacology, University of California, Davis, CA, USA.

[8]Department of Neurology, University of Kentucky, Lexington, KY, USA.

[9]Department of Physiology, Development and Neuroscience, University of Cambridge, Cambridge CB2 3EG, UK.

Correspondence: Florin Despa, Department of Pharmacology and Nutritional Sciences, College of Medicine, University of Kentucky, Wethington Building, Room 459, 900 S. Limestone, Lexington, Kentucky, 40536, USA. Phone: 859-218-0291. Fax: 859-257-3646. E-mail: f.despa@uky.edu.

Running headline: Biomarkers in diabetic microvascular dysfunction

Abstract

In type-2 diabetes, the oxygen-carrying capacity of red blood cells (RBCs) and the integrity and stability of the blood capillaries decline causing tissue hypoxia and end organ malfunction. Correcting hyperglycemia is not entirely effective at reestablishing normal cellular metabolism and function. Identification of pathological changes occurring before the development of overt hyperglycemia may lead to novel therapeutic targets for reducing the risk of microvascular dysfunction. Here we showed that the RBC-capillary interaction is altered by prediabetic hypersecretion of amylin, an amyloid-forming hormone co-synthesized with insulin, and is reversed by endothelial cell-secreted epoxyeicosatrienoic acids (EETs). In humans, we found amylin deposition in RBCs in association with type-2 diabetes, heart failure, cancer and stroke. Amylin-coated RBCs have altered shape and reduced functional (non-glycated) hemoglobin. Amylin-coated RBCs administered intravenously in control rats upregulated erythropoietin (EPO) and renal arginase expression and activity. We also found that diabetic rats expressing amyloid-forming human amylin in the pancreas (HIP rats) have increased tissue levels of hypoxia-inducible transcription factors (HIFs) compared to diabetic rats that express non-amyloid forming rat amylin (UCD rats). EPO upregulation correlated with lower hematocrit in HIP rats indicating pathologic erythropoiesis. In HIP rats, pharmacological upregulation of endogenous EETs protected the renal microvasculature against amylin deposition whilst also reducing renal accumulation of HIFs. Thus, prediabetes induces amylin dyshomeostasis and promotes amylin deposition in RBCs and the microvasculature, which alters the RBC-capillary interaction leading to activation of hypoxia signaling pathways and pathologic erythropoiesis. Amylin dyshomeostasis could be a therapeutic target for ameliorating diabetic vascular complications.

Key words: Type-2-diabetes, Amylin, Microvascular Disease, Hypoxia, Erythropoiesis.

Translational statement

Amylin accumulation in RBCs induces hypoxic-ischemic tissue injury. Detection of amylin accumulation in human RBCs, in combination with current American Heart Association guidelines to define cardiovascular risk, could result in better risk stratification for microvascular complications, improve the ability to predict progression of diabetic microvascular complications by taking a precision medicine approach, and better rationalize therapeutic strategies and response to treatment.

Introduction

Oxygen is essential for cell function and cell survival[1]. RBCs deliver oxygen to cells and tissues via mechanisms that involve the passage of RBCs through capillaries. This process is enabled by the viscoelastic properties of the RBCs, which allow them to be deformed within capillaries[2]. In type-2 diabetes, the oxygen-carrying capacity of RBCs and the integrity and stability of the capillaries decline, exacerbating the risk of tissue hypoxia and end organ malfunction[3-7]. The underlying mechanisms are complex and incompletely understood.

Physiological responses to low oxygen levels are primarily driven by the stabilization of the α subunits of the hypoxia-inducible transcription factors HIF-1 and 2[1,8,9]. HIF-2 regulates the hypoxia response by elevating the renal expression of EPO, a hormone that signals an increased demand for RBCs from the bone marrow, which then increases the production of RBCs[8]. Stabilization of HIF-2α also induces *arginase* expression[9] in vascular endothelial cells. Because arginase has the same substrate (L-arginine) as nitric oxide (NO) synthase[9], increased *arginase* production/ activation may reduce NO availability. Depleted NO production impairs relaxation of the blood vessels and affects microvascular autoregulation[1,8,9]. Thus, increased EPO coupled with arginase-NO dysregulation constitutes one of the multiple[10] molecular derangements linking systemic hypoxia with microvascular dysfunction.

Metabolic derangements that occur before the development of overt hyperglycemia may induce microvascular dysfunction[11]. In prediabetes, pancreatic β-cells compensate for insulin resistance by increasing the secretion of insulin (hyperinsulinemia)[12]. Amylin (also known as islet amyloid polypeptide; IAPP), is a 37-amino acid peptide synthesized and co-secreted with insulin in response to physiological stimuli[13-15]. It is normally soluble, crosses the blood brain barrier and binds to neurons in the feeding centers participating in the regulation of gastric fluxes[16]. Amylin from humans and a few other species, including cats, dogs and monkeys, but not rodents, has an increased propensity to aggregate, forming amyloid[17] (i.e., amylin dyshomeostasis). This triggers β-cell apoptosis by mechanisms involving

incorporation of aggregated amylin into cellular membranes[18-20]. We[21-26] and others[27-31] have shown the presence of amylin deposition in failing hearts[21-23] and kidneys[27] of patients with type-2 diabetes and in brains[28-31] of humans with dementia[32]. We also showed that rats that develop type-2 diabetes linked to amylin dyshomeostasis (i.e. the HIP rat model for type-2 diabetes[33]) develop heart dysfunction[21,23] and neurological deficits[25,34] sooner than age- and blood glucose-matched rats that develop type-2 diabetes in the absence of amylin dyshomeostasis (i.e. the UCD rat model for type-2 diabetes[35]). The upregulation of epoxyeicosatrienoic acids (EETs) in endothelial cells appeared to protect against cardiac amylin accumulation in HIP rats, which correlated with improved heart function[22]. Although we interpret these findings to support the hypothesis that reducing amylin dyshomeostasis may ameliorate diabetic vascular complications, the impact of elevated blood levels of amylin on blood cells and the microvasculature remains unknown.

Here we tested the hypothesis that systemic amylin dyshomeostasis alters the interaction between RBCs and capillaries leading to hypoxic-ischemic tissue injury. To test this hypothesis, we measured the amylin levels in RBCs from humans with and without diabetes, and used transgenic rats, RBC transfusions and pharmacological tools for mechanistic studies.

Results

Humans with type-2 diabetes have amylin deposition in RBCs.

We assessed the relationship between HbA1c level (the common marker of hyperglycemia) and amylin concentration in RBC lysates from patients with type-2 diabetes or diseases that are commonly associated with insulin resistance, including heart failure, cancer and stroke. Western blot analysis of matched plasma, RBC lysate and white blood cell (WBC) lysate from a human with type-2 diabetes (the positive control for amylin dyshomeostasis) detected both monomeric amylin (Figure 1a) and amylin-positive higher molecular weight bands (Supplementary Figure 1). RBC lysates from individuals with a primary diagnosis of type-2 diabetes (T2D) (without heart failure, cancer or stroke) had higher amylin

concentration than those from healthy individuals (H) and patients with type-1 diabetes (T1D group; the negative control for amylin) (Figure 1b). Patients with a primary diagnosis of heart failure (HF), cancer (C), or stroke (S) also had elevated RBC amylin levels independent of type-2 diabetes as a secondary diagnosis (Figure 1b). Lighter colored symbols in the HF and C groups indicate heart failure or cancer without type-2 diabetes. RBC amylin and HbA1c levels were highly variable in all groups (Figure 1c-i), except in patients with HF and type-2 diabetes in whom higher HbA1c levels correlated with RBC amylin accumulation. There were non-significant inverse correlations between HbA1c and RBC amylin levels in the HF without diabetes (Figure 1f), cancer with diabetes (Figure 1g) and stroke (Figure 1i) groups.

These results suggest that type-2 diabetes and diseases associated with insulin resistance such as heart failure, cancer and stroke promote amylin accumulation in RBCs in humans.

Amylin deposition in RBCs results from hypersecretion of amyloid-forming human amylin.

The HIP rat is a unique animal model for late-life onset type-2 diabetes as it is characterized by pancreatic expression of the human (amyloid-forming) variant of amylin[33], whereas other rodent models for type-2 diabetes express only the native, non-amyloid forming amylin[17]. As in humans[14], the development of type-2 diabetes in HIP rats is associated with pancreatic amyloid[33] (Supplementary Figure 2). We compared the amylin content in RBCs, WBCs, and plasma from diabetic HIP rats and non-diabetic WT littermates (Figure 2a). Amylin was concentrated in RBCs and the *difference* in amylin levels between WT and diabetic HIP rats was greater in RBCs than in plasma or WBCs (Figure 2a).

Analysis of freshly packed RBCs by flow cytometry (Figure 2b) and amylin ELISA (Figure 2c) revealed a correlation between RBC amylin levels and different levels of non-fasted blood glucose (normal, ≤ 11 mM, 6-8 months old; prediabetic, 11-14 mM on two consecutive measurements separated by >3 days, 10-12 months old; and diabetic, >14 mM on two consecutive measurements, separated by >3 days; 14-16 months old).

Confocal microscopy analysis of RBCs that were double-stained for amylin and hemoglobin showed amylin deposition on RBCs from HIP rats (Figure 2d). Amylin appeared to co-localize with glycophorin A (Figure 2e), a membrane protein that is specific to RBCs, suggesting amylin accumulation on the RBC membrane. The analysis of RBCs co-stained for amylin and glycophorin A using super-resolution imaging (STORM) showed the presence of amylin within the RBC membrane with some dense patches on the outer part of the cell membrane (Figure 2f). Electron microscopic examination of immunogold-labeled thin sections of epoxy resin-embedded RBCs indicated the presence of amylin within the cell membrane (Supplementary Figure 3; arrowhead pointing to amylin deposits).

The results demonstrate that hypersecretion of the amyloid-forming human variant of amylin leads to amylin deposition within circulating RBCs.

Amylin-coated RBCs have lower deformability and functional (non-glycated) hemoglobin.

Next, we investigated pathophysiological characteristics of RBCs from diabetic HIP rats and RBCs from diabetic rats without amylin dyshomeostasis (UCD rats) and non-diabetic WT rats, as they express only the non-amyloid forming rat amylin. Compared to RBCs from WT rats, RBCs from HIP rats contained less functional (non-glycated) hemoglobin (Figure 3a), whereas there was no difference between UCD and WT rats. RBCs of HIP, UCD and WT rats (~ 12 months old rats) had similar oxygen dissociation curves (Figure 3b) indicating that the affinity of hemoglobin for oxygen, the release of bound oxygen and the partial oxygen pressure for maintaining oxygen saturation are not significantly affected by amylin dyshomeostasis or hyperglycemia.

In flow cytometry experiments, the distribution of the forward scattering (FSC) signals by RBCs from WT rats (Figure 3c; orange) was bimodal, which reflects the biconcave disk shape of normal RBCs. In the case of amylin-coated RBCs from diabetic HIP rats, the FSC distribution was monomodal (Figure 3c; pink), indicating changes in RBC morphology towards a more spherical shape. The Pearson coefficient of dissymmetry (PCD), which indicates the departure from sphericity, suggested distinct morphological

changes in RBCs from HIP rats compared to WT and UCD rats (Figure 3c). Incubation of RBCs from WT rats with aggregated human amylin for 4 hours (as described in our previous studies[26,36]) replicated the morphological change observed in HIP rat RBCs (Supplementary Figure 4). Altered shape of RBCs from HIP and UCD rats did not affect the response to an osmotic resistance test, as the propensity for hemolysis in hypo-osmotic solutions was comparable for RBCs from all three rat groups (Figure 3d).

These results show that amylin deposition in RBCs is associated with lower hemoglobin concentrations and reduced RBC deformability, independently of effects of chronic glucose levels. At an early stage of diabetes, the cumulative effects of amylin dyshomeostasis and hyperglycemia (as in HIP rats) or hyperglycemia alone (as in UCD rats) do not appear to induce significant changes in hemolysis and oxygen dissociation.

The microvasculature is disrupted in kidneys of rats with amylin dyshomeostasis.

Next we investigated the structural integrity of the capillary network and the stability of the capillary beds in kidneys from age- and blood glucose-matched HIP and UCD rats. We used immunohistochemistry with antibodies against amylin (brown) and collagen IV (Col IV; green), a component of the basement membrane, to anatomically localize amylin deposition with respect to the vasculature. In HIP rat kidneys, there were patches of amylin deposits in arterioles, interstitial tissue between the tubules (Figure 3e) and glomeruli (Figure 3f). Vascular amylin deposition correlated with accumulation of macrophages, as indicated by co-staining for amylin and the ionized calcium-binding adapter molecule 1 (IBA1), a marker of macrophage activation (Figure 3g). There were macrophages in areas of amylin deposition, which may indicate a potential role for these cells in the clearance of vascular amylin deposition. Staining with ED1 (Figure 3h), an antibody against the cluster of differentiation (CD) 68 protein (that is highly expressed by circulating macrophages), supports the increased activity of macrophages in areas of vascular amylin deposition. In contrast, vascular amylin deposits and macrophage infiltration were not found in kidneys from diabetic UCD rats.

These data suggest that amylin dyshomeostasis injures the capillaries, which may be associated with systemic inflammatory responses leading to macrophage infiltration that may exacerbate ischemic vascular injury in HIP rats.

Amylin dyshomeostasis activates renal hypoxia signaling pathways.

The kidney is a critical component of a regulatory feedback loop that controls the hematocrit via EPO production[8]. Both HIP and UCD rats had renal dysfunction, as indicated by polyuria and albuminuria (Supplementary Figures 5a and 5b). Creatinine clearance was elevated in diabetic HIP rats compared with WT littermates and diabetic UCD rats (Supplementary Figure 5c). The plasma level of EPO, the hormone that signals an increased demand for RBCs to the bone marrow, was higher in diabetic HIP rats than in WT littermates (Figure 4a) and tended to be higher in age-matched diabetic UCD rats vs. WT rats ($P = 0.27$). The reticulocyte count was also higher in HIP than in WT rats (Figure 4b). Despite elevated plasma EPO levels, the average hematocrit was not different in HIP rats compared with WT littermates, but was lower in HIP compared to UCD rats (Figure 4c). The spleen, a major blood reservoir, had lower weight in diabetic HIP rats compared to age-matched WT rats (Supplementary Figure 6). Compared with diabetic UCD rats and healthy WT rats, diabetic HIP rats had elevated levels of HIF-1α and HIF-2α in whole kidney tissue homogenates (Figure 4d and 4e). Consistent with elevated HIF-2α, HIP rat kidneys also had upregulated arginase-1 and 2 proteins (Figure 4f and 4g) and greater arginase activity (Figure 4h). Increased stabilization of HIF α units in HIP rat kidney tissue correlated with a trend towards downregulation of the von Hippel-Lindau (vHL) tumor suppressor protein (Supplementary Figure 7) suggesting impaired degradation of HIF α units.

These results suggest that activation of hypoxia signaling in kidneys and downstream upregulation of EPO are associated with pathologic erythropoiesis and amylin deposition in RBCs.

Blocking of adhesion proteins in endothelium reverses amylin dyshomeostasis and HIF activation.

The adhesion of RBCs to cultured vascular endothelial cells (ECs) under flow condition tended to be greater for HIP rat RBCs than RBCs from UCD rats (P = 0.17) and from WT rats (P = 0.17) (Figure 5a). Greater adhesion of RBCs from HIP rats to ECs was found in experiments without flow condition (Figure 5b) in an adhesion test in which RBCs from WT rats that were incubated with 50 μM synthetic human amylin for 4 hours is shown in Figure 5c. Analysis of kidney capillary lysates by Western blot (A) and ELISA (B) showed a trend towards upregulation of the expression of vascular cell adhesion molecule 1 (VCAM-1) in HIP rats (Supplementary Figure 8). Taken together, these results suggest that the cell membrane adhesion proteins may play a role in amylin accumulation at the RBC-capillary interface. To test this hypothesis, we used EETs, which are primarily expressed by vascular ECs[37] and RBCs[38] and are known to downregulate the expression of VCAM-1 in endothelium[39]. We found that *ex vivo* incubation with (±)14(15)-EET reduced the adhesion of HIP rat RBCs to cultured endothelial cells (Figure 5d). Upregulation of EETs by treatment with an inhibitor of soluble epoxide hydrolase, the enzyme that degrades endogenous EETs[37], was associated with lower amylin deposition in renal microvasculature (the HIP-T group; Figure 5e). The treatment lowered renal accumulation of HIF-2α (Figure 5f) and HIF-1α (Figure 5g) and had variable effects on arginase expression and arginase activation (Supplementary Fig 9) in HIP rat kidneys.

Taken together, these results indicate that 1) reduced capillary RBC flux owing to amylin deposition on RBCs and the capillary wall likely contributes to tissue hypoxia in HIP rats and 2) EETs reduce this effect by downregulation of adhesion proteins in the vascular endothelium.

Transfused amylin-coated RBCs upregulate EPO through HIF-2α activation in kidneys.

RBCs act as both oxygen carriers and mediators of oxygen sensing and signaling pathways within ECs[8,9]. To determine whether amylin deposition on RBCs activates hypoxia signaling pathways in tissues, amylin-coated RBCs from HIP rats were administered to WT rats. Rats were given 300 μl freshly packed RBCs/day for seven days. WT rats given similar volumes of RBCs from diabetic UCD rats were used as

positive controls for the possible effects of hyperglycemia on RBC function, whereas WT rats receiving RBCs from WT rats served as negative controls. Plasma levels of EPO were elevated in WT rats receiving amylin-coated RBCs from HIP rats compared to WT rats that received either RBCs from diabetic UCD rats or WT rats (Figure 6a). Kidneys of WT rats receiving HIP rat RBCs had increased stabilization of HIF-1α (Figure 6b) but no difference in HIF-2α levels (Figure 6c), compared with rats in the two control groups.

To examine further a possible 'amylin stress" on oxygen-sensing pathways, aggregated human amylin (hA) (0.08 μg/g body weight) was intravenously administered to diabetic UCD rats, daily, for one week. Intravenous infusion of aggregated human amylin in UCD rats led to amylin deposition on RBCs (Figure 6d). This acute "amylin stress" provoked an increase in plasma EPO level (Figure 6e; the "after hA inj" rat group) and no difference in renal HIF-2α and HIF-1α levels in whole kidney tissue homogenate (Figure 6f). Arginase 1 protein levels were elevated in kidney tissue homogenates from amylin-infused UCD rats, whereas there was no significant change of arginase 2 protein expression (Figure 6g).

These data indicate elevated EPO and accumulation of HIFs in kidneys as a direct response to circulating amylin-coated RBCs (Figure 6h).

Discussion

We found that hypersecretion of human amylin is associated with amylin deposition in the microvasculature and RBCs leading to impaired RBC-capillary interaction and activation of hypoxia signaling pathways. Impairment of tissue oxygen-sensing found in diabetic HIP rats was mirrored in control rats that were given amylin-coated RBCs intravenously and in diabetic UCD rats that were given human amylin intravenously. These results indicate that amylin-coated RBCs are a trigger of hypoxia signaling pathways. These deleterious effects result in part from a reduced flux of amylin-coated RBCs through the capillaries that may involve adhesion proteins. Blocking the expression of adhesion proteins in the vascular endothelium by upregulation of EETs reduces amylin dyhomeostasis and HIF activation.

Future studies need to identify the ligand pairs for the amylin-mediated adhesive interaction between vascular ECs and RBCs. Candidate ligand pairs may include the VCAM-1-α4β1-integrin pair of proteins that appears to be involved in sickle cell disease[40].

This link between prediabetes-induced systemic amylin dyshomeostasis and tissue hypoxia has broad implications for health care because: 1) accumulating evidence demonstrates the presence of amylin deposition in vital organs[21-31] and RBCs (as shown by the present human data) that may provide a therapeutic target reducing vascular injury prior the development of overt diabetes, 2) the public health impact of type-2 diabetes; and 3) the lack of drugs that counter amylin dyshomeostasis.

Glycated hemoglobin has a higher affinity for oxygen than adult hemoglobin A (functional hemoglobin), and can disrupt the supply of oxygen to tissues[41]. Indeed, RBCs from hyperglycemic UCD rats have decreased deformability and functional hemoglobin compared with WT rats. RBC deformability and hemoglobin levels are even lower in HIP rats, which may explain, in part, the higher hypoxic response in control WT rats receiving RBCs from HIP rats compared to control rats receiving similar volumes of RBCs from UCD rats.

Elevated EPO and microvascular dysfunction identify diabetic patients with increased risk of death[42-44]. In diabetic HIP rats, elevated plasma EPO does not correlate with an increase in hematocrit. HIP rat kidneys have amylin deposits in the microvasculature that co-localized with macrophage activation. Taken together, the results suggest that systemic amylin dyshomeostasis may upregulate eryptosis via macrophage activation. The results also indicate that amylin dyshomeostasis injures capillaries and is associated with inflammatory responses exacerbating ischemic vascular injury.

There are inherent limitations to our study of the interaction between pancreatic amylin secretion and RBCs. In the human study, we were not able to control for the potential effects of glucose, steroids, anti-diabetic drugs or specific forms of anesthesia given to individual patients, which can affect pancreatic function including amylin and insulin secretion.

In conclusion, systemic amylin dyshomeostasis promotes amylin deposition in RBCs and the microvasculature associated with pathologic erythropoiesis, macrophage activation and macrophage accumulation in blood vessels. Future studies should determine whether the RBC amylin levels affect the course of microvascular complications.

Methods

Detailed Methods are included in Supplementary Materials.

Human studies

This research employed de-identified blood specimens matched with medical record data obtained from the biobank of the Center for Clinical and Translational Science at University of Kentucky. Sample collection and storage were approved by the Institutional Review Board. We assessed the relationship between HbA1c level and amylin concentration in RBC lysates from individuals with primary diagnosis of type-2 diabetes or diseases that are commonly associated with insulin resistance, including heart failure, cancer and stroke. RBC specimens were divided into groups based on the primary diagnosis of type-2 diabetes, heart failure, cancer or stroke. Most humans in the heart failure and cancer groups had type-2 diabetes as a second diagnosis. The negative control for amylin was RBC lysates from patients with over 15 years of type-1 diabetes (and, therefore, depleted β-cell mass) who were otherwise healthy. The healthy control group included individuals without diabetes, heart failure, stroke or cancer. Exclusion criteria were based on conditions that may affect the pancreatic secretion of amylin such as transplant recipients (less than 6 months after the transplant), patients with liver disease, patients with HIV and pregnant or lactating women. Table 1 summarizes the diabetes status, co-morbidities, age, sex and body mass index (BMI) of the patients who provided the blood used in these analyses.

Experimental Animals

All animal experiments conform to the NIH guide for the care and use of laboratory animals and were approved by the Institutional Animal Care and Use Committee at University of Kentucky. We compared rats that develop type-2 diabetes linked to expression of human amylin in the pancreas (HIP rats; n=65), with rats that develop type-2 diabetes in the absence of amyloid, as they express the non-amyloidogenic rat amylin (UCD rats; n=40) and control, non-diabetic rats (WT rats; n=53).

Treatment

We performed a retrospective analysis of kidney tissue from a prior study[22] in which HIP rats were treated for 10 weeks with a soluble epoxide inhibitor APAU (UC1153) added to their drinking water in order to upregulate the endogenous EET levels. APAU was formulated in polypropylene glycol at a concentration of 10 mg/mL with 30 minutes sonication. The APAU aliquot was added to the drinking water at a final content of 1%.

Renal function analysis

Urine and blood were collected from rats in metabolic cages. Creatinine concentration in plasma and urine was measured using the kinetic Jaffé method[45]. Creatinine clearance (Ccr) was calculated using the formula: Ccr (ml/min) = (urine creatinine/plasma creatinine) × urine flow rate. Urinary albumin was measured by ELISA.

Tissue extraction and RBC isolation

For measurements of hypoxia markers (hypoxia-inducible transcription factors 1α, HIF1-α, and 2α, HIF2-α, arginase 1, arginase 2 and von Hippel-Lindau factor, vHL) and arginase activity, kidney tissue was extracted in PBS with protease and phosphatase inhibitors, followed by three consecutive cycles of freezing to -80°C and thawing. For other biochemical assays, tissues were extracted in homogenization buffer containing Triton X-100, SDS and protease and phosphatase inhibitors.

RBCs were isolated immediately after blood collection by centrifugation at 1,000g. For some experiments, RBCs were lysed in lysis buffer containing 10% NP-40.

RBC transfusion

Isolated RBCs were combined with storage solution (150 mM HCl, 45 mM dextrose, 45.5 mM mannitol, and 2.2 mM adenine) in a 3:1 v/v ratio, transferred to sterile tubes and stored at 4°C in the dark before injection. Rats received 300 µL of pre-warmed (at 37º C) RBC solution once daily for 7 days via tail vein injection.

Hematocrit and hemoglobin measurements

Hematocrit was measured with an i-STAT analyzer using i-STAT CG8+ cartridges according to the manufacturer's protocol. Hemoglobin content was calculated from the optical density at 405 nm.

Assessment of RBC shape and amylin deposition on RBCs by flow cytometry

RBCs were incubated with an anti-amylin antibody followed by incubation with an anti-rabbit Alexa Fluor® 488 secondary antibody. Flow cytometry was performed with a Becton Dickinson LSRII instrument. To assess cell shape, RBCs were first gated on a forward scatter (FSC)/side scatter (SSC) plot. The region 1 (R1) events were visualized using a FSC-A/FSC-H dot plot. For detecting amylin deposited on RBCs, cells were first gated on a forward scatter (FSC)/side scatter (SSC) plot. RBCs were further gated to determine the amylin signal (Alexa 488), using negative control (no antibody) and positive control (RBCs incubated with 50 µM of synthetic amylin peptide) to set the upper and lower boundaries.

Immunofluorescence

Isolated RBCs were incubated with primary antibodies against human amylin and glycophorin A, followed by incubation secondary antibodies, and imaged with a Nikon A1R confocal microscope. For hemoglobin staining, blood smears on glass slide were fixed and incubated with primary antibodies against

hemoglobin and human amylin. Smears were then incubated with secondary antibodies, mounted in mounting media and imaged.

Biochemical assays

ELISA for human amylin, erythropoietin, HIF1-α, HIF2-α, arginase 1, arginase 2 and vHL were performed according to the manufacturer's protocols. Arginase activity was measured in kidney homogenates using a colorimetric assay. Western blots were performed on plasma, WBC lysates, RBC lysates from humans and using a primary antibody against amylin and on kidney capillary lysates from rats using a primary antibody against VCAM-1 (1:1000, ab134047, Abcam).

Immunohistochemistry

Immunohistochemical staining was performed on rat kidney slices using antibodies against amylin, collagen IV, IBA-1, and ED1). The staining area for amylin was analyzed in ImageJ.

Statistical analysis

Statistical differences between groups were determined using Student's t-test, one-way ANOVA or two-way ANOVA, as appropriate. Multiple comparison and P values were calculated by Bonferroni correction for human data. P value for each regression analysis was calculated by the Spearman correlation test.

Disclosures: The authors have declared that no conflict of interest exists.

Supplementary Materials

Supplementary Figure Legends

Supplementary Figure S1. *Left*) Representative western blot analysis of high molecular weight amylin oligomers in plasma, RBC lysate and white blood cell (WBC) lysate from an individual with type-2 diabetes. (*Right*) The Ponceau S staining of the blot show in *Left* panel.

Supplementary Figure S2. Representative images of Thioflavin S (green) and amylin (red) staining in the pancreas from a diabetic HIP and a control WT rat (n=3/group). Scale bar, 30 μm.

Supplementary Figure S3. Representative TEM images showing RBCs from HIP and WT rats, stained with human amylin primary antibody and gold (10nm) labelled secondary antibody. (Scale bar 1μm)

Supplementary Figure S4. PCD for WT rat RBCs and WT rat RBCs incubated ex vivo with oligomerized human amylin (n=5 preparations/group).

Supplementary Figure S5. Volume of urine excretion (A), albuminuria (B) and creatinine clearance rate (C) in 16 months old WT, diabetic UCD and diabetic HIP rats (n=6 rats/group). $^{**}P \leq 0.01$; $^{***}P \leq 0.001$ by One-way ANOVA.

Supplementary Figure S6. Gross spleen weights of 16 months old WT rats and diabetic HIP rats (n=10 spleens/group). Data are means ± SEM. $^{*}P < 0.05$

Supplementary Figure S7. Levels of von Hippel-Lindau (vHL) protein in the renal tissues from 16 months old WT rats and diabetic HIP rats (n=5 rats/group). Data are means ± SEM.

Supplementary Figure S8. Western blot and ELISA analyses for VCAM-1 expression in kidney capillaries lysates of WT and HIP rats (n= 3 rats/group).

Supplementary Figure S9. Reduced amylin deposition in kidneys correlated with partially reduced imbalance of arginase expression and arginase activation in HIP rat kidney tissues. (n=4 rats/group). Data are means ± SEM. *P <0.05

Supplementary Methods

Supplementary References

Supplementary information is available at www.kidney-international.org

References

1. Semenza GL. Life with oxygen. *Science.* 2007;318:62-64.

2. Mohandas N, Gallagher PG. Red cell membrane: past, present, and future. *Blood.* 2008;112:3939-3948.

3. McMillan DE, Utterback NG, La Puma J. Reduced erythrocyte deformability in diabetes. *Diabetes.* 1978;27: 895-901.

4. Tonelli M, Sacks F, Arnold M, et al. Relation between Red Blood Cell Distribution Width and Cardiovascular Event Rate in People with Coronary Disease. *Circulation.* 2008;117:163-168.

5. Thomas MC. Anemia in diabetes: marker or mediator of microvascular disease? *Nat. Clin. Pract. Nephrol.* 2007;3:20-30.

6. Maddox TM, Stanislawski MA, Grunwald GK, et al. Nonobstructive coronary artery disease and risk of myocardial infarction. *JAMA.* 2014;312:1754-1763.

7. Barrett EJ, Liu Z, Khamaisi M, et al. Diabetic Microvascular Disease: An Endocrine Society Scientific Statement. *J Clin Endocrinol Metab.* 2017;102:4343-4410.

8. Semenza GL. Involvement of oxygen-sensing pathways in physiologic and pathologic erythropoiesis. *Blood*. 2009;114:2015-2019.

9. Samanta D, Prabhakar NR, Semenza GL. Systems biology of oxygen homeostasis. *Wiley Interdiscip. Rev. Syst. Biol. Med*. 2017;9: e1382.

10. Wong BW, Marsch E, Treps L, et al. Endothelial cell metabolism in health and disease: impact of hypoxia. *EMBO J.* 2017;36:2187-2203.

11. Gerstein HC, Bosch J, Dagenais GR, et al. ORIGIN Trial Investigators. Basal insulin and cardiovascular and other outcomes in dysglycemia. *N Engl J Med*. 2012;367:319-328.

12. Dankner R, Chetrit A, Shanik MH, et al. Basal state hyperinsulinemia in healthy normoglycemic adults heralds dysglycemia after more than two decades of follow up. *Diabetes. Metab. Res. Rev.* 2012;28:618-624.

13. Butler PC, Chou J, Carter WB, et al. Effects of meal ingestion on plasma amylin concentration in NIDDM and nondiabetic humans. *Diabetes.* 1990;39:752-756.

14. Westermark P, Andersson A, Westermark GT. Islet amyloid polypeptide, islet amyloid, and diabetes mellitus. *Physiol. Rev.* 2011;91:795-826.

15. Kahn SE, D'Alessio DA, Schwartz MW, et al. Evidence of cosecretion of islet amyloid polypeptide and insulin by beta-cells. *Diabetes.* 1990;39:634-638.

16. Lutz TA. The role of amylin in the control of energy homeostasis. *Am. J. Physiol. Regul. Integr. Comp. Physiol.* 2010;298:R1475-R1484.

17. Westermark P, Engstrom U, Johnson KH, et al. Islet amyloid polypeptide: pinpointing amino acid residues linked to amyloid fibril formation. *Proc. Natl. Acad. Sci. USA.* 1990;87:5036-5040.

18. Janson J, Ashley RH, Harrison D, et al. The mechanism of islet amyloid polypeptide toxicity is membrane disruption by intermediate-sized toxic amyloid particles. *Diabetes.* 1999;48:491-498.

19. Zraika S1, Hull RL, Udayasankar J, et al. Oxidative stress is induced by islet amyloid formation and time-dependently mediates amyloid-induced beta cell apoptosis. *Diabetologia.* 2009;52:626-635.

20. Huang CJ, Haataja L, Gurlo T, et al. Induction of endoplasmic reticulum stress-induced beta-cell apoptosis and accumulation of polyubiquitinated proteins by human islet amyloid polypeptide. *Am. J. Physiol. Endocrinol. Metab.* 2007;293:E1656-E1662.

21. Despa S, Margulies KB, Chen L, et al. Hyperamylinemia contributes to cardiac dysfunction in obesity and diabetes: A study in humans and rats. *Circ. Res.* 2012;110:598-608.

22. Despa S, Sharma S, Harris TR, et al. Cardioprotection by controlling hyperamylinemia in a "humanized" diabetic rat model. *J. Am. Heart. Assoc.* 2014;3:pii: e001015.

23. Liu M, Verma N, Peng X, et al. Hyperamylinemia increases IL-1β synthesis in the heart via peroxidative sarcolemmal injury. *Diabetes.* 2016;65:2772-2783.

24. Jackson K, Barisone GA, Diaz E, et al. Amylin deposition in the brain: A second amyloid in Alzheimer disease? *Ann. Neurol.* 2013;74:517-526.

25. Verma N, Ly H, Liu M, et al. Intraneuronal amylin deposition, peroxidative membrane injury and increased IL-1β synthesis in brains of Alzheimer's disease patients with type-2 diabetes and in diabetic HIP rats. *J. Alzheimers. Dis.* 2016;53:259-272.

26. Ly H, Verma N, Wu F, et al. Brain microvascular injury and white matter disease provoked by diabetes-associated hyperamylinemia. *Ann. Neurol.* 2017;82:208-222.

27. Gong W, Liu ZH, Zeng CH, et al. Amylin deposition in the kidney of patients with diabetic nephropathy. *Kidney Int.* 2007;72:213-218.

28. Fawver JN, Ghiwot Y, Koola C, et al. Islet amyloid polypeptide (IAPP): A second amyloid in Alzheimer's disease. *Curr. Alzheimer. Res.* 2014;1:928-940.

29. Oskarsson ME, Paulsson JF, Schultz SW, et al. In vivo seeding and cross-seeding of localized amyloidosis: A molecular link between type 2 diabetes and Alzheimer disease. *Am. J. Pathol.* 2015;185:834-846.

30. Schultz N, Byman E, Fex M, et al. Amylin alters human brain pericyte viability and NG2 expression. *J. Cereb. Blood Flow Metab.* 2007;37:1470-1482.

31. Schultz N, Byman E, Netherlands BB, et al. Levels of retinal IAPP are altered in Alzheimer's disease patients and correlate with vascular changes and hippocampal IAPP levels. *Neurobiol. Aging.* 2018;69:94-101.

32. Biessels GJ, Despa F. Cognitive decline and dementia in diabetes mellitus: mechanisms and clinical implications. *Nat. Rev. Endocrinol.* 2018;14:591-604.

33. Butler AE, Jang J, Gurlo T, et al. Diabetes due to a progressive defect in beta-cell mass in rats transgenic for human islet amyloid polypeptide (HIP Rat): a new model for type 2 diabetes. *Diabetes*. 2004;53:1509-1516.

34. Srodulski S, Sharma S, Bachstetter AB, et al Neuroinflammation and neurologic deficits in diabetes linked to brain accumulation of amylin. *Mol. Neurodegener.* 2014;9:30.

35. Cummings BP, Digitale EK, Stanhope KL, et al. Development and characterization of a novel rat model of type 2 diabetes mellitus: the UC Davis type 2 diabetes mellitus UCD-T2DM rat. *Am. J. Physiol. Regul. Integr. Comp. Physiol.* 2008;295:R1782-R1793.

36. Liu M, Hoskins A, Verma N, et al. Amylin and diabetic cardiomyopathy - amylin-induced sarcolemmal Ca^{2+} leak is independent of diabetic remodeling of myocardium. *Biochim. Biophys. Acta. Mol. Basis Dis.* 2018;1864:1923-1930.

37. Imig JD. Epoxides and soluble epoxide hydrolase in cardiovascular physiology. *Physiol Rev*. 2012;92:101-130.

38. Jiang H, Anderson GD, McGiff JC. Red blood cells (RBCs), epoxyeicosatrienoic acids (EETs) and adenosine triphosphate (ATP). *Pharmacol Rep*. 2010;62:468-474.

39. Node K, Huo Y, Ruan X, et al. Anti-inflammatory properties of cytochrome P450 epoxygenase-derived eicosanoids. *Science.* 1999;285:1276-1279.

40. White J, Lancelot M, Sarnaik S, et al. Increased erythrocyte adhesion to VCAM-1 during pulsatile flow: Application of a microfluidic flow adhesion bioassay. *Clin. Hemorheol. Microcirc*. 2015;60:201-13

41. Jain SK, McVie R, Duett J, et al. Erythrocyte membrane lipid peroxidation and glycosylated hemoglobin in diabetes. *Diabetes.* 1989;38:1539-1543.

42. Wagner M, Alam A, Zimmermann J, et al. Endogenous erythropoietin and the association with inflammation and mortality in diabetic chronic kidney disease. *Clin. J. Am. Soc. Nephrol.* 2011 6:1573-1579.

43. Thomas MC. Type 2 Diabetes and Heart Failure: Challenges and Solutions. *Curr. Cardiol. Rev.* 2016;12:249-255.

44. Thomas MC, Brownlee M, Susztak K, et al Diabetic kidney disease. *Nat. Rev. Dis. Primers.* 2015;1:15018.

45. Peake M, Whiting M. Measurement of serum creatinine- current status and future goals. *Clin Biochem Rev*. 2006;27:173-84.

Acknowledgements:

Author Contributions: N.V., M.L. and H.L. conducted the experiments; (#) N.V. and M.L. contributed equally; A.L. analyzed the kidney function data; K.S.C. contributed the RBC samples and clinical data stored in the CCTS Biobank; M.L., N.V., H.L, S.D. and F.D. analyzed the data; H.B. provided advice on the statistical methods and interpretation of the statistical analyses; P.A.K, P.A.J., H.T., D.M.B, L.B.G and S.D. provided advice on the interpretation of the data analyses; A.J.M designed and assisted with the interpretation of the hypoxia experiments; F.D. conceived the study and wrote the manuscript with contributions from all authors.

Sources of Funding: This research was supported by National Institutes of Health HL118474 (F.D.), HL135000 (S.D.), AG057290 (F.D.) and AG053999 (F.D.), American Heart Association 16GRNT310200 (F.D.) and 18PRE33990154 (H.L.) and Alzheimer's Association VMF-15-363458 (F.D.). The University

of Kentucky CCTS Biostatistics, Epidemiology & Research Design (BERD) and Biospecimens Cores are funded by the CTSA grant UL1 TR001998.

Figure Legends

Fig. 1. Amylin-coated RBCs in human pathology. (a) Representative Western blots showing the amylin monomer in matched plasma, RBC and white blood cell (WBC) lysates from an individual with type-2 diabetes. Recombinant human amylin served as control. (b) Whisker box plots comparing the concentration of amylin, measured by ELISA, in RBCs from healthy individuals (h; dark green; n=66) versus individuals with various diseases or combination thereof, including type-2 diabetes (T2D; blue; n=69), heart failure (HF) with diabetes (HF-T2D; dark red; n=49) and without diabetes (HF w/o T2D; light red; n=59), cancer with diabetes (C-T2D; black; n=33) and without diabetes (C; gray; n=58), and stroke (S; yellow; n=13). RBC lysates from patients with type 1 diabetes (T1D; black; n=5) are the negative control for amylin. Statistical significance of the differences in amylin level was assessed using One-way ANOVA with the Bonferroni post-test for comparing all pairs of columns. *P<0.05, **P <0.01, ***P <0.001, ****P <0.0001. The correlation between RBC amylin and HbA1c in groups of healthy (c) and diseased individuals (d-i) described in (b). Out-of axis amylin-HbA1c levels: 25.2-5.8 and 12.2-4.6 in (d); 16.3-5.5 in (f) and 10.7-5.3 and 13.1-5.1 in (i), respectively. The Spearman nonparametric correlation analysis was performed in GraphPad and the values for the Spearman r and P are indicated on the plots.

Fig. 2. Accumulation of amyloid-forming human amylin in RBCs from diabetic rats. (a) Amylin concentration, measured by ELISA, in matched plasma and lysates of WBCs and RBCs from HIP rats and WT littermates (n=4/group). (b) Representative flow cytometry graphs (upper) and mean intensity (lower) for amylin/Alexa Fluor 488 fluorescence in RBCs from healthy, prediabetic and diabetic HIP rats (n=5 rats/group). (c) Amylin concentration in RBC lysates from 16 months old WT rats (n=7) and healthy

(n=6), prediabetic (n=15) and diabetic (n=16) HIP rats measured by ELISA. (d and e) Representative images of co-staining for amylin and hemoglobin (d) and amylin and glycophorin A (e) in RBCs from age-matched WT and diabetic HIP rats (n=3 rats/group). Scale bar, 10 µm (top row) and 5 µm (midle and bottom rows). (f) Representative STORM images showing RBCS from HIP and WT rats stained for human amylin (red) and Glycophorin A (green). (Scale bar 2µm). (n=3 for each rat group). *P <0.05; **P <0.01 by t-test (a) and One-way ANOVA (b and c).

Fig. 3. Pathophysiological changes induced by amyloid-forming amylin in RBCs. (a) Hemoglobin levels in RBCs from WT, HIP and UCD rats (n=11 rats/group). (b) Oxygen dissociation curve for RBCs from WT, HIP and UCD rats (n=5 rats/group). (c) Representative example of cell shape distribution of RBCs from WT (orange), UCD (blue) and HIP (pink) rats (n=6 rats/group) and the Pearson coefficient of dissymmetry (PCD) calculated from these data. (d) Percentage of RBC hemolysis in hypo-osmotic solutions. The NaCl concentration for 50% hemolysis of WT, HIP and UCD RBCs is indicated in the inset. (n=4 rats/group). (e and f) Representative images of co-staining for amylin and collagen IV (Col IV) in kidney tissue sections showing amylin deposition in arterioles and interstitial tissue (e) and in the glomerulus (f) in diabetic HIP rats but not in diabetic UCD rats (n=3 rats/group). (g) Representative images of co-staining for amylin and ionized calcium binding adaptor molecule 1 (IBA1) in kidney tissue sections from diabetic HIP and diabetic UCD rats (n=3 rats/group). (h) Representative images of staining for the cluster of differentiation 68 (CD68; ED1) in kidney tissue section from diabetic HIP and diabetic UCD rats (n=3 rats/group). (Scale bar 50µm) *P<0.05; **P<0.01 by One-way ANOVA with Tukey's post-test (a and c).

Fig. 4. Modulation of renal hypoxia markers by amylin dyshomeostasis. (a) EPO levels in plasma from 16 months WT rats (n=17), diabetic UCD rats (n=8) and diabetic HIP rats (n=17). (b) Percentage

number of reticulocytes over total numbers of RBCs in blood of WT, HIP and UCD rats (n=3 for each rat group). (c) Hematocrit levels in diabetic HIP and UCD rats and WT controls (n=6 rats/group). (d-h) Protein levels of HIF-1α (d), HIF-2α (e), arginase-1 (f) and arginase-2 (g) and arginase activity (h) measured by ELISA in renal tissues from 16 months old WT rats and diabetic UCD and HIP rats (n=10 rats/group). *P <0.05; **P <0.01; ***P <0.001 by One-way ANOVA with Tukey's post-test.

Fig. 5. Effect of increasing endogenous EETs on RBC-capillary coupling and renal hypoxia signaling. (a) Average numbers of RBCs adhered to cultured vascular endothelial cells when fixed hematocrit of RBCs flowed over cultured EC at constant rate for constant time of 20 minutes (n=3/ group). (b) Analysis of the adhesion of RBCs isolated from HIP rats and WT littermates to cultured vascular endothelial cells (n=8/group). (c) Adhesion of WT rat RBCs to cultured vascular endothelial cells with/without incubation with recombinant human amylin (50 μM) for 2 hours (n=5/group). (d) Attachment of RBCs from WT and diabetic HIP rats to vascular endothelial cells in the absence or in the presence of various amounts of EETs (n=8 rats/group). (e) Representative images of staining for amylin and Col IV in kidney sections from diabetic HIP rats (HIP-UT) and diabetic HIP rats with pharmacologically upregulated EETs (HIP-T). The scatterplot shows the percentage of the tissue area that is positive for amylin (n=3 rats/group). (f-g) Protein levels of HIF-2α (f) and HIF-1α (g) in whole kidney tissue homogenate from rats in the HIP-UT and HIP-T groups (n=4 rats/group). *P <0.05; **P <0.01; ***P <0.001 by t-test.

Fig. 6. Altered oxygen sensing in kidneys following transfusion with amylin-loaded RBCs

(a) Plasma EPO levels in WT rats transfused with RBCs from i) WT rats (n=7); ii) diabetic UCD rats (n=7) and iii) diabetic HIP rats (n=7). (b and c) Protein levels of HIF-1α (b) and HIF-2α (c) in renal tissue homogenate from the rats described in (a). (d) Representative images of amylin and glycophorin A co-

staining (left panel) and of amylin and hemoglobin co-staining (right panel) in RBCs from UCD rats infused with aggregated human amylin (daily injection of 0.08 µg/g body weight for 7 days; n=3 rats/group). (e) Plasma EPO levels in diabetic UCD rats (n=3) at baseline and at the end of the acute intravenous treatment with aggregated human amylin (hA). (f-g) Protein levels of HIF-2α and HIF-1α (f) and arginase-1 and arginase-2 (g) in renal tissue homogenates from diabetic UCD rats injected with human amylin versus non-injected diabetic UCD control rats (n=3 rats/group). (h) Cartoon illustrating the proposed mechanism through which "human" hyperamylinemia exacerbates hypoxia signalingin diabetic rats with pancreatic expression of non-amyloid forming amylin rat amylin (UCD rats). *P <0.05; **P <0.01; ***P <0.001 by One-way ANOVA with Tukey's post-test (a-c) or two-tailed t-test (e-g).

Diabetic Microcirculatory Disturbances and Pathologic Erythropoiesis Provoked by Deposition of Amyloid-Forming Amylin in Red Blood Cells and Capillaries

Nirmal Verma, Ph.D[1#], Miao Liu, Ph.D[1#], Han Ly, BS[1], Analia Loria, Ph.D[1], Kenneth S. Campbell, Ph.D[2], Heather Bush, Ph.D[3], Philip A. Kern, M.D.[4], Pedro A. Jose, M.D., Ph.D.[5], Heinrich Taegtmeyer, M.D., D.Phil.[6], Donald M. Bers, Ph.D[7], Sanda Despa, Ph.D[1], Larry B. Goldstein, M.D.[8], Andrew J. Murray, Ph.D.[9] and Florin Despa, Ph.D[1,8]

[1]Department of Pharmacology and Nutritional Sciences, University of Kentucky, Lexington, KY, USA.

[2]Department of Physiology, University of Kentucky, Lexington, KY, USA.

[3]Department of Biostatistics, College of Public Health, University of Kentucky, Lexington, KY, USA.

[4]Division of Endocrinology, Department of Medicine, University of Kentucky, Lexington, KY, USA.

[5]Department of Medicine, Division of Renal Diseases & Hypertension, The George Washington University School of Medicine & Health Sciences, Washington, DC, USA.

[6]Department of Internal Medicine, McGovern Medical School at UT Health, Houston, TX, USA

[7]Department of Pharmacology, University of California, Davis, CA, USA.

[8]Department of Neurology, University of Kentucky, Lexington, KY, USA.

[9]Department of Physiology, Development and Neuroscience, University of Cambridge, Cambridge CB2 3EG, UK.

Correspondence: Florin Despa, Department of Pharmacology and Nutritional Sciences, College of Medicine, University of Kentucky, Wethington Building, Room 459, 900 S. Limestone, Lexington, Kentucky, 40536, USA. Phone: 859-218-0291. Fax: 859-257-3646. E-mail: f.despa@uky.edu.

Running headline: Biomarkers in diabetic microvascular dysfunction

Abstract

In type-2 diabetes, the oxygen-carrying capacity of red blood cells (RBCs) and the integrity and stability of the blood capillaries decline causing tissue hypoxia and end organ malfunction. Correcting hyperglycemia is not entirely effective at reestablishing normal cellular metabolism and function. Identification of pathological changes occurring before the development of overt hyperglycemia may lead to novel therapeutic targets for reducing the risk of microvascular dysfunction. Here we showed that the RBC-capillary interaction is altered by prediabetic hypersecretion of amylin, an amyloid-forming hormone co-synthesized with insulin, and is reversed by endothelial cell-secreted epoxyeicosatrienoic acids (EETs). In humans, we found amylin deposition in RBCs in association with type-2 diabetes, heart failure, cancer and stroke. Amylin-coated RBCs have altered shape and reduced functional (non-glycated) hemoglobin. Amylin-coated RBCs administered intravenously in control rats upregulated erythropoietin (EPO) and renal arginase expression and activity. We also found that diabetic rats expressing amyloid-forming human amylin in the pancreas (HIP rats) have increased tissue levels of hypoxia-inducible transcription factors (HIFs) compared to diabetic rats that express non-amyloid forming rat amylin (UCD rats). EPO upregulation correlated with lower hematocrit in HIP rats indicating pathologic erythropoiesis. In HIP rats, pharmacological upregulation of endogenous EETs protected the renal microvasculature against amylin deposition whilst also reducing renal accumulation of HIFs. Thus, prediabetes induces amylin dyshomeostasis and promotes amylin deposition in RBCs and the microvasculature, which alters the RBC-capillary interaction leading to activation of hypoxia signaling pathways and pathologic erythropoiesis. Amylin dyshomeostasis could be a therapeutic target for ameliorating diabetic vascular complications.

Key words: Type-2-diabetes, Amylin, Microvascular Disease, Hypoxia, Erythropoiesis.

Translational statement

Amylin accumulation in RBCs induces hypoxic-ischemic tissue injury. Detection of amylin accumulation in human RBCs, in combination with current American Heart Association guidelines to define cardiovascular risk, could result in better risk stratification for microvascular complications, improve the ability to predict progression of diabetic microvascular complications by taking a precision medicine approach, and better rationalize therapeutic strategies and response to treatment.

Introduction

Oxygen is essential for cell function and cell survival[1]. RBCs deliver oxygen to cells and tissues via mechanisms that involve the passage of RBCs through capillaries. This process is enabled by the viscoelastic properties of the RBCs, which allow them to be deformed within capillaries[2]. In type-2 diabetes, the oxygen-carrying capacity of RBCs and the integrity and stability of the capillaries decline, exacerbating the risk of tissue hypoxia and end organ malfunction[3-7]. The underlying mechanisms are complex and incompletely understood.

Physiological responses to low oxygen levels are primarily driven by the stabilization of the α subunits of the hypoxia-inducible transcription factors HIF-1 and 2[1,8,9]. HIF-2 regulates the hypoxia response by elevating the renal expression of EPO, a hormone that signals an increased demand for RBCs from the bone marrow, which then increases the production of RBCs[8]. Stabilization of HIF-2α also induces *arginase* expression[9] in vascular endothelial cells. Because arginase has the same substrate (L-arginine) as nitric oxide (NO) synthase[9], increased *arginase* production/ activation may reduce NO availability. Depleted NO production impairs relaxation of the blood vessels and affects microvascular autoregulation[1,8,9]. Thus, increased EPO coupled with arginase-NO dysregulation constitutes one of the multiple[10] molecular derangements linking systemic hypoxia with microvascular dysfunction.

Metabolic derangements that occur before the development of overt hyperglycemia may induce microvascular dysfunction[11]. In prediabetes, pancreatic β-cells compensate for insulin resistance by increasing the secretion of insulin (hyperinsulinemia)[12]. Amylin (also known as islet amyloid polypeptide; IAPP), is a 37-amino acid peptide synthesized and co-secreted with insulin in response to physiological stimuli[13-15]. It is normally soluble, crosses the blood brain barrier and binds to neurons in the feeding centers participating in the regulation of gastric fluxes[16]. Amylin from humans and a few other species, including cats, dogs and monkeys, but not rodents, has an increased propensity to aggregate, forming amyloid[17] (i.e., amylin dyshomeostasis). This triggers β-cell apoptosis by mechanisms involving

incorporation of aggregated amylin into cellular membranes[18-20]. We[21-26] and others[27-31] have shown the presence of amylin deposition in failing hearts[21-23] and kidneys[27] of patients with type-2 diabetes and in brains[28-31] of humans with dementia[32]. We also showed that rats that develop type-2 diabetes linked to amylin dyshomeostasis (i.e. the HIP rat model for type-2 diabetes[33]) develop heart dysfunction[21,23] and neurological deficits[25,34] sooner than age- and blood glucose-matched rats that develop type-2 diabetes in the absence of amylin dyshomeostasis (i.e. the UCD rat model for type-2 diabetes[35]). The upregulation of epoxyeicosatrienoic acids (EETs) in endothelial cells appeared to protect against cardiac amylin accumulation in HIP rats, which correlated with improved heart function[22]. Although we interpret these findings to support the hypothesis that reducing amylin dyshomeostasis may ameliorate diabetic vascular complications, the impact of elevated blood levels of amylin on blood cells and the microvasculature remains unknown.

Here we tested the hypothesis that systemic amylin dyshomeostasis alters the interaction between RBCs and capillaries leading to hypoxic-ischemic tissue injury. To test this hypothesis, we measured the amylin levels in RBCs from humans with and without diabetes, and used transgenic rats, RBC transfusions and pharmacological tools for mechanistic studies.

Results

Humans with type-2 diabetes have amylin deposition in RBCs.

We assessed the relationship between HbA1c level (the common marker of hyperglycemia) and amylin concentration in RBC lysates from patients with type-2 diabetes or diseases that are commonly associated with insulin resistance, including heart failure, cancer and stroke. Western blot analysis of matched plasma, RBC lysate and white blood cell (WBC) lysate from a human with type-2 diabetes (the positive control for amylin dyshomeostasis) detected both monomeric amylin (Figure 1a) and amylin-positive higher molecular weight bands (Supplementary Figure 1). RBC lysates from individuals with a primary diagnosis of type-2 diabetes (T2D) (without heart failure, cancer or stroke) had higher amylin

concentration than those from healthy individuals (H) and patients with type-1 diabetes (T1D group; the negative control for amylin) (Figure 1b). Patients with a primary diagnosis of heart failure (HF), cancer (C), or stroke (S) also had elevated RBC amylin levels independent of type-2 diabetes as a secondary diagnosis (Figure 1b). Lighter colored symbols in the HF and C groups indicate heart failure or cancer without type-2 diabetes. RBC amylin and HbA1c levels were highly variable in all groups (Figure 1c-i), except in patients with HF and type-2 diabetes in whom higher HbA1c levels correlated with RBC amylin accumulation. There were non-significant inverse correlations between HbA1c and RBC amylin levels in the HF without diabetes (Figure 1f), cancer with diabetes (Figure 1g) and stroke (Figure 1i) groups.

These results suggest that type-2 diabetes and diseases associated with insulin resistance such as heart failure, cancer and stroke promote amylin accumulation in RBCs in humans.

Amylin deposition in RBCs results from hypersecretion of amyloid-forming human amylin.

The HIP rat is a unique animal model for late-life onset type-2 diabetes as it is characterized by pancreatic expression of the human (amyloid-forming) variant of amylin[33], whereas other rodent models for type-2 diabetes express only the native, non-amyloid forming amylin[17]. As in humans[14], the development of type-2 diabetes in HIP rats is associated with pancreatic amyloid[33] (Supplementary Figure 2). We compared the amylin content in RBCs, WBCs, and plasma from diabetic HIP rats and non-diabetic WT littermates (Figure 2a). Amylin was concentrated in RBCs and the *difference* in amylin levels between WT and diabetic HIP rats was greater in RBCs than in plasma or WBCs (Figure 2a).

Analysis of freshly packed RBCs by flow cytometry (Figure 2b) and amylin ELISA (Figure 2c) revealed a correlation between RBC amylin levels and different levels of non-fasted blood glucose (normal, ≤ 11 mM, 6-8 months old; prediabetic, 11-14 mM on two consecutive measurements separated by >3 days, 10-12 months old; and diabetic, >14 mM on two consecutive measurements, separated by >3 days; 14-16 months old).

Confocal microscopy analysis of RBCs that were double-stained for amylin and hemoglobin showed amylin deposition on RBCs from HIP rats (Figure 2d). Amylin appeared to co-localize with glycophorin A (Figure 2e), a membrane protein that is specific to RBCs, suggesting amylin accumulation on the RBC membrane. The analysis of RBCs co-stained for amylin and glycophorin A using super-resolution imaging (STORM) showed the presence of amylin within the RBC membrane with some dense patches on the outer part of the cell membrane (Figure 2f). Electron microscopic examination of immunogold-labeled thin sections of epoxy resin-embedded RBCs indicated the presence of amylin within the cell membrane (Supplementary Figure 3; arrowhead pointing to amylin deposits).

The results demonstrate that hypersecretion of the amyloid-forming human variant of amylin leads to amylin deposition within circulating RBCs.

Amylin-coated RBCs have lower deformability and functional (non-glycated) hemoglobin.

Next, we investigated pathophysiological characteristics of RBCs from diabetic HIP rats and RBCs from diabetic rats without amylin dyshomeostasis (UCD rats) and non-diabetic WT rats, as they express only the non-amyloid forming rat amylin. Compared to RBCs from WT rats, RBCs from HIP rats contained less functional (non-glycated) hemoglobin (Figure 3a), whereas there was no difference between UCD and WT rats. RBCs of HIP, UCD and WT rats (~ 12 months old rats) had similar oxygen dissociation curves (Figure 3b) indicating that the affinity of hemoglobin for oxygen, the release of bound oxygen and the partial oxygen pressure for maintaining oxygen saturation are not significantly affected by amylin dyshomeostasis or hyperglycemia.

In flow cytometry experiments, the distribution of the forward scattering (FSC) signals by RBCs from WT rats (Figure 3c; orange) was bimodal, which reflects the biconcave disk shape of normal RBCs. In the case of amylin-coated RBCs from diabetic HIP rats, the FSC distribution was monomodal (Figure 3c; pink), indicating changes in RBC morphology towards a more spherical shape. The Pearson coefficient of dissymmetry (PCD), which indicates the departure from sphericity, suggested distinct morphological

changes in RBCs from HIP rats compared to WT and UCD rats (Figure 3c). Incubation of RBCs from WT rats with aggregated human amylin for 4 hours (as described in our previous studies[26,36]) replicated the morphological change observed in HIP rat RBCs (Supplementary Figure 4). Altered shape of RBCs from HIP and UCD rats did not affect the response to an osmotic resistance test, as the propensity for hemolysis in hypo-osmotic solutions was comparable for RBCs from all three rat groups (Figure 3d).

These results show that amylin deposition in RBCs is associated with lower hemoglobin concentrations and reduced RBC deformability, independently of effects of chronic glucose levels. At an early stage of diabetes, the cumulative effects of amylin dyshomeostasis and hyperglycemia (as in HIP rats) or hyperglycemia alone (as in UCD rats) do not appear to induce significant changes in hemolysis and oxygen dissociation.

The microvasculature is disrupted in kidneys of rats with amylin dyshomeostasis.

Next we investigated the structural integrity of the capillary network and the stability of the capillary beds in kidneys from age- and blood glucose-matched HIP and UCD rats. We used immunohistochemistry with antibodies against amylin (brown) and collagen IV (Col IV; green), a component of the basement membrane, to anatomically localize amylin deposition with respect to the vasculature. In HIP rat kidneys, there were patches of amylin deposits in arterioles, interstitial tissue between the tubules (Figure 3e) and glomeruli (Figure 3f). Vascular amylin deposition correlated with accumulation of macrophages, as indicated by co-staining for amylin and the ionized calcium-binding adapter molecule 1 (IBA1), a marker of macrophage activation (Figure 3g). There were macrophages in areas of amylin deposition, which may indicate a potential role for these cells in the clearance of vascular amylin deposition. Staining with ED1 (Figure 3h), an antibody against the cluster of differentiation (CD) 68 protein (that is highly expressed by circulating macrophages), supports the increased activity of macrophages in areas of vascular amylin deposition. In contrast, vascular amylin deposits and macrophage infiltration were not found in kidneys from diabetic UCD rats.

These data suggest that amylin dyshomeostasis injures the capillaries, which may be associated with systemic inflammatory responses leading to macrophage infiltration that may exacerbate ischemic vascular injury in HIP rats.

Amylin dyshomeostasis activates renal hypoxia signaling pathways.

The kidney is a critical component of a regulatory feedback loop that controls the hematocrit via EPO production[8]. Both HIP and UCD rats had renal dysfunction, as indicated by polyuria and albuminuria (Supplementary Figures 5a and 5b). Creatinine clearance was elevated in diabetic HIP rats compared with WT littermates and diabetic UCD rats (Supplementary Figure 5c). The plasma level of EPO, the hormone that signals an increased demand for RBCs to the bone marrow, was higher in diabetic HIP rats than in WT littermates (Figure 4a) and tended to be higher in age-matched diabetic UCD rats vs. WT rats ($P = 0.27$). The reticulocyte count was also higher in HIP than in WT rats (Figure 4b). Despite elevated plasma EPO levels, the average hematocrit was not different in HIP rats compared with WT littermates, but was lower in HIP compared to UCD rats (Figure 4c). The spleen, a major blood reservoir, had lower weight in diabetic HIP rats compared to age-matched WT rats (Supplementary Figure 6). Compared with diabetic UCD rats and healthy WT rats, diabetic HIP rats had elevated levels of HIF-1α and HIF-2α in whole kidney tissue homogenates (Figure 4d and 4e). Consistent with elevated HIF-2α, HIP rat kidneys also had upregulated arginase-1 and 2 proteins (Figure 4f and 4g) and greater arginase activity (Figure 4h). Increased stabilization of HIF α units in HIP rat kidney tissue correlated with a trend towards downregulation of the von Hippel-Lindau (vHL) tumor suppressor protein (Supplementary Figure 7) suggesting impaired degradation of HIF α units.

These results suggest that activation of hypoxia signaling in kidneys and downstream upregulation of EPO are associated with pathologic erythropoiesis and amylin deposition in RBCs.

Blocking of adhesion proteins in endothelium reverses amylin dyshomeostasis and HIF activation.

The adhesion of RBCs to cultured vascular endothelial cells (ECs) under flow condition tended to be greater for HIP rat RBCs than RBCs from UCD rats (P = 0.17) and from WT rats (P = 0.17) (Figure 5a). Greater adhesion of RBCs from HIP rats to ECs was found in experiments without flow condition (Figure 5b) in an adhesion test in which RBCs from WT rats that were incubated with 50 μM synthetic human amylin for 4 hours is shown in Figure 5c. Analysis of kidney capillary lysates by Western blot (A) and ELISA (B) showed a trend towards upregulation of the expression of vascular cell adhesion molecule 1 (VCAM-1) in HIP rats (Supplementary Figure 8). Taken together, these results suggest that the cell membrane adhesion proteins may play a role in amylin accumulation at the RBC-capillary interface. To test this hypothesis, we used EETs, which are primarily expressed by vascular ECs[37] and RBCs[38] and are known to downregulate the expression of VCAM-1 in endothelium[39]. We found that *ex vivo* incubation with (±)14(15)-EET reduced the adhesion of HIP rat RBCs to cultured endothelial cells (Figure 5d). Upregulation of EETs by treatment with an inhibitor of soluble epoxide hydrolase, the enzyme that degrades endogenous EETs[37], was associated with lower amylin deposition in renal microvasculature (the HIP-T group; Figure 5e). The treatment lowered renal accumulation of HIF-2α (Figure 5f) and HIF-1α (Figure 5g) and had variable effects on arginase expression and arginase activation (Supplementary Fig 9) in HIP rat kidneys.

Taken together, these results indicate that 1) reduced capillary RBC flux owing to amylin deposition on RBCs and the capillary wall likely contributes to tissue hypoxia in HIP rats and 2) EETs reduce this effect by downregulation of adhesion proteins in the vascular endothelium.

Transfused amylin-coated RBCs upregulate EPO through HIF-2α activation in kidneys.

RBCs act as both oxygen carriers and mediators of oxygen sensing and signaling pathways within ECs[8,9]. To determine whether amylin deposition on RBCs activates hypoxia signaling pathways in tissues, amylin-coated RBCs from HIP rats were administered to WT rats. Rats were given 300 μl freshly packed RBCs/day for seven days. WT rats given similar volumes of RBCs from diabetic UCD rats were used as

positive controls for the possible effects of hyperglycemia on RBC function, whereas WT rats receiving RBCs from WT rats served as negative controls. Plasma levels of EPO were elevated in WT rats receiving amylin-coated RBCs from HIP rats compared to WT rats that received either RBCs from diabetic UCD rats or WT rats (Figure 6a). Kidneys of WT rats receiving HIP rat RBCs had increased stabilization of HIF-1α (Figure 6b) but no difference in HIF-2α levels (Figure 6c), compared with rats in the two control groups.

To examine further a possible 'amylin stress" on oxygen-sensing pathways, aggregated human amylin (hA) (0.08 μg/g body weight) was intravenously administered to diabetic UCD rats, daily, for one week. Intravenous infusion of aggregated human amylin in UCD rats led to amylin deposition on RBCs (Figure 6d). This acute "amylin stress" provoked an increase in plasma EPO level (Figure 6e; the "after hA inj" rat group) and no difference in renal HIF-2α and HIF-1α levels in whole kidney tissue homogenate (Figure 6f). Arginase 1 protein levels were elevated in kidney tissue homogenates from amylin-infused UCD rats, whereas there was no significant change of arginase 2 protein expression (Figure 6g).

These data indicate elevated EPO and accumulation of HIFs in kidneys as a direct response to circulating amylin-coated RBCs (Figure 6h).

Discussion

We found that hypersecretion of human amylin is associated with amylin deposition in the microvasculature and RBCs leading to impaired RBC-capillary interaction and activation of hypoxia signaling pathways. Impairment of tissue oxygen-sensing found in diabetic HIP rats was mirrored in control rats that were given amylin-coated RBCs intravenously and in diabetic UCD rats that were given human amylin intravenously. These results indicate that amylin-coated RBCs are a trigger of hypoxia signaling pathways. These deleterious effects result in part from a reduced flux of amylin-coated RBCs through the capillaries that may involve adhesion proteins. Blocking the expression of adhesion proteins in the vascular endothelium by upregulation of EETs reduces amylin dyhomeostasis and HIF activation.

Future studies need to identify the ligand pairs for the amylin-mediated adhesive interaction between vascular ECs and RBCs. Candidate ligand pairs may include the VCAM-1-α4β1-integrin pair of proteins that appears to be involved in sickle cell disease[40].

This link between prediabetes-induced systemic amylin dyshomeostasis and tissue hypoxia has broad implications for health care because: 1) accumulating evidence demonstrates the presence of amylin deposition in vital organs[21-31] and RBCs (as shown by the present human data) that may provide a therapeutic target reducing vascular injury prior the development of overt diabetes, 2) the public health impact of type-2 diabetes; and 3) the lack of drugs that counter amylin dyshomeostasis.

Glycated hemoglobin has a higher affinity for oxygen than adult hemoglobin A (functional hemoglobin), and can disrupt the supply of oxygen to tissues[41]. Indeed, RBCs from hyperglycemic UCD rats have decreased deformability and functional hemoglobin compared with WT rats. RBC deformability and hemoglobin levels are even lower in HIP rats, which may explain, in part, the higher hypoxic response in control WT rats receiving RBCs from HIP rats compared to control rats receiving similar volumes of RBCs from UCD rats.

Elevated EPO and microvascular dysfunction identify diabetic patients with increased risk of death[42-44]. In diabetic HIP rats, elevated plasma EPO does not correlate with an increase in hematocrit. HIP rat kidneys have amylin deposits in the microvasculature that co-localized with macrophage activation. Taken together, the results suggest that systemic amylin dyshomeostasis may upregulate eryptosis via macrophage activation. The results also indicate that amylin dyshomeostasis injures capillaries and is associated with inflammatory responses exacerbating ischemic vascular injury.

There are inherent limitations to our study of the interaction between pancreatic amylin secretion and RBCs. In the human study, we were not able to control for the potential effects of glucose, steroids, anti-diabetic drugs or specific forms of anesthesia given to individual patients, which can affect pancreatic function including amylin and insulin secretion.

In conclusion, systemic amylin dyshomeostasis promotes amylin deposition in RBCs and the microvasculature associated with pathologic erythropoiesis, macrophage activation and macrophage accumulation in blood vessels. Future studies should determine whether the RBC amylin levels affect the course of microvascular complications.

Methods

Detailed Methods are included in Supplementary Materials.

Human studies

This research employed de-identified blood specimens matched with medical record data obtained from the biobank of the Center for Clinical and Translational Science at University of Kentucky. Sample collection and storage were approved by the Institutional Review Board. We assessed the relationship between HbA1c level and amylin concentration in RBC lysates from individuals with primary diagnosis of type-2 diabetes or diseases that are commonly associated with insulin resistance, including heart failure, cancer and stroke. RBC specimens were divided into groups based on the primary diagnosis of type-2 diabetes, heart failure, cancer or stroke. Most humans in the heart failure and cancer groups had type-2 diabetes as a second diagnosis. The negative control for amylin was RBC lysates from patients with over 15 years of type-1 diabetes (and, therefore, depleted β-cell mass) who were otherwise healthy. The healthy control group included individuals without diabetes, heart failure, stroke or cancer. Exclusion criteria were based on conditions that may affect the pancreatic secretion of amylin such as transplant recipients (less than 6 months after the transplant), patients with liver disease, patients with HIV and pregnant or lactating women. Table 1 summarizes the diabetes status, co-morbidities, age, sex and body mass index (BMI) of the patients who provided the blood used in these analyses.

Experimental Animals

All animal experiments conform to the NIH guide for the care and use of laboratory animals and were approved by the Institutional Animal Care and Use Committee at University of Kentucky. We compared rats that develop type-2 diabetes linked to expression of human amylin in the pancreas (HIP rats; n=65), with rats that develop type-2 diabetes in the absence of amyloid, as they express the non-amyloidogenic rat amylin (UCD rats; n=40) and control, non-diabetic rats (WT rats; n=53).

Treatment

We performed a retrospective analysis of kidney tissue from a prior study[22] in which HIP rats were treated for 10 weeks with a soluble epoxide inhibitor APAU (UC1153) added to their drinking water in order to upregulate the endogenous EET levels. APAU was formulated in polypropylene glycol at a concentration of 10 mg/mL with 30 minutes sonication. The APAU aliquot was added to the drinking water at a final content of 1%.

Renal function analysis

Urine and blood were collected from rats in metabolic cages. Creatinine concentration in plasma and urine was measured using the kinetic Jaffé method[45]. Creatinine clearance (Ccr) was calculated using the formula: Ccr (ml/min) = (urine creatinine/plasma creatinine) × urine flow rate. Urinary albumin was measured by ELISA.

Tissue extraction and RBC isolation

For measurements of hypoxia markers (hypoxia-inducible transcription factors 1α, HIF1-α, and 2α, HIF2-α, arginase 1, arginase 2 and von Hippel-Lindau factor, vHL) and arginase activity, kidney tissue was extracted in PBS with protease and phosphatase inhibitors, followed by three consecutive cycles of freezing to -80°C and thawing. For other biochemical assays, tissues were extracted in homogenization buffer containing Triton X-100, SDS and protease and phosphatase inhibitors.

RBCs were isolated immediately after blood collection by centrifugation at 1,000g. For some experiments, RBCs were lysed in lysis buffer containing 10% NP-40.

RBC transfusion

Isolated RBCs were combined with storage solution (150 mM HCl, 45 mM dextrose, 45.5 mM mannitol, and 2.2 mM adenine) in a 3:1 v/v ratio, transferred to sterile tubes and stored at 4°C in the dark before injection. Rats received 300 µL of pre-warmed (at 37º C) RBC solution once daily for 7 days via tail vein injection.

Hematocrit and hemoglobin measurements

Hematocrit was measured with an i-STAT analyzer using i-STAT CG8+ cartridges according to the manufacturer's protocol. Hemoglobin content was calculated from the optical density at 405 nm.

Assessment of RBC shape and amylin deposition on RBCs by flow cytometry

RBCs were incubated with an anti-amylin antibody followed by incubation with an anti-rabbit Alexa Fluor® 488 secondary antibody. Flow cytometry was performed with a Becton Dickinson LSRII instrument. To assess cell shape, RBCs were first gated on a forward scatter (FSC)/side scatter (SSC) plot. The region 1 (R1) events were visualized using a FSC-A/FSC-H dot plot. For detecting amylin deposited on RBCs, cells were first gated on a forward scatter (FSC)/side scatter (SSC) plot. RBCs were further gated to determine the amylin signal (Alexa 488), using negative control (no antibody) and positive control (RBCs incubated with 50 µM of synthetic amylin peptide) to set the upper and lower boundaries.

Immunofluorescence

Isolated RBCs were incubated with primary antibodies against human amylin and glycophorin A, followed by incubation secondary antibodies, and imaged with a Nikon A1R confocal microscope. For hemoglobin staining, blood smears on glass slide were fixed and incubated with primary antibodies against

hemoglobin and human amylin. Smears were then incubated with secondary antibodies, mounted in mounting media and imaged.

Biochemical assays

ELISA for human amylin, erythropoietin, HIF1-α, HIF2-α, arginase 1, arginase 2 and vHL were performed according to the manufacturer's protocols. Arginase activity was measured in kidney homogenates using a colorimetric assay. Western blots were performed on plasma, WBC lysates, RBC lysates from humans and using a primary antibody against amylin and on kidney capillary lysates from rats using a primary antibody against VCAM-1 (1:1000, ab134047, Abcam).

Immunohistochemistry

Immunohistochemical staining was performed on rat kidney slices using antibodies against amylin, collagen IV, IBA-1, and ED1). The staining area for amylin was analyzed in ImageJ.

Statistical analysis

Statistical differences between groups were determined using Student's t-test, one-way ANOVA or two-way ANOVA, as appropriate. Multiple comparison and P values were calculated by Bonferroni correction for human data. P value for each regression analysis was calculated by the Spearman correlation test.

Disclosures: The authors have declared that no conflict of interest exists.

Supplementary Materials

Supplementary Figure Legends

Supplementary Figure S1. *Left*) Representative western blot analysis of high molecular weight amylin oligomers in plasma, RBC lysate and white blood cell (WBC) lysate from an individual with type-2 diabetes. (*Right*) The Ponceau S staining of the blot show in *Left* panel.

Supplementary Figure S2. Representative images of Thioflavin S (green) and amylin (red) staining in the pancreas from a diabetic HIP and a control WT rat (n=3/group). Scale bar, 30 µm.

Supplementary Figure S3. Representative TEM images showing RBCs from HIP and WT rats, stained with human amylin primary antibody and gold (10nm) labelled secondary antibody. (Scale bar 1µm)

Supplementary Figure S4. PCD for WT rat RBCs and WT rat RBCs incubated ex vivo with oligomerized human amylin (n=5 preparations/group).

Supplementary Figure S5. Volume of urine excretion (A), albuminuria (B) and creatinine clearance rate (C) in 16 months old WT, diabetic UCD and diabetic HIP rats (n=6 rats/group). $^{**}P \leq 0.01$; $^{***}P \leq 0.001$ by One-way ANOVA.

Supplementary Figure S6. Gross spleen weights of 16 months old WT rats and diabetic HIP rats (n=10 spleens/group). Data are means ± SEM. $^{*}P < 0.05$

Supplementary Figure S7. Levels of von Hippel-Lindau (vHL) protein in the renal tissues from 16 months old WT rats and diabetic HIP rats (n=5 rats/group). Data are means ± SEM.

Supplementary Figure S8. Western blot and ELISA analyses for VCAM-1 expression in kidney capillaries lysates of WT and HIP rats (n= 3 rats/group).

Supplementary Figure S9. Reduced amylin deposition in kidneys correlated with partially reduced imbalance of arginase expression and arginase activation in HIP rat kidney tissues. (n=4 rats/group). Data are means ± SEM. *P <0.05

Supplementary Methods

Supplementary References

Supplementary information is available at www.kidney-international.org

References

1. Semenza GL. Life with oxygen. *Science.* 2007;318:62-64.

2. Mohandas N, Gallagher PG. Red cell membrane: past, present, and future. *Blood.* 2008;112:3939-3948.

3. McMillan DE, Utterback NG, La Puma J. Reduced erythrocyte deformability in diabetes. *Diabetes.* 1978;27: 895-901.

4. Tonelli M, Sacks F, Arnold M, et al. Relation between Red Blood Cell Distribution Width and Cardiovascular Event Rate in People with Coronary Disease. *Circulation.* 2008;117:163-168.

5. Thomas MC. Anemia in diabetes: marker or mediator of microvascular disease? *Nat. Clin. Pract. Nephrol.* 2007;3:20-30.

6. Maddox TM, Stanislawski MA, Grunwald GK, et al. Nonobstructive coronary artery disease and risk of myocardial infarction. *JAMA.* 2014;312:1754-1763.

7. Barrett EJ, Liu Z, Khamaisi M, et al. Diabetic Microvascular Disease: An Endocrine Society Scientific Statement. *J Clin Endocrinol Metab.* 2017;102:4343-4410.

8. Semenza GL. Involvement of oxygen-sensing pathways in physiologic and pathologic erythropoiesis. *Blood*. 2009;114:2015-2019.

9. Samanta D, Prabhakar NR, Semenza GL. Systems biology of oxygen homeostasis. *Wiley Interdiscip. Rev. Syst. Biol. Med*. 2017;9: e1382.

10. Wong BW, Marsch E, Treps L, et al. Endothelial cell metabolism in health and disease: impact of hypoxia. *EMBO J.* 2017;36:2187-2203.

11. Gerstein HC, Bosch J, Dagenais GR, et al. ORIGIN Trial Investigators. Basal insulin and cardiovascular and other outcomes in dysglycemia. *N Engl J Med*. 2012;367:319-328.

12. Dankner R, Chetrit A, Shanik MH, et al. Basal state hyperinsulinemia in healthy normoglycemic adults heralds dysglycemia after more than two decades of follow up. *Diabetes. Metab. Res. Rev.* 2012;28:618-624.

13. Butler PC, Chou J, Carter WB, et al. Effects of meal ingestion on plasma amylin concentration in NIDDM and nondiabetic humans. *Diabetes.* 1990;39:752-756.

14. Westermark P, Andersson A, Westermark GT. Islet amyloid polypeptide, islet amyloid, and diabetes mellitus. *Physiol. Rev.* 2011;91:795-826.

15. Kahn SE, D'Alessio DA, Schwartz MW, et al. Evidence of cosecretion of islet amyloid polypeptide and insulin by beta-cells. *Diabetes.* 1990;39:634-638.

16. Lutz TA. The role of amylin in the control of energy homeostasis. *Am. J. Physiol. Regul. Integr. Comp. Physiol.* 2010;298:R1475-R1484.

17. Westermark P, Engstrom U, Johnson KH, et al. Islet amyloid polypeptide: pinpointing amino acid residues linked to amyloid fibril formation. *Proc. Natl. Acad. Sci. USA.* 1990;87:5036-5040.

18. Janson J, Ashley RH, Harrison D, et al. The mechanism of islet amyloid polypeptide toxicity is membrane disruption by intermediate-sized toxic amyloid particles. *Diabetes.* 1999;48:491-498.

19. Zraika S1, Hull RL, Udayasankar J, et al. Oxidative stress is induced by islet amyloid formation and time-dependently mediates amyloid-induced beta cell apoptosis. *Diabetologia.* 2009;52:626-635.

20. Huang CJ, Haataja L, Gurlo T, et al. Induction of endoplasmic reticulum stress-induced beta-cell apoptosis and accumulation of polyubiquitinated proteins by human islet amyloid polypeptide. *Am. J. Physiol. Endocrinol. Metab.* 2007;293:E1656-E1662.

21. Despa S, Margulies KB, Chen L, et al. Hyperamylinemia contributes to cardiac dysfunction in obesity and diabetes: A study in humans and rats. *Circ. Res.* 2012;110:598-608.

22. Despa S, Sharma S, Harris TR, et al. Cardioprotection by controlling hyperamylinemia in a "humanized" diabetic rat model. *J. Am. Heart. Assoc.* 2014;3:pii: e001015.

23. Liu M, Verma N, Peng X, et al. Hyperamylinemia increases IL-1β synthesis in the heart via peroxidative sarcolemmal injury. *Diabetes.* 2016;65:2772-2783.

24. Jackson K, Barisone GA, Diaz E, et al. Amylin deposition in the brain: A second amyloid in Alzheimer disease? *Ann. Neurol.* 2013;74:517-526.

25. Verma N, Ly H, Liu M, et al. Intraneuronal amylin deposition, peroxidative membrane injury and increased IL-1β synthesis in brains of Alzheimer's disease patients with type-2 diabetes and in diabetic HIP rats. *J. Alzheimers. Dis.* 2016;53:259-272.

26. Ly H, Verma N, Wu F, et al. Brain microvascular injury and white matter disease provoked by diabetes-associated hyperamylinemia. *Ann. Neurol.* 2017;82:208-222.

27. Gong W, Liu ZH, Zeng CH, et al. Amylin deposition in the kidney of patients with diabetic nephropathy. *Kidney Int.* 2007;72:213-218.

28. Fawver JN, Ghiwot Y, Koola C, et al. Islet amyloid polypeptide (IAPP): A second amyloid in Alzheimer's disease. *Curr. Alzheimer. Res.* 2014;1:928-940.

29. Oskarsson ME, Paulsson JF, Schultz SW, et al. In vivo seeding and cross-seeding of localized amyloidosis: A molecular link between type 2 diabetes and Alzheimer disease. *Am. J. Pathol.* 2015;185:834-846.

30. Schultz N, Byman E, Fex M, et al. Amylin alters human brain pericyte viability and NG2 expression. *J. Cereb. Blood Flow Metab.* 2007;37:1470-1482.

31. Schultz N, Byman E, Netherlands BB, et al. Levels of retinal IAPP are altered in Alzheimer's disease patients and correlate with vascular changes and hippocampal IAPP levels. *Neurobiol. Aging.* 2018;69:94-101.

32. Biessels GJ, Despa F. Cognitive decline and dementia in diabetes mellitus: mechanisms and clinical implications. *Nat. Rev. Endocrinol.* 2018;14:591-604.

33. Butler AE, Jang J, Gurlo T, et al. Diabetes due to a progressive defect in beta-cell mass in rats transgenic for human islet amyloid polypeptide (HIP Rat): a new model for type 2 diabetes. *Diabetes*. 2004;53:1509-1516.

34. Srodulski S, Sharma S, Bachstetter AB, et al Neuroinflammation and neurologic deficits in diabetes linked to brain accumulation of amylin. *Mol. Neurodegener.* 2014;9:30.

35. Cummings BP, Digitale EK, Stanhope KL, et al. Development and characterization of a novel rat model of type 2 diabetes mellitus: the UC Davis type 2 diabetes mellitus UCD-T2DM rat. *Am. J. Physiol. Regul. Integr. Comp. Physiol.* 2008;295:R1782-R1793.

36. Liu M, Hoskins A, Verma N, et al. Amylin and diabetic cardiomyopathy - amylin-induced sarcolemmal Ca^{2+} leak is independent of diabetic remodeling of myocardium. *Biochim. Biophys. Acta. Mol. Basis Dis.* 2018;1864:1923-1930.

37. Imig JD. Epoxides and soluble epoxide hydrolase in cardiovascular physiology. *Physiol Rev*. 2012;92:101-130.

38. Jiang H, Anderson GD, McGiff JC. Red blood cells (RBCs), epoxyeicosatrienoic acids (EETs) and adenosine triphosphate (ATP). *Pharmacol Rep*. 2010;62:468-474.

39. Node K, Huo Y, Ruan X, et al. Anti-inflammatory properties of cytochrome P450 epoxygenase-derived eicosanoids. *Science.* 1999;285:1276-1279.

40. White J, Lancelot M, Sarnaik S, et al. Increased erythrocyte adhesion to VCAM-1 during pulsatile flow: Application of a microfluidic flow adhesion bioassay. *Clin. Hemorheol. Microcirc*. 2015;60:201-13

41. Jain SK, McVie R, Duett J, et al. Erythrocyte membrane lipid peroxidation and glycosylated hemoglobin in diabetes. *Diabetes.* 1989;38:1539-1543.

42. Wagner M, Alam A, Zimmermann J, et al. Endogenous erythropoietin and the association with inflammation and mortality in diabetic chronic kidney disease. *Clin. J. Am. Soc. Nephrol.* 2011 6:1573-1579.

43. Thomas MC. Type 2 Diabetes and Heart Failure: Challenges and Solutions. *Curr. Cardiol. Rev.* 2016;12:249-255.

44. Thomas MC, Brownlee M, Susztak K, et al Diabetic kidney disease. *Nat. Rev. Dis. Primers.* 2015;1:15018.

45. Peake M, Whiting M. Measurement of serum creatinine- current status and future goals. *Clin Biochem Rev*. 2006;27:173-84.

Acknowledgements:

Author Contributions: N.V., M.L. and H.L. conducted the experiments; (#) N.V. and M.L. contributed equally; A.L. analyzed the kidney function data; K.S.C. contributed the RBC samples and clinical data stored in the CCTS Biobank; M.L., N.V., H.L, S.D. and F.D. analyzed the data; H.B. provided advice on the statistical methods and interpretation of the statistical analyses; P.A.K, P.A.J., H.T., D.M.B, L.B.G and S.D. provided advice on the interpretation of the data analyses; A.J.M designed and assisted with the interpretation of the hypoxia experiments; F.D. conceived the study and wrote the manuscript with contributions from all authors.

Sources of Funding: This research was supported by National Institutes of Health HL118474 (F.D.), HL135000 (S.D.), AG057290 (F.D.) and AG053999 (F.D.), American Heart Association 16GRNT310200 (F.D.) and 18PRE33990154 (H.L.) and Alzheimer's Association VMF-15-363458 (F.D.). The University

of Kentucky CCTS Biostatistics, Epidemiology & Research Design (BERD) and Biospecimens Cores are funded by the CTSA grant UL1 TR001998.

Figure Legends

Fig. 1. Amylin-coated RBCs in human pathology. (a) Representative Western blots showing the amylin monomer in matched plasma, RBC and white blood cell (WBC) lysates from an individual with type-2 diabetes. Recombinant human amylin served as control. (b) Whisker box plots comparing the concentration of amylin, measured by ELISA, in RBCs from healthy individuals (h; dark green; n=66) versus individuals with various diseases or combination thereof, including type-2 diabetes (T2D; blue; n=69), heart failure (HF) with diabetes (HF-T2D; dark red; n=49) and without diabetes (HF w/o T2D; light red; n=59), cancer with diabetes (C-T2D; black; n=33) and without diabetes (C; gray; n=58), and stroke (S; yellow; n=13). RBC lysates from patients with type 1 diabetes (T1D; black; n=5) are the negative control for amylin. Statistical significance of the differences in amylin level was assessed using One-way ANOVA with the Bonferroni post-test for comparing all pairs of columns. *P<0.05, **P <0.01, ***P <0.001, ****P <0.0001. The correlation between RBC amylin and HbA1c in groups of healthy (c) and diseased individuals (d-i) described in (b). Out-of axis amylin-HbA1c levels: 25.2-5.8 and 12.2-4.6 in (d); 16.3-5.5 in (f) and 10.7-5.3 and 13.1-5.1 in (i), respectively. The Spearman nonparametric correlation analysis was performed in GraphPad and the values for the Spearman r and P are indicated on the plots.

Fig. 2. Accumulation of amyloid-forming human amylin in RBCs from diabetic rats. (a) Amylin concentration, measured by ELISA, in matched plasma and lysates of WBCs and RBCs from HIP rats and WT littermates (n=4/group). (b) Representative flow cytometry graphs (upper) and mean intensity (lower) for amylin/Alexa Fluor 488 fluorescence in RBCs from healthy, prediabetic and diabetic HIP rats (n=5 rats/group). (c) Amylin concentration in RBC lysates from 16 months old WT rats (n=7) and healthy

(n=6), prediabetic (n=15) and diabetic (n=16) HIP rats measured by ELISA. (d and e) Representative images of co-staining for amylin and hemoglobin (d) and amylin and glycophorin A (e) in RBCs from age-matched WT and diabetic HIP rats (n=3 rats/group). Scale bar, 10 µm (top row) and 5 µm (midle and bottom rows). (f) Representative STORM images showing RBCS from HIP and WT rats stained for human amylin (red) and Glycophorin A (green). (Scale bar 2µm). (n=3 for each rat group). *P <0.05; **P <0.01 by t-test (a) and One-way ANOVA (b and c).

Fig. 3. Pathophysiological changes induced by amyloid-forming amylin in RBCs. (a) Hemoglobin levels in RBCs from WT, HIP and UCD rats (n=11 rats/group). (b) Oxygen dissociation curve for RBCs from WT, HIP and UCD rats (n=5 rats/group). (c) Representative example of cell shape distribution of RBCs from WT (orange), UCD (blue) and HIP (pink) rats (n=6 rats/group) and the Pearson coefficient of dissymmetry (PCD) calculated from these data. (d) Percentage of RBC hemolysis in hypo-osmotic solutions. The NaCl concentration for 50% hemolysis of WT, HIP and UCD RBCs is indicated in the inset. (n=4 rats/group). (e and f) Representative images of co-staining for amylin and collagen IV (Col IV) in kidney tissue sections showing amylin deposition in arterioles and interstitial tissue (e) and in the glomerulus (f) in diabetic HIP rats but not in diabetic UCD rats (n=3 rats/group). (g) Representative images of co-staining for amylin and ionized calcium binding adaptor molecule 1 (IBA1) in kidney tissue sections from diabetic HIP and diabetic UCD rats (n=3 rats/group). (h) Representative images of staining for the cluster of differentiation 68 (CD68; ED1) in kidney tissue section from diabetic HIP and diabetic UCD rats (n=3 rats/group). (Scale bar 50µm) *P<0.05; **P<0.01 by One-way ANOVA with Tukey's post-test (a and c).

Fig. 4. Modulation of renal hypoxia markers by amylin dyshomeostasis. (a) EPO levels in plasma from 16 months WT rats (n=17), diabetic UCD rats (n=8) and diabetic HIP rats (n=17). (b) Percentage

number of reticulocytes over total numbers of RBCs in blood of WT, HIP and UCD rats (n=3 for each rat group). (c) Hematocrit levels in diabetic HIP and UCD rats and WT controls (n=6 rats/group). (d-h) Protein levels of HIF-1α (d), HIF-2α (e), arginase-1 (f) and arginase-2 (g) and arginase activity (h) measured by ELISA in renal tissues from 16 months old WT rats and diabetic UCD and HIP rats (n=10 rats/group). *P <0.05; **P <0.01; ***P <0.001 by One-way ANOVA with Tukey's post-test.

Fig. 5. Effect of increasing endogenous EETs on RBC-capillary coupling and renal hypoxia signaling. (a) Average numbers of RBCs adhered to cultured vascular endothelial cells when fixed hematocrit of RBCs flowed over cultured EC at constant rate for constant time of 20 minutes (n=3/ group). (b) Analysis of the adhesion of RBCs isolated from HIP rats and WT littermates to cultured vascular endothelial cells (n=8/group). (c) Adhesion of WT rat RBCs to cultured vascular endothelial cells with/without incubation with recombinant human amylin (50 μM) for 2 hours (n=5/group). (d) Attachment of RBCs from WT and diabetic HIP rats to vascular endothelial cells in the absence or in the presence of various amounts of EETs (n=8 rats/group). (e) Representative images of staining for amylin and Col IV in kidney sections from diabetic HIP rats (HIP-UT) and diabetic HIP rats with pharmacologically upregulated EETs (HIP-T). The scatterplot shows the percentage of the tissue area that is positive for amylin (n=3 rats/group). (f-g) Protein levels of HIF-2α (f) and HIF-1α (g) in whole kidney tissue homogenate from rats in the HIP-UT and HIP-T groups (n=4 rats/group). *P <0.05; **P <0.01; ***P <0.001 by t-test.

Fig. 6. Altered oxygen sensing in kidneys following transfusion with amylin-loaded RBCs

(a) Plasma EPO levels in WT rats transfused with RBCs from i) WT rats (n=7); ii) diabetic UCD rats (n=7) and iii) diabetic HIP rats (n=7). (b and c) Protein levels of HIF-1α (b) and HIF-2α (c) in renal tissue homogenate from the rats described in (a). (d) Representative images of amylin and glycophorin A co-

staining (left panel) and of amylin and hemoglobin co-staining (right panel) in RBCs from UCD rats infused with aggregated human amylin (daily injection of 0.08 µg/g body weight for 7 days; n=3 rats/group). (e) Plasma EPO levels in diabetic UCD rats (n=3) at baseline and at the end of the acute intravenous treatment with aggregated human amylin (hA). (f-g) Protein levels of HIF-2α and HIF-1α (f) and arginase-1 and arginase-2 (g) in renal tissue homogenates from diabetic UCD rats injected with human amylin versus non-injected diabetic UCD control rats (n=3 rats/group). (h) Cartoon illustrating the proposed mechanism through which "human" hyperamylinemia exacerbates hypoxia signalingin diabetic rats with pancreatic expression of non-amyloid forming amylin rat amylin (UCD rats). *P <0.05; **P <0.01; ***P <0.001 by One-way ANOVA with Tukey's post-test (a-c) or two-tailed t-test (e-g).

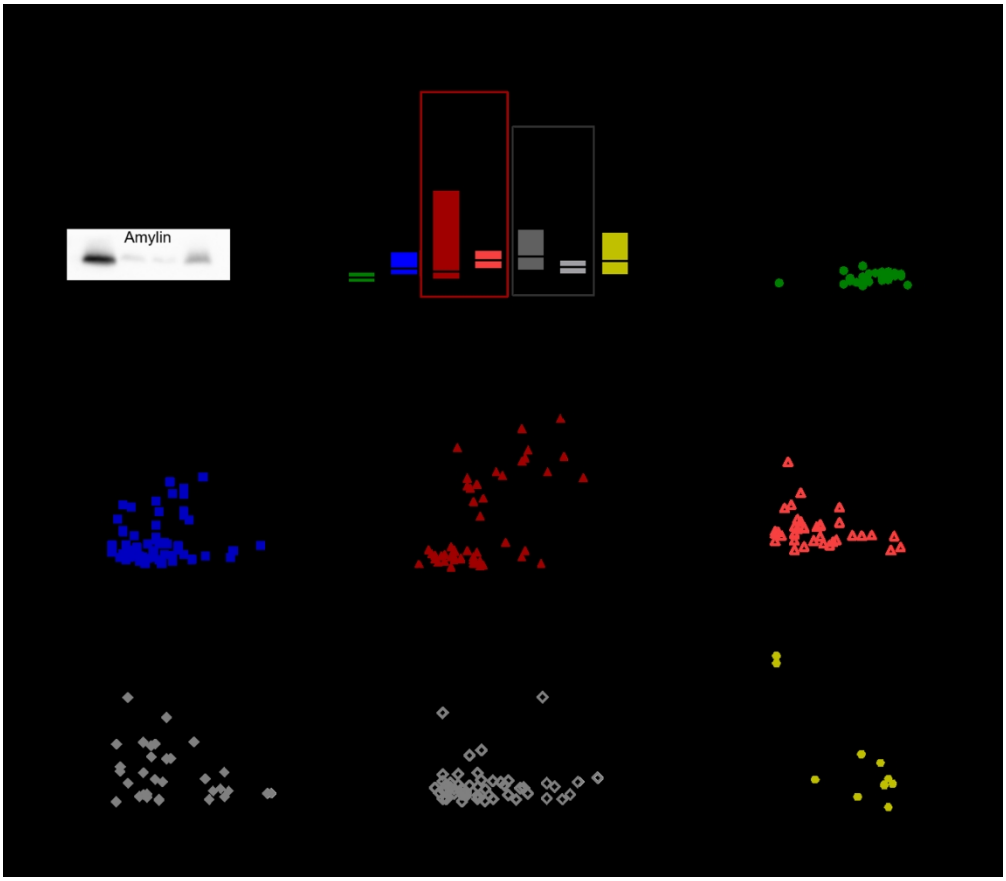

Amylin-coated RBCs in human pathology

225x196mm (300 x 300 DPI)

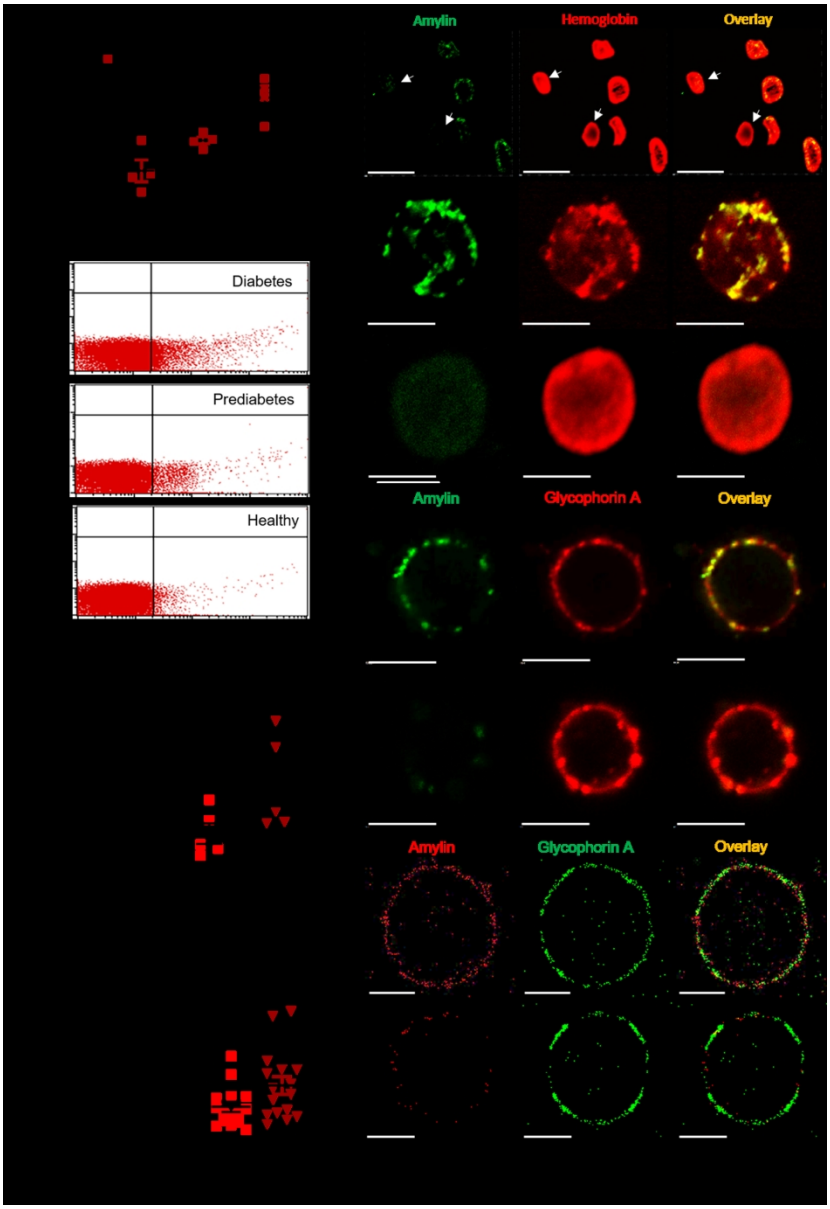

Accumulation of amyloid-forming human amylin in RBCs from diabetic rats

189x275mm (300 x 300 DPI)

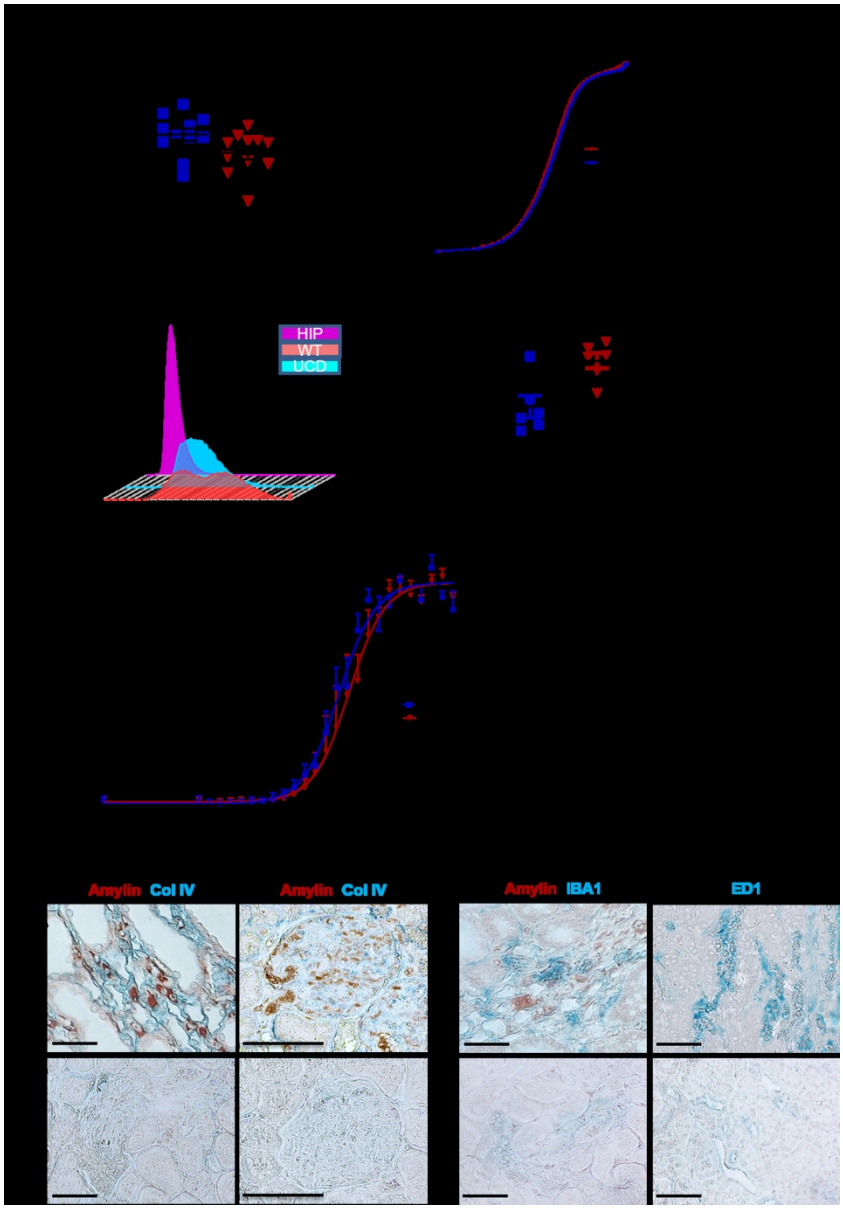

Pathophysiological changes induced by amyloid-forming amylin in RBCs

187x269mm (300 x 300 DPI)

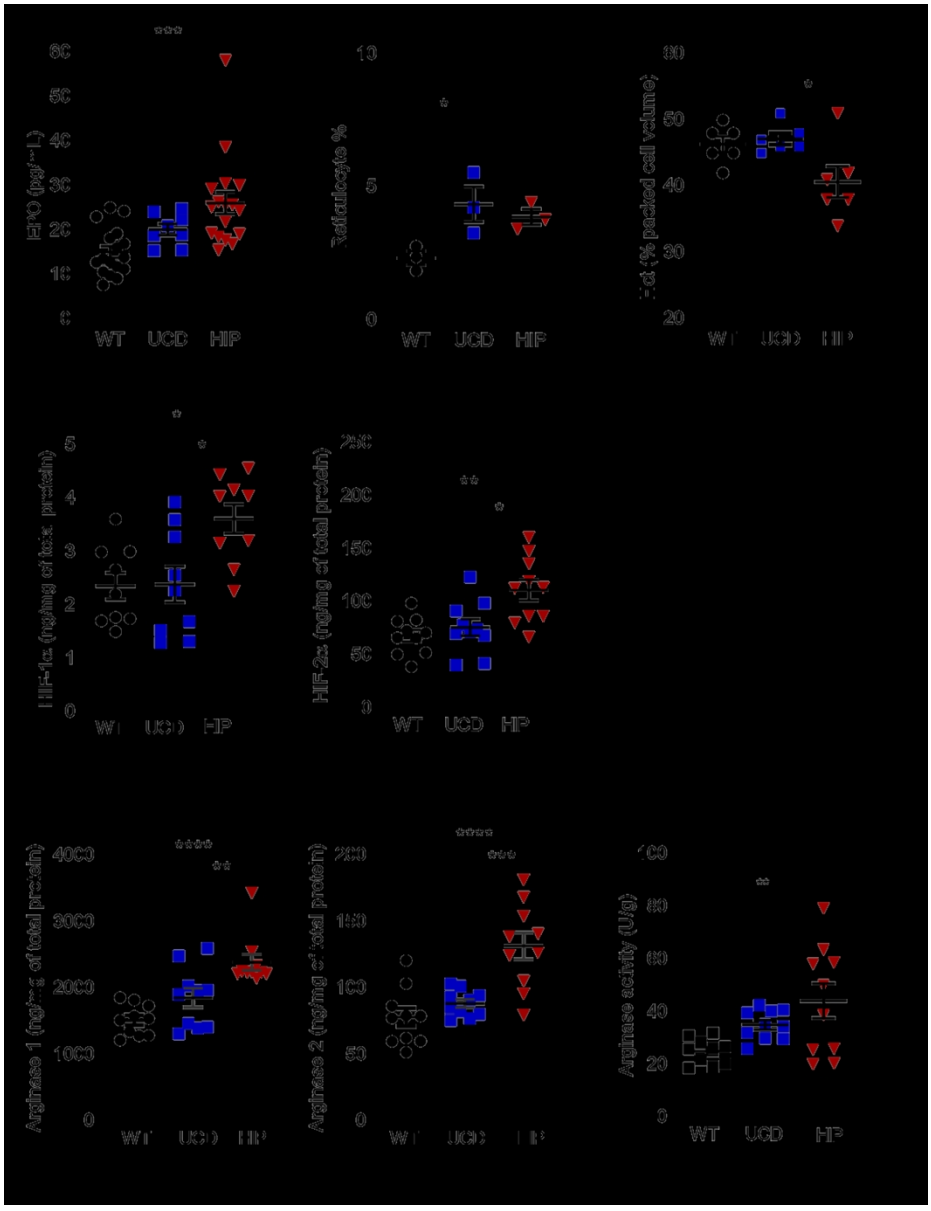

Modulation of renal hypoxia markers by amylin dyshomeostasis

176x228mm (300 x 300 DPI)

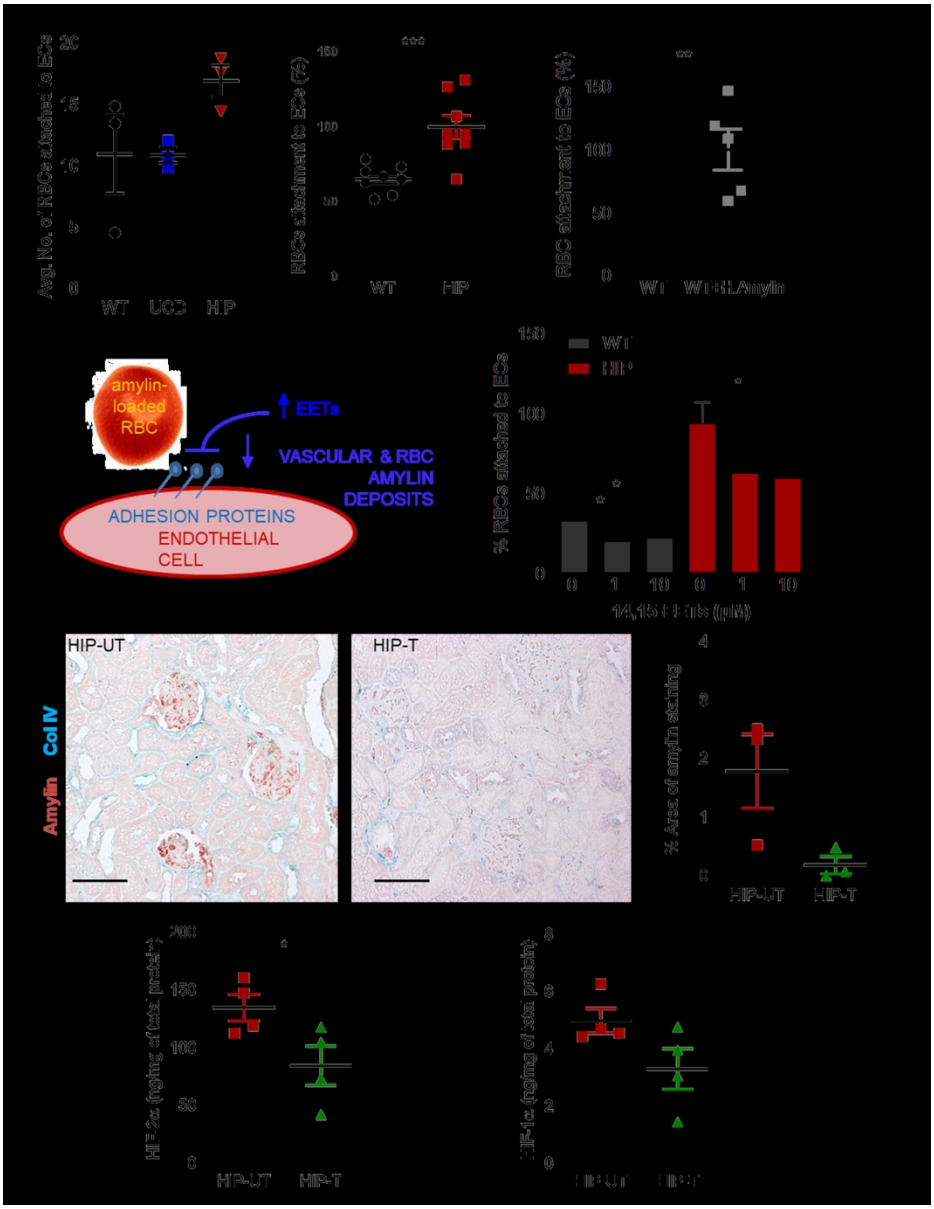

Effect of increasing endogenous EETs on RBC-capillary coupling and renal hypoxia signaling

184x238mm (300 x 300 DPI)

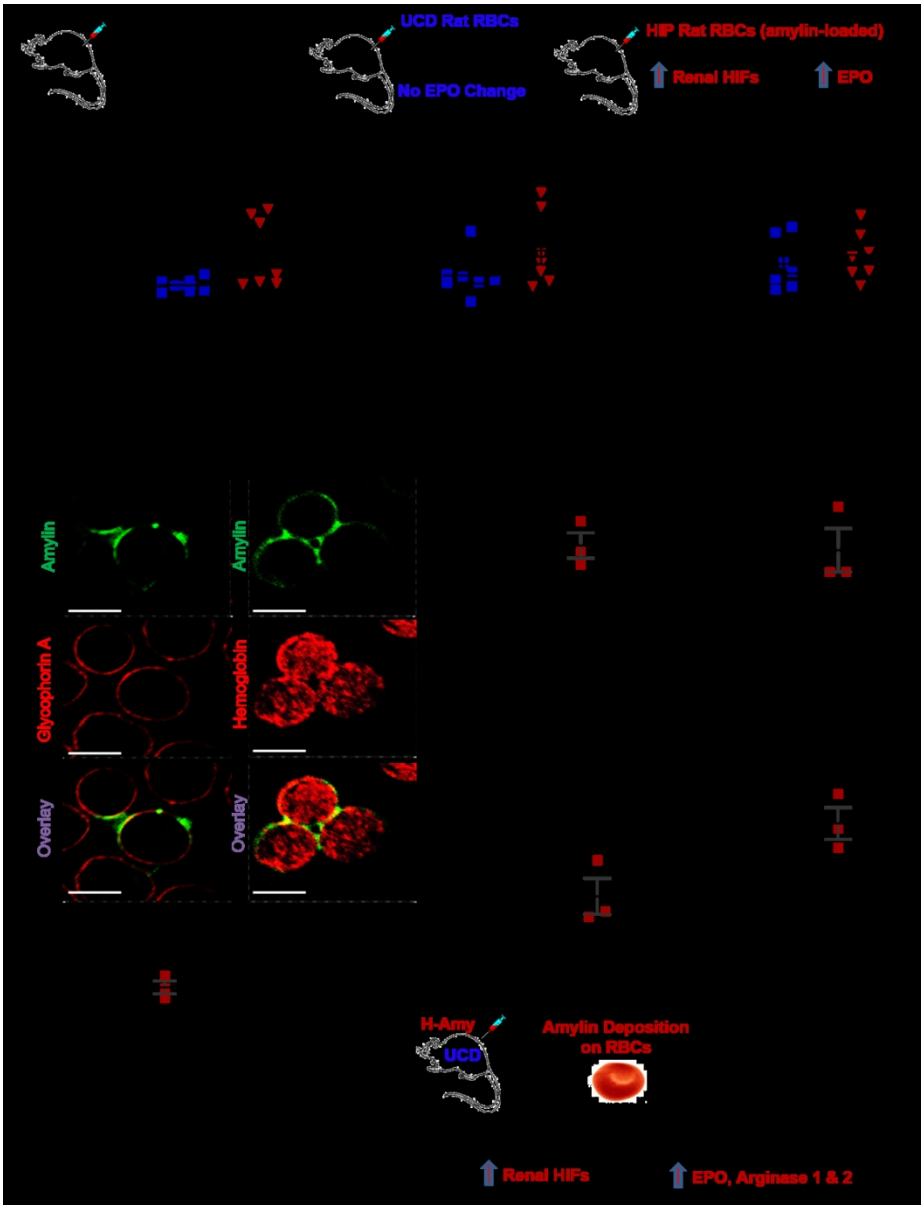

Altered oxygen sensing in kidneys following transfusion with amylin-loaded RBCs

193x252mm (300 x 300 DPI)

Table 1. Characteristics of the individuals providing the RBC samples, including age, sex, body mass index (BMI), diabetes status and co-morbidities.

Sample size	n = 353	
	Disease	**Healthy (n=66)**
Age	55±1 years	43±2 years
Female sex	127(45%)	29(45%)
Obesity (BMI>30)	116(41%)	14(21%)
Heart Failure	108(38%)	
Type-2 Diabetes	69(24%)	
Cancer	91(32%)	
Stroke	13(5%)	
Type-1 Diabetes	5(2%)	

Diabetic Microcirculatory Disturbances and Pathologic Erythropoiesis Provoked by Deposition of Amyloid-Forming Amylin in Red Blood Cells and Capillaries

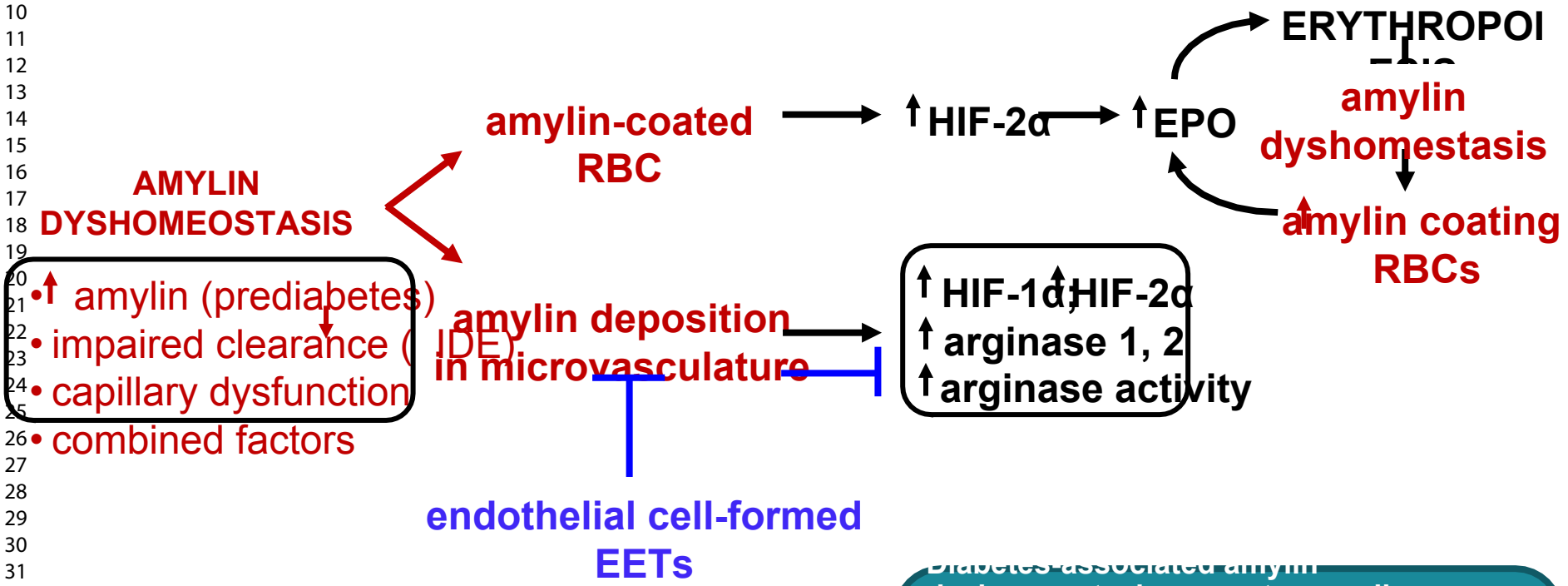

Verma, 2019

CONCLUSION: Diabetes-associated amylin dyshomeostasis promotes amylin deposition in red blood cells (RBCs) and capillaries leading to tissue hypoxic-ischemic injury.

kidney INTERNATIONAL
OFFICIAL JOURNAL OF THE INTERNATIONAL SOCIETY OF NEPHROLOGY
KI REPORTS
KIReports.org

Supplementary Figures

Supplementary Figure S1. (*Left*) Representative western blot analysis of high molecular weight amylin oligomers in plasma, RBC lysate and white blood cell (WBC) lysate from an individual with type-2 diabetes. (*Right*) The Ponceau S staining of the blot show in *Left* panel.

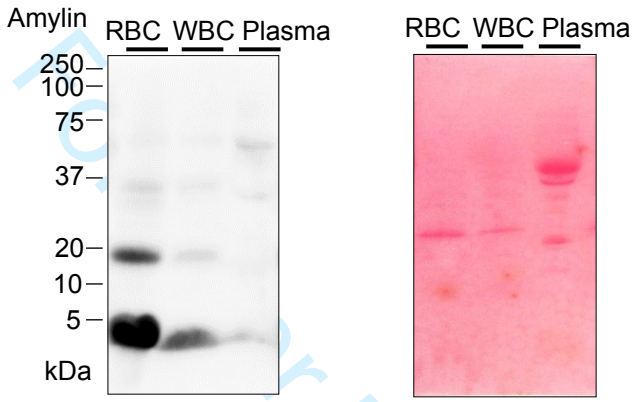

Supplementary Figure S2. Representative images of Thioflavin S (green) and amylin (red) staining in the pancreas from a diabetic HIP and a control WT rat (n=3/group). Scale bar, 30 μm.

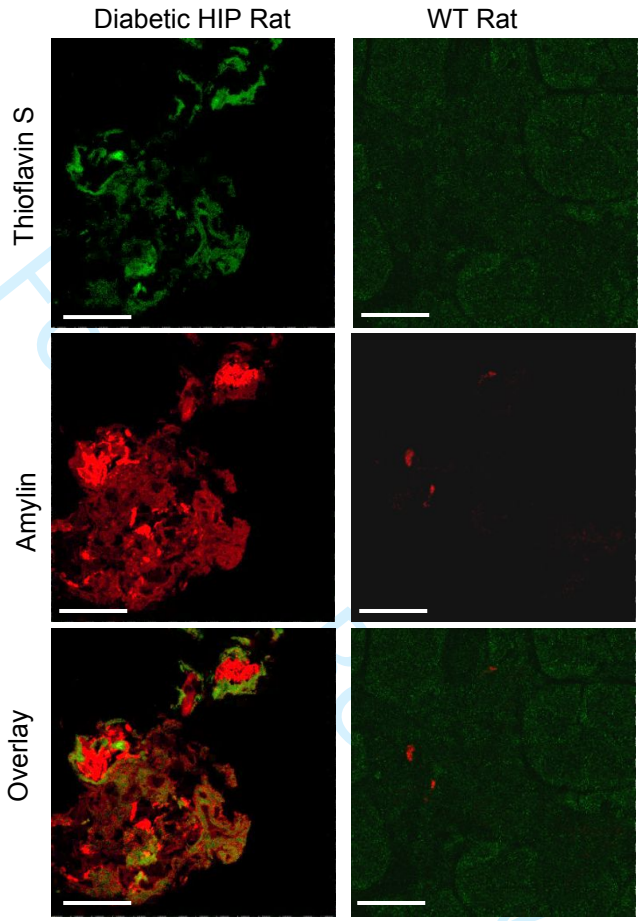

Supplementary Figure S3. Representative TEM images showing RBCs from HIP and WT rats, stained with human amylin primary antibody and gold (10nm) labelled secondary antibody. (Scale bar 1μm)

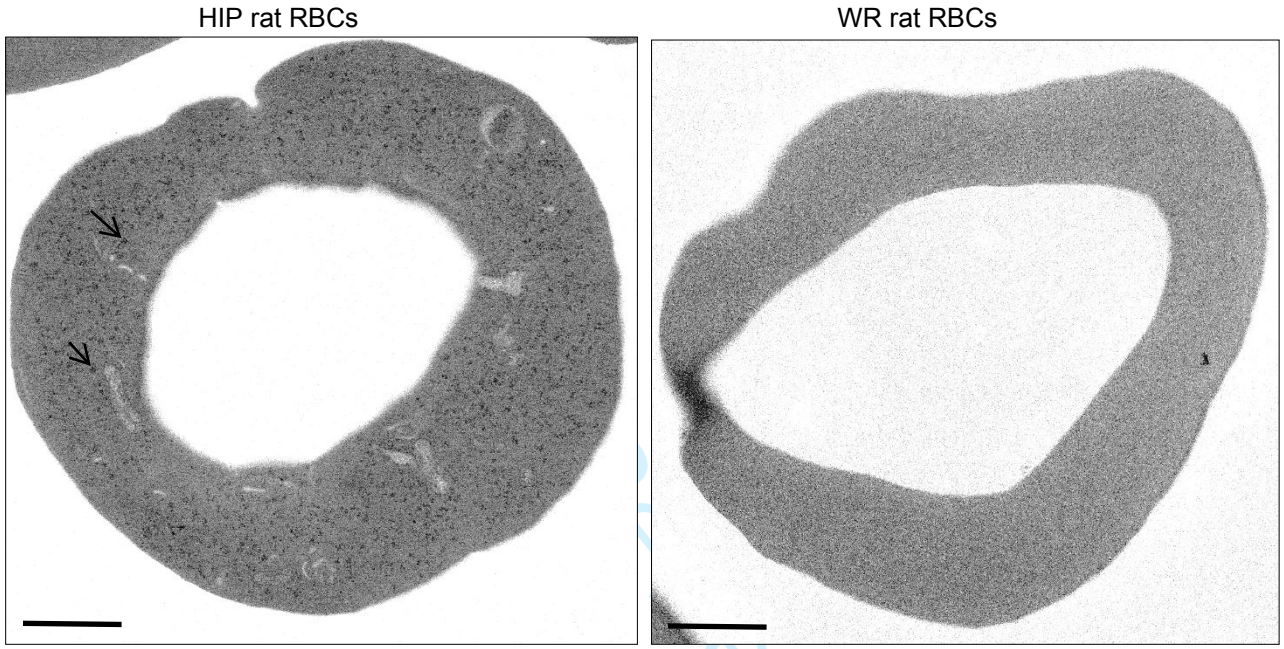

Supplementary Figure S4. PCD for WT rat RBCs and WT rat RBCs incubated ex vivo with oligomerized human amylin (n=5 preparations/group).

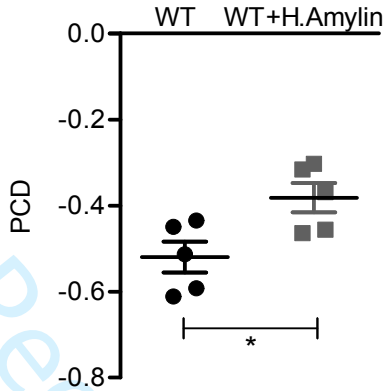

Supplementary Figure S5. Volume of urine excretion (A), albuminuria (B) and creatinine clearance rate (C) in 16 months old WT, diabetic UCD and diabetic HIP rats (n=6 rats/group). ** $P \leq 0.01$; *** $P \leq 0.001$ by One-way ANOVA.

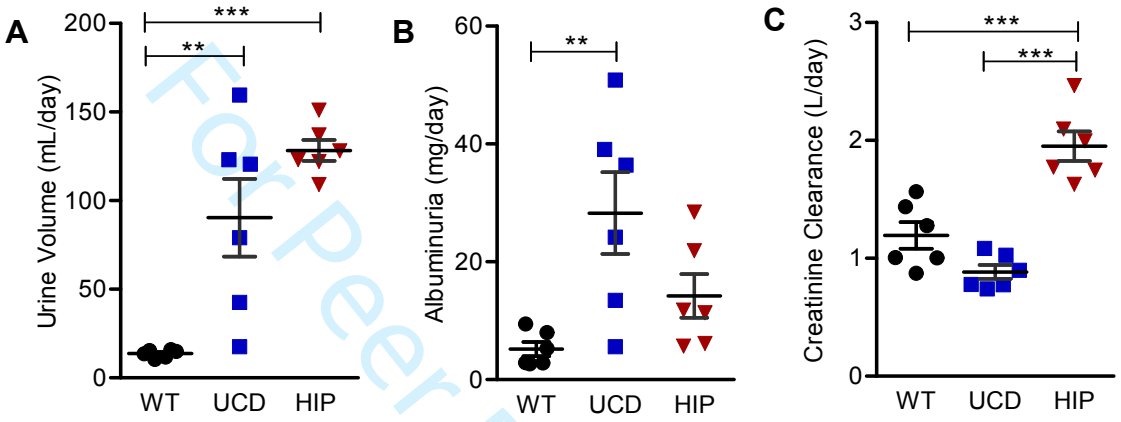

Supplementary Figure S6. Gross spleen weights of 16 months old WT rats and diabetic HIP rats (n=10 spleens/group). Data are means ± SEM. **P* <0.05

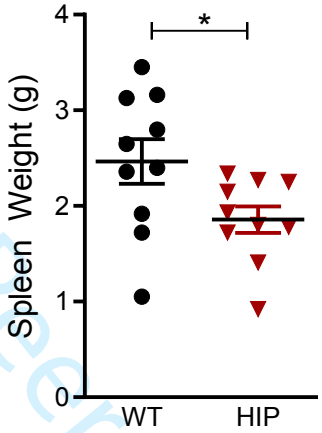

Supplementary Figure S7. Levels of von Hippel-Lindau (vHL) protein in the renal tissues from 16 months old WT rats and diabetic HIP rats (n=5 rats/group). Data are means ± SEM.

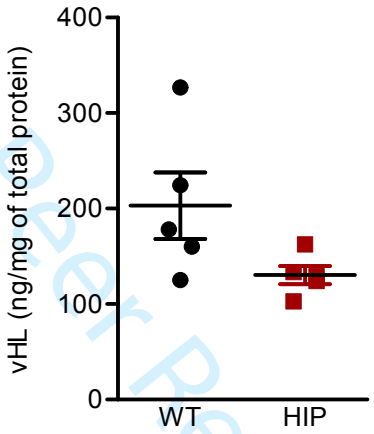

Supplementary Figure S8. Western blot and ELISA analyses for VCAM-1 expression in kidney capillaries lysates of WT and HIP rats (n= 3 rats/group).

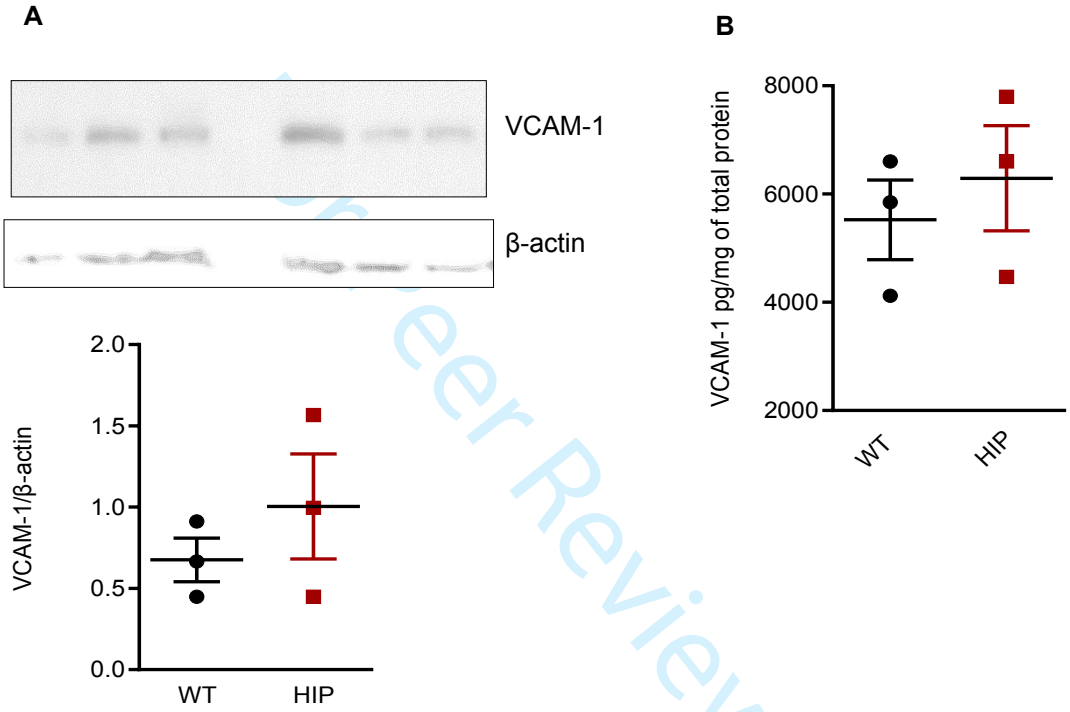

Supplementary Figure S9. Reduced amylin deposition in kidneys correlated with partially reduced imbalance of arginase expression and arginase activation in HIP rat kidney tissues. (n=4 rats/group). Data are means ± SEM. *P <0.05

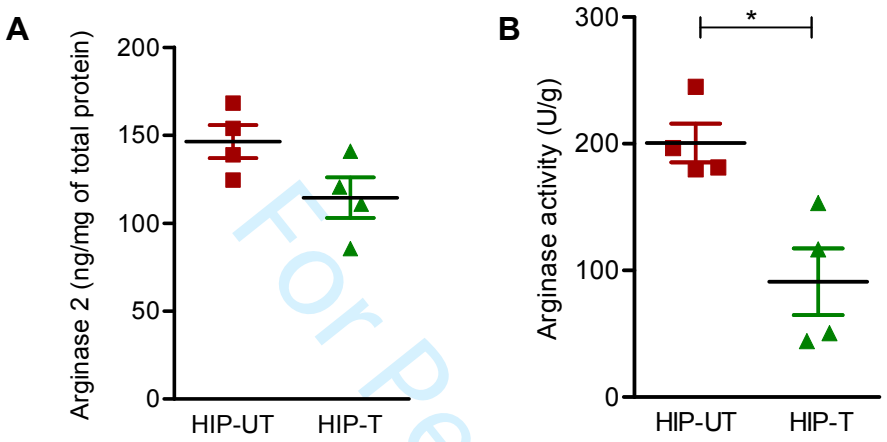

Supplementary Figures

Supplementary Figure S1. (*Left*) Representative western blot analysis of high molecular weight amylin oligomers in plasma, RBC lysate and white blood cell (WBC) lysate from an individual with type-2 diabetes. (*Right*) The Ponceau S staining of the blot show in *Left* panel.

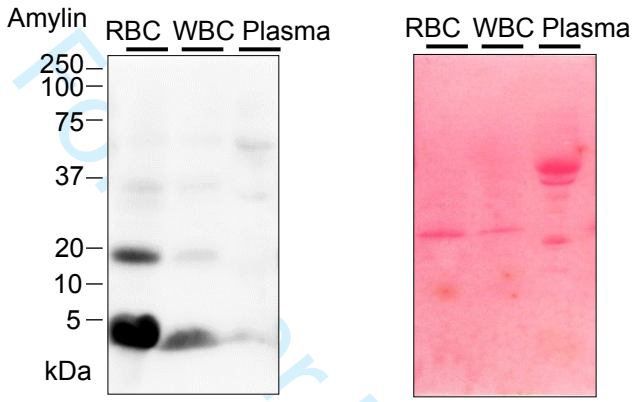

Supplementary Figure S2. Representative images of Thioflavin S (green) and amylin (red) staining in the pancreas from a diabetic HIP and a control WT rat (n=3/group). Scale bar, 30 μm.

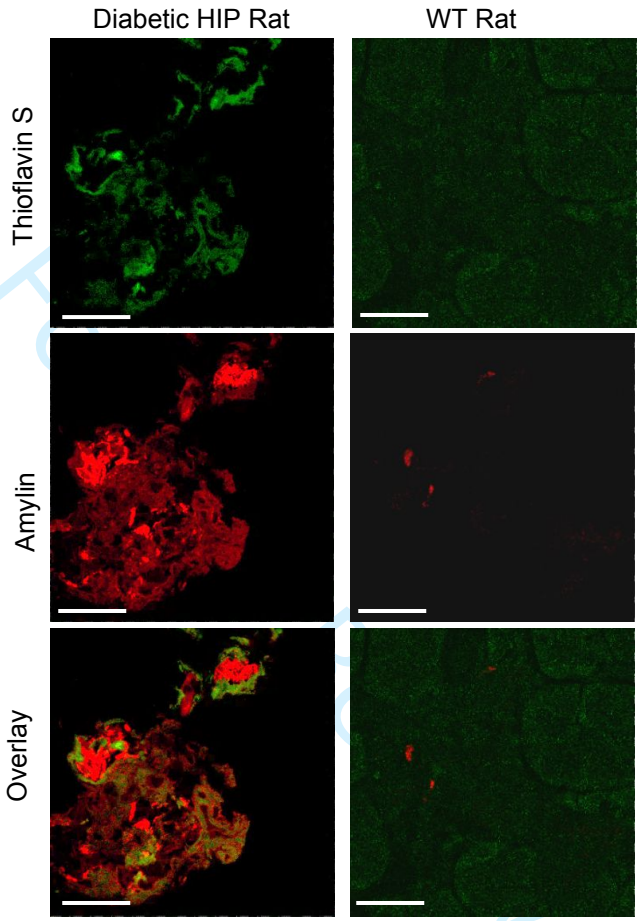

Supplementary Figure S3. Representative TEM images showing RBCs from HIP and WT rats, stained with human amylin primary antibody and gold (10nm) labelled secondary antibody. (Scale bar 1μm)

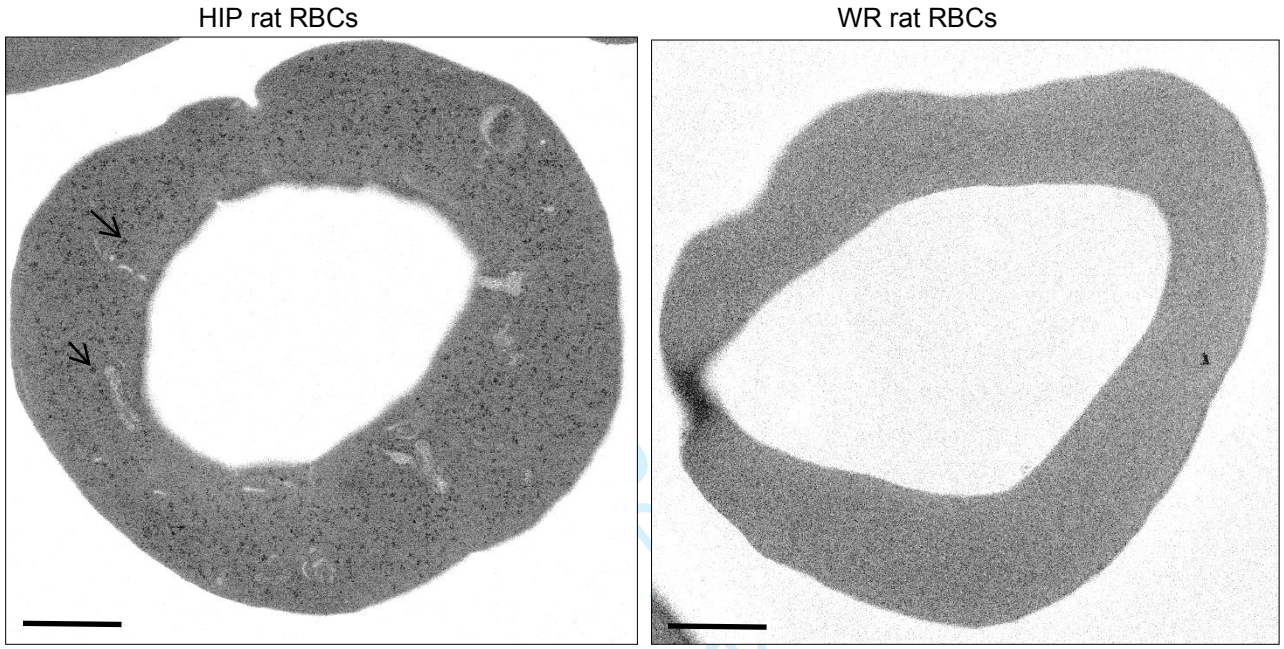

Supplementary Figure S4. PCD for WT rat RBCs and WT rat RBCs incubated ex vivo with oligomerized human amylin (n=5 preparations/group).

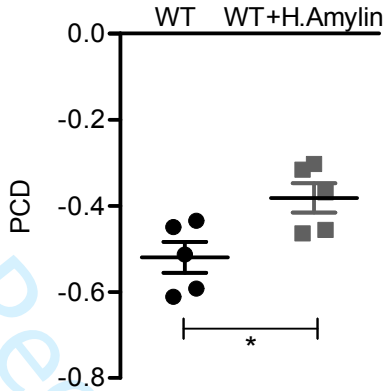

Supplementary Figure S5. Volume of urine excretion (A), albuminuria (B) and creatinine clearance rate (C) in 16 months old WT, diabetic UCD and diabetic HIP rats (n=6 rats/group). $^{**}P \leq 0.01$; $^{***}P \leq 0.001$ by One-way ANOVA.

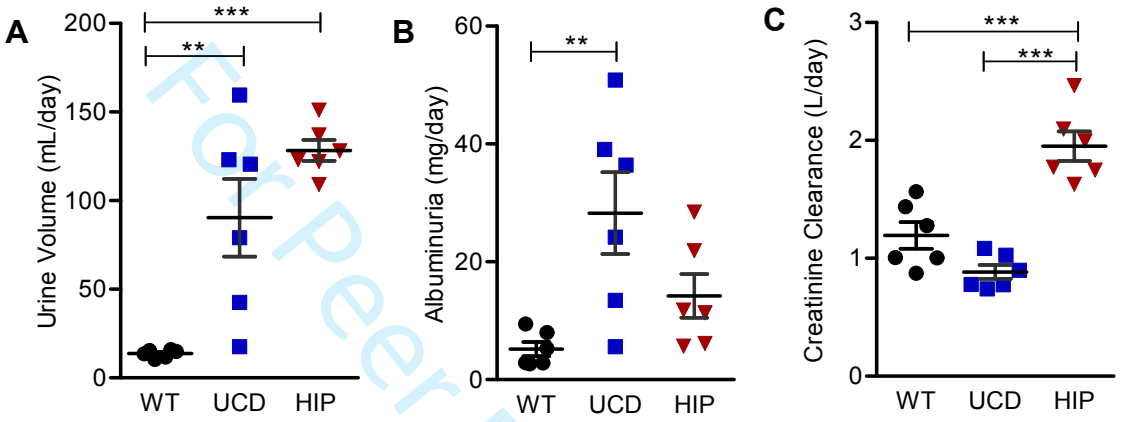

Supplementary Figure S6. Gross spleen weights of 16 months old WT rats and diabetic HIP rats (n=10 spleens/group). Data are means ± SEM. *P <0.05

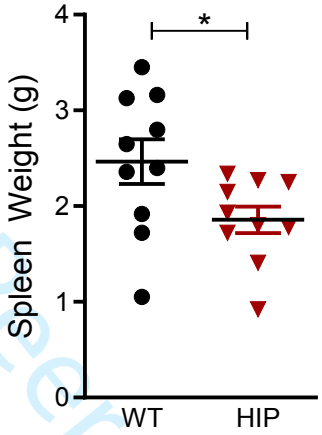

Supplementary Figure S7. Levels of von Hippel-Lindau (vHL) protein in the renal tissues from 16 months old WT rats and diabetic HIP rats (n=5 rats/group). Data are means ± SEM.

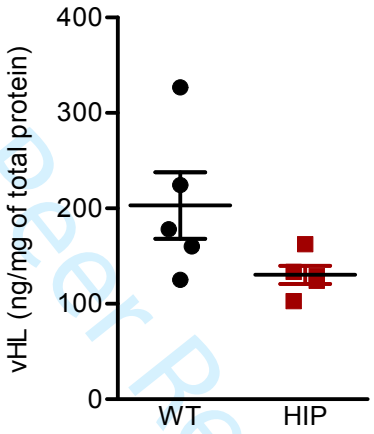

Supplementary Figure S8. Western blot and ELISA analyses for VCAM-1 expression in kidney capillaries lysates of WT and HIP rats (n= 3 rats/group).

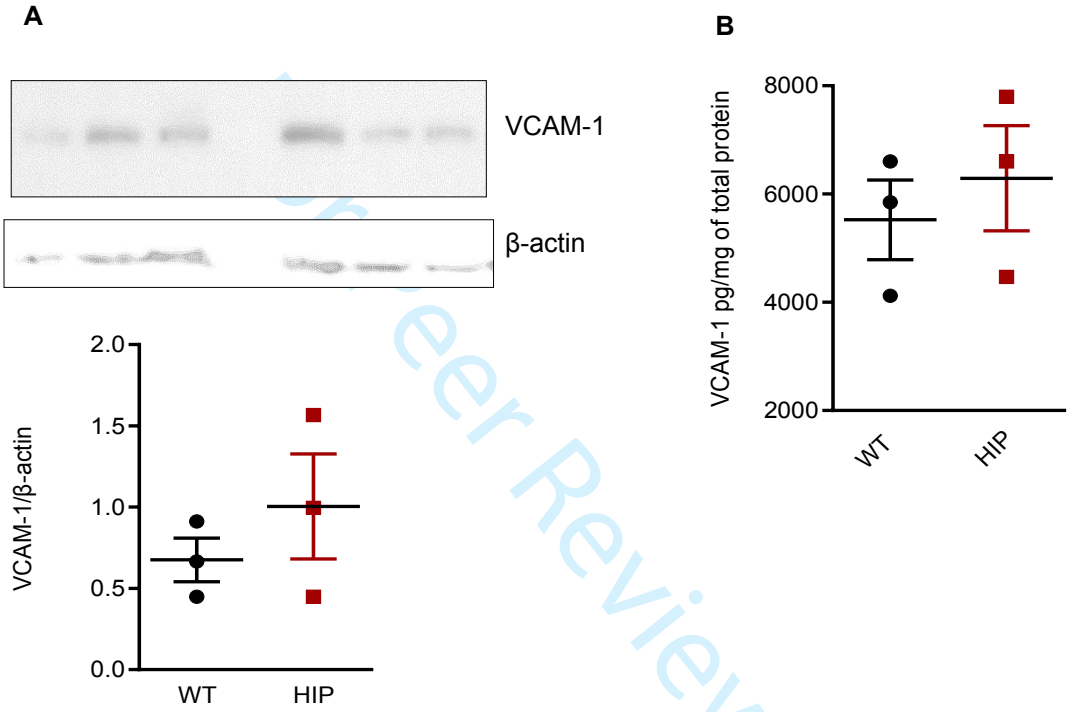

Supplementary Figure S9. Reduced amylin deposition in kidneys correlated with partially reduced imbalance of arginase expression and arginase activation in HIP rat kidney tissues. (n=4 rats/group). Data are means ± SEM. *P <0.05

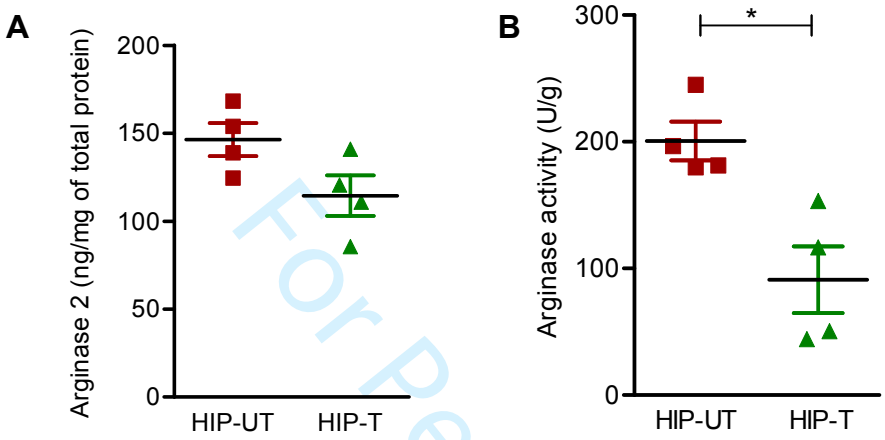

Supplemental Methods

Human studies

This research employed de-identified blood specimens matched with medical record data obtained from the biobank of the Center for Clinical and Translational Science at University of Kentucky (UK-CCTS). Sample collection and storage was approved by the Institutional Review Board at the University of Kentucky. Written informed consent was received from each individual prior to donating the blood sample. Specimens from transplant recipients (less than 6 months from the transplant), patients with liver disease, patients with HIV and pregnant or lactating women, which may affect the pancreatic secretion of amylin, were excluded from the study. RBCs from patients with type-2 diabetes were the amylin positive control, whereas patients with over 15 years of type-1 diabetes (and, therefore, depleted β-cell mass) but otherwise healthy served as the negative control for amylin. The latter samples were collected under a different IRB-approved protocol and de-identified.

RBC specimens were divided into groups based on the primary diagnosis of heart failure, cancer or stroke. Most individuals in the disease group had type-2 diabetes as the second diagnosis. Diabetes status, co-morbidities and characteristics of the individuals providing the blood samples, such as age, sex and body mass index (BMI) are summarized in Table 1. The control group represents individuals without diabetes, heart failure, stroke or cancer.

Statistics and defining and handling of outliers for the human study

The Spearman nonparametric correlation analysis was used to examine the relationship between RBC amylin levels and HbA1c (Fig 1c-i), respectively, in healthy individuals and disease groups. We computed the Whisker plot (Fig 1b) from amylin levels in human RBC across different groups.

In each group, the median, first and third quartiles were calculated. The interquartile range was calculated by subtracting the lower quartile value from the upper quartile value. Points falling more than 1.5 times the interquartile range above the third quartile were considered outliers. The outliers were indicated in the caption of Figure 1 and included in statistical analyses. One-way ANOVA with the Bonferroni post-test was used to compare amylin levels in the 8 groups. All analyses were performed using GraphPad Prism 5.0 software.

Hemoglobin A1c (HbA1c) measurement

Hemoglobin A1c or HbA1c levels were measured in human blood samples by A1CNow^{+} kit (Polymer Technology Systems,Inc. IN, USA) as per manufacturer's protocol provided with the kit..

Animal studies

Experimental Animals

All animal experiments were approved by the Institutional Animal Care and Use Committee at University of Kentucky and conforms to the Guide for the Care and Use of Laboratory Animals, the 8th Edition, published by the National Academies Press, Washington (DC); 2011. We compared rats that develop type-2 diabetes (T2D) linked to expression of human amylin in the pancreas (HIP rats; n=65) with rats that develop T2D in the absence of amyloid, as they express solely the non-amyloid forming rat amylin (UCD rats; n=40) and control, non-diabetic rats (WT rats; n=53). Only males were used because HIP females become diabetic at a more advanced age. [S1,S2]

HIP rats are Sprague-Dawley (SD) rats that overexpress (3-fold) human amylin specifically in the pancreatic β-cells on the insulin II promoter.[S1] HIP rats develop amylin dyshomeostasis and amylin amyloid deposition in pancreatic islets leading to β-cell apoptosis and hyperglycemia with

regular diet. Breeding pairs were obtained from Charles River Laboratory. The presence of the human amylin gene was confirmed by genotyping using the following primers:

Rip1: 5'- GTC ATG TGC ACC TAA AGG GGC AAG TAA TTC A-3'

Rip2: 5'- CGA GTG GGC TAT GGG TTT GT -3'

Mus-a-actinF1: 5'-CAC CAC ACC TTC TAC AAT GAG CTG-3'

Mus-a-actinR1: 5'-TCA TCA GGT AGT CAG TGA GGT CGC -3'

Actin was used as the internal control. WT littermates were used as the non-diabetic control.

UCD rats were generated as described in Ref *3* by crossing obese Sprague-Dawley rats with Zucker diabetic fatty (ZDF) lean rats. ZDF-lean founder rats were purchased from Charles River Laboratories. These rats have functional leptin receptors and the autosomal recessive β-cell defect.[S3] The breeding strategy was to maintain the obese phenotype from obese Sprague-Dawley rats and selecting for individuals homozygous for the autosomal recessive β-cell defect. In the seventh generation (F7) all animals were homozygous for the β-cell defect and increased genetic propensity to develop diabetes.

Rats were housed (singly) in individually ventilated cages (ACE, Allentown, NJ, USA) with Sani-Chip bedding (Harlan-Teklad) and maintained on a standard chow diet (Teklad Global 18% Protein Rodent Diet #2018, VA, USA) and reverse osmosis drinking water for the duration of the study. Nesting material (Enviro-Dri®, Shepherd Specialty Papers) and aspen chew blocks (Lomir Biomedical Inc. IL,USA) were provided for environmental enrichment. All animals were maintained on a 12:12 hour light:dark cycle at temperatures between 21-24 °C.

Treatment

We performed a retrospective analysis of kidney tissue from HIP rats with pharmacologically elevated EETs used in a prior study.[S4] Briefly, pre-diabetic male HIP rats were randomized to treatment (HIP-T) and no treatment (HIP-UT) groups by a blinded observer. To increase the endogenous levels of EETs, pre-diabetic HIP rats were treated with a soluble epoxide hydrolase inhibitor APAU (UC1153) added in drinking water for 10 weeks. APAU was formulated in polypropylene glycol at a concentration of 10 mg/mL with 30 minutes sonication. The APAU aliquot was added to the drinking water at a final content of 1%.

Renal function analysis

Rats were placed in metabolic cages. After 2 days of acclimation, 24-hours cycle urine collections were taken at baseline and day 2. Blood sampling (500 µl) was obtained from tail vein for determination of creatinine level. Creatinine concentration in plasma and urine was measured using the kinetic Jaffé method[S5] with 10% picric acid solution in NaOH. After 15 min, absorbance reading was obtained in a microplate set for dual wavelengths at 490 nm (read) and 620 nm (reference). Creatinine clearance (Ccr) was calculated using the following formula: Ccr (ml/min) = (urine creatinine/plasma creatinine) × urine flow rate. Urinary excretion rate of albumin was measured using a commercially available ELISA kit (E110-125, Bethil Laboratories, Inc, TX).

Tissue extraction and red blood cell (RBC) isolation

For measurements of hypoxia markers (HIF-1α, HIF-2α, Arginase 1, Arginase 2 and vHL) by ELISA and arginase activity assay, tissues were extracted in 1xPBS with 1% (v/v) protease and phosphatase inhibitors. The homogenate was frozen at -80°C and thawed on ice for 3 consecutive cycles to break cell membranes. For other biochemical assays, tissues were extracted in homogenization buffer (150 mM NaCl, 50 mM Tris, 50 mM NaF, 2% Triton X-100, 0.1% SDS

and 1% (v/v) protease and phosphatase inhibitors). All homogenates were then centrifuged at 17,000 xg for 30 minutes at 4°C.

Rat blood samples were collected into sterile K2-EDTA vacutainer tubes. RBCs were isolated from plasma by centrifugation at 1,000 xg for 10 minutes, at 4°C, immediately after blood collection. To obtain RBCs lysates for biochemical analyses, RBCs were incubated with cell lysate buffer (10% NP-40, 150 mM NaCl, 10 mM Tris, 2 mM EGTA and 50 mM NaF, 1% (v/v) protease and phosphatase inhibitors) for 30 minutes on the rotor at 4°C, followed by centrifugation at 17000 xg for 30 minutes at 4°C. Supernatant was used for experiments.

RBC transfusion

RBCs were isolated into a heparin lithium tube, washed twice with sterile 1xPBS, combined with storage solution (150 mM HCl, 45 mM dextrose, 45.5 mM mannitol, and 2.2 mM adenine) in a 3:1 v/v ratio, transferred to sterile tubes and stored at 4°C in the dark before injection. Rats received 300 µL of pre-warmed (at 37° C) RBCs solution once daily for 7 days via tail vein injection.

Hematocrit measurements

The ratio of RBCs to total blood volume (hematocrit; Hct) was measured with an i-SATA analyzer (VetScan i-STAT 1 Handheld Analyzer, ABAXIS, CA, USA) using i-STAT CG8+ cartridges (VetScan i-SATA CG8+ cartridge, Cat# 600-9001-25, ABAXIS) according to the manufacturer's protocol.

Hemoglobin measurements

Isolated RBCs were first suspended to a hematocrit 2.5% in Hank's Balanced Salt Solution (HBSS) containing 0.5% BSA (HBSS/A). 10 µL of RBCs suspension was further diluted in 990 µL

HBSS/A and 100 µL of this RBCs dilution was incubated with 200 µL 0.5% SDS for 5 hours. Total hemoglobin in the 100 µL RBCs diluted suspension was calculated from the optical density (at 540 nm) measured with a spectrophotometer (Molecular Devices, Menlo Park, CA, USA).

Assessment of RBC shape and amylin deposition on RBCs by flow cytometry

RBCs ($1x10^7$ cells) were aliquoted to assay tubes, washed twice with 2 mL incubation buffer (0.5 % BSA in PBS), and resuspended in 100 µL incubation buffer. RBCs were incubated with an anti-amylin antibody (1:200, T-4157, Bachem-Peninsula Laboratories, CA, USA) for 1 hour on ice, washed twice with PBS by centrifugation at 1000 xg for 1 minute and then incubated with goat anti-rabbit Alexa Fluor® 488 (A11029, Invitrogen, MA, USA) for 30 min on ice. RBCs were then washed twice before re-suspension in 200 µl PBS, and analyzed by flow cytometer (Becton Dickinson LSRII) within 90 min. To assess the cell shape, RBCs were first gated on a forward scatter (FSC)/side scatter (SSC) plot. The R1 events are visualized using a FSC-A/FSC-H dot plot. For detecting amylin deposited on RBCs, the cells were first gated on a forward scatter (FSC)/side scatter (SSC) plot. RBCs were further gated to determine the amylin signal (Alexa 488), using negative control (no antibody) and positive control to set the upper and lower boundaries.

RBC adhesion assay

Adult rat microvascular endothelial cells (RA-6024, Cell Biologics, IL, USA) were cultured on 96-wells cell culture plate coated with cell attachment factor solution (123-100, Sigma, MO, USA). Cells were allowed to attach for 24 hours and used for experiments when they reached 70%-90% confluency. Isolated RBCs were washed twice with cold HBSS and once with HBSS/A. RBCs

were suspended to hematocrit 2.5% in HBSS/A. 10µL of RBCs suspension was used to measure the hemoglobin content as described above. Another 300µL of RBC suspension aliquot (hematocrit 2.5% in HBSS/A) was gently layered on confluent endothelial cells pre-incubated with 150 µL of media containing different concentrations of (±)14(15)-EET (50651, Cayman Chemical, MI). The plate was incubated at 37° C for 40 min. An additional 83 µL of HBSS/A was gently added to create a slight convex meniscus over each well, and the plate was covered with an adhesive plastic film (89087-692, VWR, IL, USA). The plate was then inverted and allowed to sit for an additional 30 min at 37° C. With the plate maintained in the inverted position, the adhesive sheet was removed and the remaining fluid was removed by aspiration. 200 µL 0.5% SDS was added to each well, followed by 5 hours incubation at room temperature. The amount of hemoglobin in each well was measured from the optical density (OD) as described above. Adherence was calculated as the percentage of OD of adhered hemoglobin/ (OD of total hemoglobin x dilution factor).

RBC adherence assay in flow condition

Freshly isolated red blood cells were diluted to 0.5 hematocrit in saline solution and passed at a fixed rate for 20 minutes over endothelial cells plated on a coverslip in recording and imaging chamber (ALA scientific instruments). The coverslip was then mounted over a glass slide and the number of RBCs attached to endothelial cells was counted under light microscope at 10 different places on coverslip.

Immunofluorescence

Isolated RBCs were washed 3 times with 1xPBS, blocked with 10% goat serum for 15 minutes at 37^{o} C, incubated with primary antibodies against human amylin (1:200, T-4157, Bachem-Peninsula Laboratories) and Glycophorin A (1:100, sc-71159, Santa Cruz Biotechnology, TX,

USA) for 15 min at 37° C, followed by incubation with anti-mouse IgG and anti-rabbit IgG secondary antibodies for 15 min at 37° C. Cells were hemolyzed in 1% saponin in PBS, centrifuged at 8000g for 5 min and the pellet was re-suspended in 1xPBS for microscopy. Images were obtained on a Nikon A1R confocal microscope (Nikon, NY, USA).

For hemoglobin staining, blood smears on glass slide were fixed in acetone/ethanol/methanol (6:2:2) for 20 minutes at RT. Smears were air-dried and re-hydrated in 1xPBS for 5 minutes, rinsed briefly in distilled water, and incubated with pre warmed (37°C) trypsin solution (0.1% in calcium chloride 0.1% pH 7.8) for 15 minutes in humidity chamber. Next, smears were washed in PBS for 5 minutes with gentle agitation, rinsed in distilled water and air dried. Smears were then incubated at 37°C with primary antibodies against hemoglobin (1:100, ab92492, Abcam, MA, USA) and human amylin (1:100, SC-377530, Santa Cruz Biotech, TX, USA) in humidity chamber for 30-40 minutes. They were next washed, air-dried and covered with anti-mouse IgG and anti-rabbit IgG secondary antibodies for 20-30 minutes at 37°C. After incubation smears were washed with PBS, rinsed in water, air dried and mounted in mounting media. Thin sections of paraffin embedded pancreatic tissues were co-stained with Thioflavin S and an anti-amylin antibody.

Enzyme-linked immunosorbent assay (ELISA)

ELISA assays for human amylin (EZHA-52K, Millipore, MA; EIA-AMY-5, Raybiotech, GA, USA), erythropoietin (EPO; 442807, Biolegend, CA, USA), hypoxia-inducible transcription factor 1α (HIF1-α; MBS764727, MyBioSource, CA, USA), hypoxia-inducible transcription factor 2α (HIF2-α; MBS2601406, MyBioSource), arginase 1 (MBS289817, MyBioSource), arginase 2 (MBS7216305, MyBioSource), von Hippel-Lindau (vHL; MBS288882, MyBioSource) and

VCAM-1 (LS-F24285, LifeSpan BioSciences, Inc, WA, USA) were performed according to the manufacturer's protocols..

Arginase activity assay

Arginase activity was measured in kidney homogenates using a colorimetric assay (MAK112, Sigma, MO, USA). To eliminate urine from kidney samples, 300µL of kidney homogenate were filtered through a 10kD spin column (88513, ThermoFisher, MA, USA) with centrifugation at 15000g for 60 min, 4°C. Collected remnant was used for experiments. Assay was performed according to the manufacturer's protocol. Briefly, filtered kidney samples were incubated with reaction substrate mix for 2 hours at 37° C. The stop solution was applied, followed by incubation at 37° C for 35 min. Absorbance reading was taken at 430 nm. Arginase activity was calculated based on manufacturer's analysis instruction.

Isolation of kidney capillaries

Kidney capillaries were isolated by using the protocol used for the isolation of brain capillaries as describes previously[S2]. Briefly, kidneys were homogenized in ice cold cPBS and were mixed with 30% Ficoll solution by gently inverting tubes and then centrifuged 5800g for 20 minutes at 4°C. Pellets were re-suspended in ice cold cPBS with 1%BSA and were passed through the glass beads column. Beads were agitated in cPBS with 1%PBS using 25mL pipette and solutions were taken equally in two 50mL tubes. Tubes were centrifuged and pellets were dissolved in 0.5 to 1mL cPBS and used for experiment.

Immunoblot

Western blot analysis was performed on plasma, WBC lysates, and RBC lysates from humans using a primary antibody against amylin (1:2,000, T-4157, Bachem-Peninsula Laboratories).

Western blot analysis for VCAM-1 (1:1000, ab134047, Abcam) was done on kidney capillary lysates from WT and HIP rats

Immunohistochemistry

Immunohistochemical staining was performed on rat kidney slices using antibodies against amylin (1:200, SC-377530, Santa Cruz), collagen IV (1:1000, ab6586, Abcam), IBA-1(1:200, 019-19741, Wako, VA, USA), and EDI (1:100, MCA341GA, Biorad, PA, USA). Biotinylated anti-mouse (1:400, BA2000, Vector lab, CA, USA), AP conjugated anti-mouse and anti-rabbit IgG (1:50, A3562, A3687, Sigma) were the secondary antibodies. The staining area for amylin was analyzed by ImageJ. The imaging area is 1280 x 1024 pixels; 1 pixel^2 is 0.053 μm^2 for 40X objective lens.

Transmission electron microscopy

Fresh red blood cells were fixed in 0.1M Sorensen's phosphate buffer with 4% PFA and 0.2% glutaraldehyde for 1-2 hours. Cells were then washed in 0.1M Sorensen's buffer and blocked in 0.1% sodium borohydride for 15 minutes and incubated in AURION blocking solution (AURION blocking solution, 50-247-65, fisher scientific) for 60 minutes. Cells were washed with incubation buffer and incubated with primary antibody (anti-human amylin; T-4157; Peninsula lab) for 2 hours at RT. Cells were rinsed with incubation buffer and incubated with secondary antibody (anti-Rabbit IgG-10nm Gold; ab27234, Abcam) overnight at 4 ºC. Cells were then washed in PBS and post-fixed in 2% glutaraldehyde for 2 hours. Cells were silver stained using Silver enhancement kit (ab170732, Abcam) and fixed in 0.5% OsO4 in 0.1M Sorensen's buffer for 15 minutes. Cells were embedded in Epoxy resin and thin sections were prepared over nickel grid (T300-Ni, Electron microscopy science) for imaging in Transmission Electron Microscope (FEI Talos F200X, Thermo Scientific).

High resolution Stochastic Optical Reconstruction Microscopy (STORM)

Fresh red blood cells were stained using the same protocol as for immunofluorescence using primary antibodies (anti-human amylin; T-4157; Peninsula lab and anti-glycophorin A; sc-71159Santacuz biotech) and secondary antibodies (rabbit IgG-atto 647 and mouse IgG-atto 488). Cells were kept in STORM imaging buffer {7µl GLOX (oxygen scavenger)+ 70µl of MEA (Cysteamine hydrochloride)+ 620µl of buffer B (Tris-HCL/NaCl)} during imaging on Nikon N-SIM N-STORM (Nikon) microscope.

RBCs osmotic resistance test

The osmotic resistance of RBCs was assessed by measuring hemolysis at various concentrations of NaCl. Solutions with NaCl concentrations between 0 and 9g/L were obtained by mixing normal saline solution (containing 9g/L NaCl) with distilled water in various proportions. 285µl of each solution was placed in an Eppendorf tube. 4µl of RBC lysate was then added to tubes, mixed and incubated at room temperature for 30 min. The tubes were then centrifuged at 600 × g for 5 min. The supernatant was collected and the amount of hemoglobin released was detected by measuring the O.D. at 540 nm. For each sample, the % hemolysis at a given NaCl concentration was calculated assuming that complete hemolysis occurs in distilled water. All samples were run in duplicate.

Oxygen dissociation curve

Fresh heparinized blood was oxygenated by blowing air on its surface in small vessels with swirling for a few seconds. 200µl of buffer (20mM phosphate in isotonic NaCl) was pipetted in a XF96 plate (Agilent Technologies, CA, USA) and 4µl of blood and 4µl of active yeast cell suspension were added to each well. The partial pressure of oxygen was then recorded at different

time points in a Seahorse XF96 Extracellular Flux Analyzer (Agilent Technologies, CA, USA) until 100% oxygen consumption. Percentage saturation was then calculated and oxygen dissociation curve was plotted as described previously[S6].

Reticulocyte count

For reticulocyte counting, 2-3 drops of filtered new methylene blue solution (New methylene blue 1g, sodium citrate 0.6g, sodium chloride 0.7g and distilled water 100ml) mixed with equal amount of blood and incubated at 37ºC for 15 minutes. After gentle mixing, thin smear of blood was prepared in glass slide and air dried. Reticulocytes and RBCs were counted under a light microscope and the percentage of reticulocytes relative to the total number of RBCs was calculated.

Statistical analysis for animal data

Statistical differences between groups were determined using student's t-test, one-way ANOVA or two-way ANOVA, as appropriate. Data are presented as mean ± standard error. Differences between groups were considered significant when $P < 0.05$. All analyses were performed using GraphPad Prism 5.0 software.

Supplemental Methods

Human studies

This research employed de-identified blood specimens matched with medical record data obtained from the biobank of the Center for Clinical and Translational Science at University of Kentucky (UK-CCTS). Sample collection and storage was approved by the Institutional Review Board at the University of Kentucky. Written informed consent was received from each individual prior to donating the blood sample. Specimens from transplant recipients (less than 6 months from the transplant), patients with liver disease, patients with HIV and pregnant or lactating women, which may affect the pancreatic secretion of amylin, were excluded from the study. RBCs from patients with type-2 diabetes were the amylin positive control, whereas patients with over 15 years of type-1 diabetes (and, therefore, depleted β-cell mass) but otherwise healthy served as the negative control for amylin. The latter samples were collected under a different IRB-approved protocol and de-identified.

RBC specimens were divided into groups based on the primary diagnosis of heart failure, cancer or stroke. Most individuals in the disease group had type-2 diabetes as the second diagnosis. Diabetes status, co-morbidities and characteristics of the individuals providing the blood samples, such as age, sex and body mass index (BMI) are summarized in Table 1. The control group represents individuals without diabetes, heart failure, stroke or cancer.

Statistics and defining and handling of outliers for the human study

The Spearman nonparametric correlation analysis was used to examine the relationship between RBC amylin levels and HbA1c (Fig 1c-i), respectively, in healthy individuals and disease groups. We computed the Whisker plot (Fig 1b) from amylin levels in human RBC across

different groups. In each group, the median, first and third quartiles were calculated. The interquartile range was calculated by subtracting the lower quartile value from the upper quartile value. Points falling more than 1.5 times the interquartile range above the third quartile were considered outliers. The outliers were indicated in the caption of Figure 1 and included in statistical analyses. One-way ANOVA with the Bonferroni post-test was used to compare amylin levels in the 8 groups. All analyses were performed using GraphPad Prism 5.0 software.

Hemoglobin A1c (HbA1c) measurement

Hemoglobin A1c or HbA1c levels were measured in human blood samples by A1CNow^{+} kit (Polymer Technology Systems,Inc. IN, USA) as per manufacturer's protocol provided with the kit..

Animal studies

Experimental Animals

All animal experiments were approved by the Institutional Animal Care and Use Committee at University of Kentucky and conforms to the Guide for the Care and Use of Laboratory Animals, the 8th Edition, published by the National Academies Press, Washington (DC); 2011. We compared rats that develop type-2 diabetes (T2D) linked to expression of human amylin in the pancreas (HIP rats; n=65) with rats that develop T2D in the absence of amyloid, as they express solely the non-amyloid forming rat amylin (UCD rats; n=40) and control, non-diabetic rats (WT rats; n=53). Only males were used because HIP females become diabetic at a more advanced age. [S1,S2]

HIP rats are Sprague-Dawley (SD) rats that overexpress (3-fold) human amylin specifically in the pancreatic β-cells on the insulin II promoter.[S1] HIP rats develop amylin

dyshomeostasis and amylin amyloid deposition in pancreatic islets leading to β-cell apoptosis and hyperglycemia with regular diet. Breeding pairs were obtained from Charles River Laboratory. The presence of the human amylin gene was confirmed by genotyping using the following primers:

Rip1: 5'- GTC ATG TGC ACC TAA AGG GGC AAG TAA TTC A-3'

Rip2: 5'- CGA GTG GGC TAT GGG TTT GT -3'

Mus-a-actinF1: 5'-CAC CAC ACC TTC TAC AAT GAG CTG-3'

Mus-a-actinR1: 5'-TCA TCA GGT AGT CAG TGA GGT CGC -3'

Actin was used as the internal control. WT littermates were used as the non-diabetic control.

UCD rats were generated as described in Ref *3* by crossing obese Sprague-Dawley rats with Zucker diabetic fatty (ZDF) lean rats. ZDF-lean founder rats were purchased from Charles River Laboratories. These rats have functional leptin receptors and the autosomal recessive β-cell defect.[S3] The breeding strategy was to maintain the obese phenotype from obese Sprague-Dawley rats and selecting for individuals homozygous for the autosomal recessive β-cell defect. In the seventh generation (F7) all animals were homozygous for the β-cell defect and increased genetic propensity to develop diabetes.

Rats were housed (singly) in individually ventilated cages (ACE, Allentown, NJ, USA) with Sani-Chip bedding (Harlan-Teklad) and maintained on a standard chow diet (Teklad Global 18% Protein Rodent Diet #2018, VA, USA) and reverse osmosis drinking water for the duration of the study. Nesting material (Enviro-Dri®, Shepherd Specialty Papers) and aspen chew blocks (Lomir Biomedical Inc. IL,USA) were provided for environmental enrichment. All animals were maintained on a 12:12 hour light:dark cycle at temperatures between 21-24 ˚C.

Treatment

We performed a retrospective analysis of kidney tissue from HIP rats with pharmacologically elevated EETs used in a prior study.[S4] Briefly, pre-diabetic male HIP rats were randomized to treatment (HIP-T) and no treatment (HIP-UT) groups by a blinded observer. To increase the endogenous levels of EETs, pre-diabetic HIP rats were treated with a soluble epoxide hydrolase inhibitor APAU (UC1153) added in drinking water for 10 weeks. APAU was formulated in polypropylene glycol at a concentration of 10 mg/mL with 30 minutes sonication. The APAU aliquot was added to the drinking water at a final content of 1%.

Renal function analysis

Rats were placed in metabolic cages. After 2 days of acclimation, 24-hours cycle urine collections were taken at baseline and day 2. Blood sampling (500 µl) was obtained from tail vein for determination of creatinine level. Creatinine concentration in plasma and urine was measured using the kinetic Jaffé method[S5] with 10% picric acid solution in NaOH. After 15 min, absorbance reading was obtained in a microplate set for dual wavelengths at 490 nm (read) and 620 nm (reference). Creatinine clearance (Ccr) was calculated using the following formula: Ccr (ml/min) = (urine creatinine/plasma creatinine) × urine flow rate. Urinary excretion rate of albumin was measured using a commercially available ELISA kit (E110-125, Bethil Laboratories, Inc, TX).

Tissue extraction and red blood cell (RBC) isolation

For measurements of hypoxia markers (HIF-1α, HIF-2α, Arginase 1, Arginase 2 and vHL) by ELISA and arginase activity assay, tissues were extracted in 1xPBS with 1% (v/v) protease and phosphatase inhibitors. The homogenate was frozen at -80°C and thawed on ice for 3

consecutive cycles to break cell membranes. For other biochemical assays, tissues were extracted in homogenization buffer (150 mM NaCl, 50 mM Tris, 50 mM NaF, 2% Triton X-100, 0.1% SDS and 1% (v/v) protease and phosphatase inhibitors). All homogenates were then centrifuged at 17,000 xg for 30 minutes at 4°C.

Rat blood samples were collected into sterile K2-EDTA vacutainer tubes. RBCs were isolated from plasma by centrifugation at 1,000 xg for 10 minutes, at 4°C, immediately after blood collection. To obtain RBCs lysates for biochemical analyses, RBCs were incubated with cell lysate buffer (10% NP-40, 150 mM NaCl, 10 mM Tris, 2 mM EGTA and 50 mM NaF, 1% (v/v) protease and phosphatase inhibitors) for 30 minutes on the rotor at 4°C, followed by centrifugation at 17000 xg for 30 minutes at 4°C. Supernatant was used for experiments.

RBC transfusion

RBCs were isolated into a heparin lithium tube, washed twice with sterile 1xPBS, combined with storage solution (150 mM HCl, 45 mM dextrose, 45.5 mM mannitol, and 2.2 mM adenine) in a 3:1 v/v ratio, transferred to sterile tubes and stored at 4°C in the dark before injection. Rats received 300 µL of pre-warmed (at 37° C) RBCs solution once daily for 7 days via tail vein injection.

Hematocrit measurements

The ratio of RBCs to total blood volume (hematocrit; Hct) was measured with an i-SATA analyzer (VetScan i-STAT 1 Handheld Analyzer, ABAXIS, CA, USA) using i-STAT CG8+ cartridges (VetScan i-SATA CG8+ cartridge, Cat# 600-9001-25, ABAXIS) according to the manufacturer's protocol.

Hemoglobin measurements

Isolated RBCs were first suspended to a hematocrit 2.5% in Hank's Balanced Salt Solution (HBSS) containing 0.5% BSA (HBSS/A). 10 µL of RBCs suspension was further diluted in 990 µL HBSS/A and 100 µL of this RBCs dilution was incubated with 200 µL 0.5% SDS for 5 hours. Total hemoglobin in the 100 µL RBCs diluted suspension was calculated from the optical density (at 540 nm) measured with a spectrophotometer (Molecular Devices, Menlo Park, CA, USA).

Assessment of RBC shape and amylin deposition on RBCs by flow cytometry

RBCs ($1x10^7$ cells) were aliquoted to assay tubes, washed twice with 2 mL incubation buffer (0.5 % BSA in PBS), and resuspended in 100 µL incubation buffer. RBCs were incubated with an anti-amylin antibody (1:200, T-4157, Bachem-Peninsula Laboratories, CA, USA) for 1 hour on ice, washed twice with PBS by centrifugation at 1000 xg for 1 minute and then incubated with goat anti-rabbit Alexa Fluor® 488 (A11029, Invitrogen, MA, USA) for 30 min on ice. RBCs were then washed twice before re-suspension in 200 µl PBS, and analyzed by flow cytometer (Becton Dickinson LSRII) within 90 min. To assess the cell shape, RBCs were first gated on a forward scatter (FSC)/side scatter (SSC) plot. The R1 events are visualized using a FSC-A/FSC-H dot plot. For detecting amylin deposited on RBCs, the cells were first gated on a forward scatter (FSC)/side scatter (SSC) plot. RBCs were further gated to determine the amylin signal (Alexa 488), using negative control (no antibody) and positive control to set the upper and lower boundaries.

RBC adhesion assay

Adult rat microvascular endothelial cells (RA-6024, Cell Biologics, IL, USA) were cultured on 96-wells cell culture plate coated with cell attachment factor solution (123-100, Sigma, MO, USA). Cells were allowed to attach for 24 hours and used for experiments when they reached 70%-90% confluency. Isolated RBCs were washed twice with cold HBSS and once with HBSS/A. RBCs were suspended to hematocrit 2.5% in HBSS/A. 10µL of RBCs suspension was used to measure the hemoglobin content as described above. Another 300µL of RBC suspension aliquot (hematocrit 2.5% in HBSS/A) was gently layered on confluent endothelial cells pre-incubated with 150 µL of media containing different concentrations of (±)14(15)-EET (50651, Cayman Chemical, MI). The plate was incubated at 37° C for 40 min. An additional 83 µL of HBSS/A was gently added to create a slight convex meniscus over each well, and the plate was covered with an adhesive plastic film (89087-692, VWR, IL, USA). The plate was then inverted and allowed to sit for an additional 30 min at 37° C. With the plate maintained in the inverted position, the adhesive sheet was removed and the remaining fluid was removed by aspiration. 200 µL 0.5% SDS was added to each well, followed by 5 hours incubation at room temperature. The amount of hemoglobin in each well was measured from the optical density (OD) as described above. Adherence was calculated as the percentage of OD of adhered hemoglobin/ (OD of total hemoglobin x dilution factor).

RBC adherence assay in flow condition

Freshly isolated red blood cells were diluted to 0.5 hematocrit in saline solution and passed at a fixed rate for 20 minutes over endothelial cells plated on a coverslip in recording and imaging chamber (ALA scientific instruments). The coverslip was then mounted over a glass slide and

the number of RBCs attached to endothelial cells was counted under light microscope at 10 different places on coverslip.

Immunofluorescence

Isolated RBCs were washed 3 times with 1xPBS, blocked with 10% goat serum for 15 minutes at 37° C, incubated with primary antibodies against human amylin (1:200, T-4157, Bachem-Peninsula Laboratories) and Glycophorin A (1:100, sc-71159, Santa Cruz Biotechnology, TX, USA) for 15 min at 37° C, followed by incubation with anti-mouse IgG and anti-rabbit IgG secondary antibodies for 15 min at 37° C. Cells were hemolyzed in 1% saponin in PBS, centrifuged at 8000g for 5 min and the pellet was re-suspended in 1xPBS for microscopy. Images were obtained on a Nikon A1R confocal microscope (Nikon, NY, USA).

For hemoglobin staining, blood smears on glass slide were fixed in acetone/ethanol/methanol (6:2:2) for 20 minutes at RT. Smears were air-dried and re-hydrated in 1xPBS for 5 minutes, rinsed briefly in distilled water, and incubated with pre warmed (37°C) trypsin solution (0.1% in calcium chloride 0.1% pH 7.8) for 15 minutes in humidity chamber. Next, smears were washed in PBS for 5 minutes with gentle agitation, rinsed in distilled water and air dried. Smears were then incubated at 37°C with primary antibodies against hemoglobin (1:100, ab92492, Abcam, MA, USA) and human amylin (1:100, SC-377530, Santa Cruz Biotech, TX, USA) in humidity chamber for 30-40 minutes. They were next washed, air-dried and covered with anti-mouse IgG and anti-rabbit IgG secondary antibodies for 20-30 minutes at 37°C. After incubation smears were washed with PBS, rinsed in water, air dried and mounted in mounting media. Thin sections of paraffin embedded pancreatic tissues were co-stained with Thioflavin S and an anti-amylin antibody.

Enzyme-linked immunosorbent assay (ELISA)

ELISA assays for human amylin (EZHA-52K, Millipore, MA; EIA-AMY-5, Raybiotech, GA, USA), erythropoietin (EPO; 442807, Biolegend, CA, USA), hypoxia-inducible transcription factor 1α (HIF1-α; MBS764727, MyBioSource, CA, USA), hypoxia-inducible transcription factor 2α (HIF2-α; MBS2601406, MyBioSource), arginase 1 (MBS289817, MyBioSource), arginase 2 (MBS7216305, MyBioSource), von Hippel-Lindau (vHL; MBS288882, MyBioSource) and VCAM-1 (LS-F24285, LifeSpan BioSciences, Inc, WA, USA) were performed according to the manufacturer's protocols..

Arginase activity assay

Arginase activity was measured in kidney homogenates using a colorimetric assay (MAK112, Sigma, MO, USA). To eliminate urine from kidney samples, 300µL of kidney homogenate were filtered through a 10kD spin column (88513, ThermoFisher, MA, USA) with centrifugation at 15000g for 60 min, 4°C. Collected remnant was used for experiments. Assay was performed according to the manufacturer's protocol. Briefly, filtered kidney samples were incubated with reaction substrate mix for 2 hours at 37° C. The stop solution was applied, followed by incubation at 37° C for 35 min. Absorbance reading was taken at 430 nm. Arginase activity was calculated based on manufacturer's analysis instruction.

Isolation of kidney capillaries

Kidney capillaries were isolated by using the protocol used for the isolation of brain capillaries as describes previously[S2]. Briefly, kidneys were homogenized in ice cold cPBS and were mixed with 30% Ficoll solution by gently inverting tubes and then centrifuged 5800g for 20 minutes at 4°C. Pellets were re-suspended in ice cold cPBS with 1%BSA and were passed through the glass

beads column. Beads were agitated in cPBS with 1%PBS using 25mL pipette and solutions were taken equally in two 50mL tubes. Tubes were centrifuged and pellets were dissolved in 0.5 to 1mL cPBS and used for experiment.

Immunoblot

Western blot analysis was performed on plasma, WBC lysates, and RBC lysates from humans using a primary antibody against amylin (1:2,000, T-4157, Bachem-Peninsula Laboratories). Western blot analysis for VCAM-1 (1:1000, ab134047, Abcam) was done on kidney capillary lysates from WT and HIP rats

Immunohistochemistry

Immunohistochemical staining was performed on rat kidney slices using antibodies against amylin (1:200, SC-377530, Santa Cruz), collagen IV (1:1000, ab6586, Abcam), IBA-1(1:200, 019-19741, Wako, VA, USA), and EDI (1:100, MCA341GA, Biorad, PA, USA). Biotinylated anti-mouse (1:400, BA2000, Vector lab, CA, USA), AP conjugated anti-mouse and anti-rabbit IgG (1:50, A3562, A3687, Sigma) were the secondary antibodies. The staining area for amylin was analyzed by ImageJ. The imaging area is 1280 x 1024 pixels; 1 pixel^2 is 0.053 μm^2 for 40X objective lens.

Transmission electron microscopy

Fresh red blood cells were fixed in 0.1M Sorensen's phosphate buffer with 4% PFA and 0.2% glutaraldehyde for 1-2 hours. Cells were then washed in 0.1M Sorensen's buffer and blocked in 0.1% sodium borohydride for 15 minutes and incubated in AURION blocking solution (AURION blocking solution, 50-247-65, fisher scientific) for 60 minutes. Cells were washed with incubation buffer and incubated with primary antibody (anti-human amylin; T-4157;

Peninsula lab) for 2 hours at RT. Cells were rinsed with incubation buffer and incubated with secondary antibody (anti-Rabbit IgG-10nm Gold; ab27234, Abcam) overnight at 4 ºC. Cells were then washed in PBS and post-fixed in 2% glutaraldehyde for 2 hours. Cells were silver stained using Silver enhancement kit (ab170732, Abcam) and fixed in 0.5% OsO4 in 0.1M Sorensen's buffer for 15 minutes. Cells were embedded in Epoxy resin and thin sections were prepared over nickel grid (T300-Ni, Electron microscopy science) for imaging in Transmission Electron Microscope (FEI Talos F200X, Thermo Scientific).

High resolution Stochastic Optical Reconstruction Microscopy (STORM)

Fresh red blood cells were stained using the same protocol as for immunofluorescence using primary antibodies (anti-human amylin; T-4157; Peninsula lab and anti-glycophorin A; sc-71159Santacuz biotech) and secondary antibodies (rabbit IgG-atto 647 and mouse IgG-atto 488). Cells were kept in STORM imaging buffer {7µl GLOX (oxygen scavenger)+ 70µl of MEA (Cysteamine hydrochloride)+ 620µl of buffer B (Tris-HCL/NaCl)} during imaging on Nikon N-SIM N-STORM (Nikon) microscope.

RBCs osmotic resistance test

The osmotic resistance of RBCs was assessed by measuring hemolysis at various concentrations of NaCl. Solutions with NaCl concentrations between 0 and 9g/L were obtained by mixing normal saline solution (containing 9g/L NaCl) with distilled water in various proportions. 285µl of each solution was placed in an Eppendorf tube. 4µl of RBC lysate was then added to tubes, mixed and incubated at room temperature for 30 min. The tubes were then centrifuged at 600 × g for 5 min. The supernatant was collected and the amount of hemoglobin released was detected by measuring the O.D. at 540 nm. For each sample, the % hemolysis at a given NaCl concentration

was calculated assuming that complete hemolysis occurs in distilled water. All samples were run in duplicate.

Oxygen dissociation curve

Fresh heparinized blood was oxygenated by blowing air on its surface in small vessels with swirling for a few seconds. 200µl of buffer (20mM phosphate in isotonic NaCl) was pipetted in a XF96 plate (Agilent Technologies, CA, USA) and 4µl of blood and 4µl of active yeast cell suspension were added to each well. The partial pressure of oxygen was then recorded at different time points in a Seahorse XF96 Extracellular Flux Analyzer (Agilent Technologies, CA, USA) until 100% oxygen consumption. Percentage saturation was then calculated and oxygen dissociation curve was plotted as described previously[S6].

Reticulocyte count

For reticulocyte counting, 2-3 drops of filtered new methylene blue solution (New methylene blue 1g, sodium citrate 0.6g, sodium chloride 0.7g and distilled water 100ml) mixed with equal amount of blood and incubated at 37ºC for 15 minutes. After gentle mixing, thin smear of blood was prepared in glass slide and air dried. Reticulocytes and RBCs were counted under a light microscope and the percentage of reticulocytes relative to the total number of RBCs was calculated.

Statistical analysis for animal data

Statistical differences between groups were determined using student's t-test, one-way ANOVA or two-way ANOVA, as appropriate. Data are presented as mean ± standard error. Differences between groups were considered significant when $P < 0.05$. All analyses were performed using GraphPad Prism 5.0 software.

Supplementary References

S1. Butler AE, Jang J, Gurlo T, Carty MD, Soeller WC, Butler PC. Diabetes due to a progressive defect in beta-cell mass in rats transgenic for human islet amyloid polypeptide (HIP Rat): a new model for type 2 diabetes. Diabetes. 2004;53:1509-1516.

S2. Ly H, Verma N, Wu F, Liu M, Saatman KE, Nelson PT, Slevin JT, Goldstein LB, Biessels GJ, Despa F. Brain microvascular injury and white matter disease provoked by diabetes-associated hyperamylinemia. *Ann. Neurol.* 2017;82:208-222.

S3. Cummings BP, Digitale EK, Stanhope KL, Graham JL, Baskin DG, Reed BJ, Sweet IR, Griffen SC, Havel PJ. Development and characterization of a novel rat model of type 2 diabetes mellitus: the UC Davis type 2 diabetes mellitus UCD-T2DM rat. Am. J. Physiol. Regul. Integr. Comp. Physiol. 2008;295:R1782-1793.

S4. Despa S, Sharma S, Harris TR, Dong H, Li N, Chiamvimonvat N, Taegtmeyer H, Margulies KB, Hammock BD, Despa F. Cardioprotection by controlling hyperamylinemia in a "humanized" diabetic rat model. J. Am. Heart. Assoc.2014;3.

S5. Peake M, Whiting M. Measurement of serum creatinine- current status and future goals. *Clin Biochem Rev.* 2006;27:173-184.

S6. Gordon L. Atkins, James Doyle. A simple method for measuring oxyhemoglobin dissociation curves in a student practical class. Biochemical Education, Volume 7, Issue 2, April 1979, Pages 34-36 Biochemical.

Full unedited gel for Figure 4a

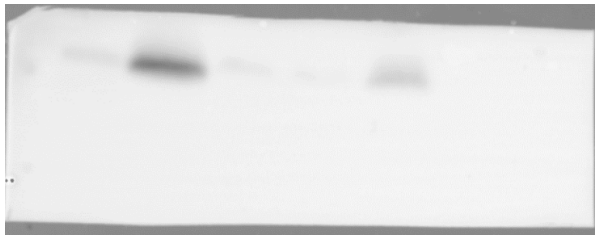

Full unedited gel for Figure S1

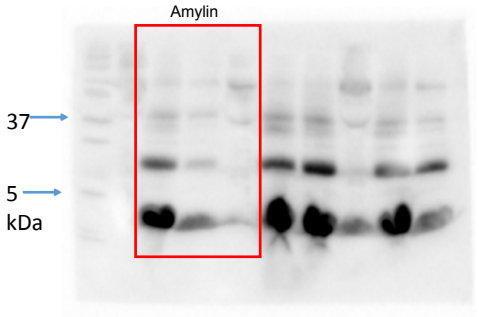

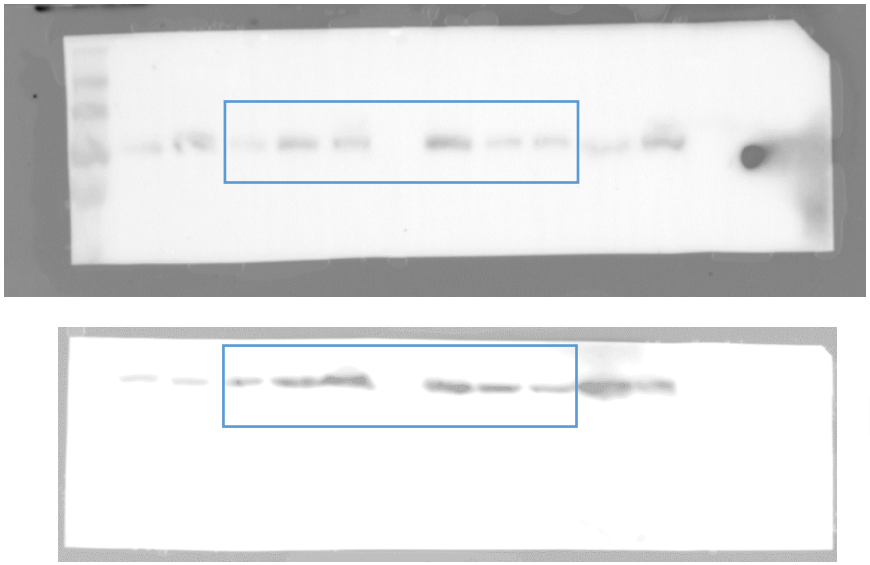
VCAM-1
β-actin

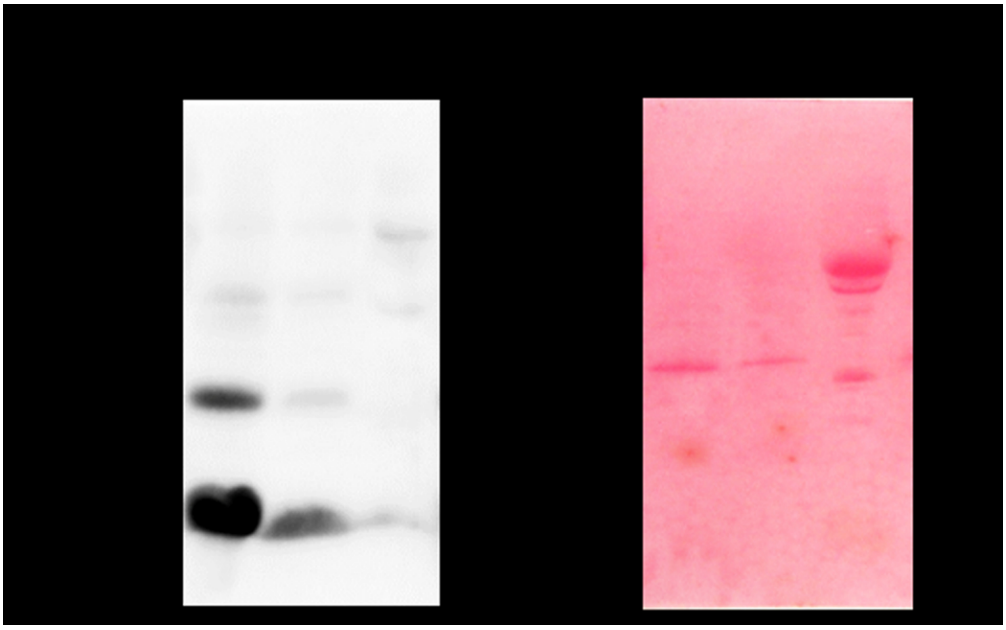

88x54mm (300 x 300 DPI)

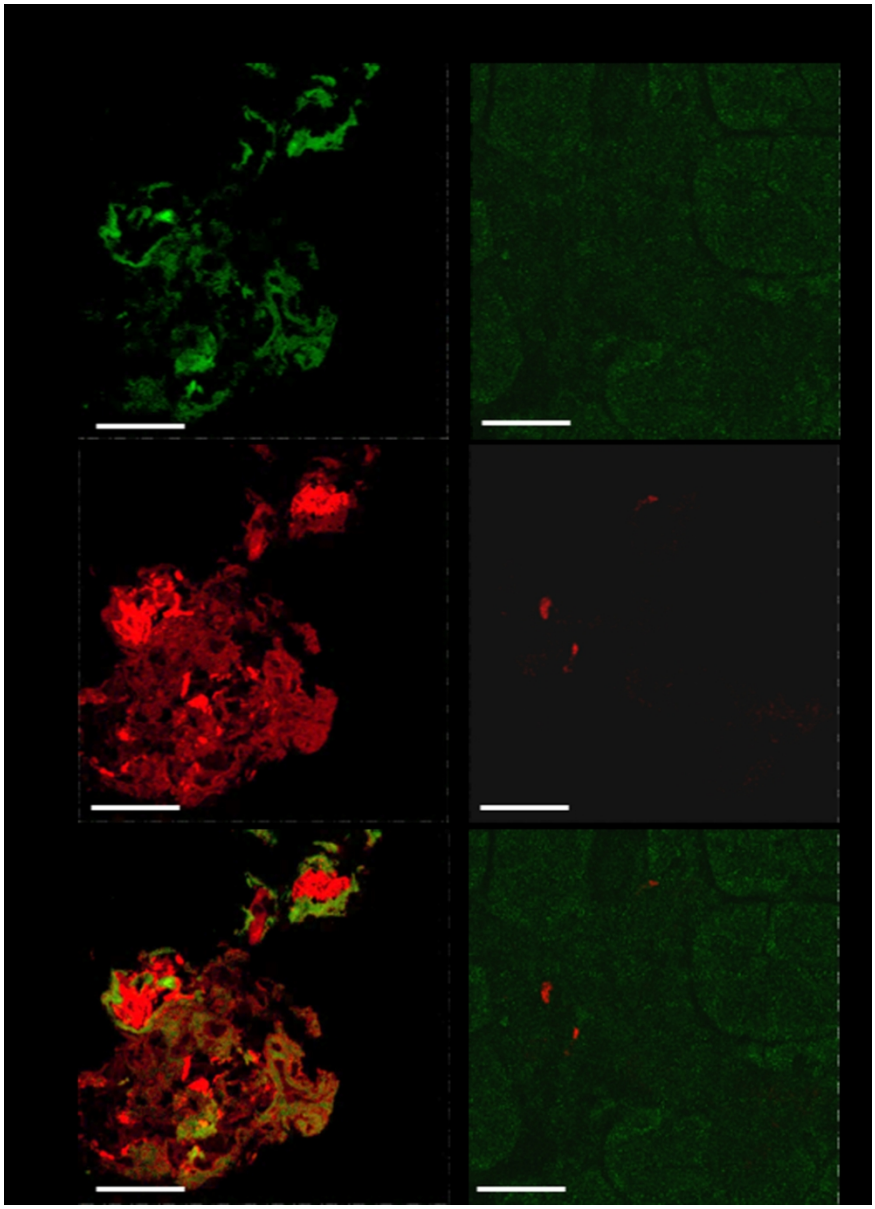

88x122mm (300 x 300 DPI)

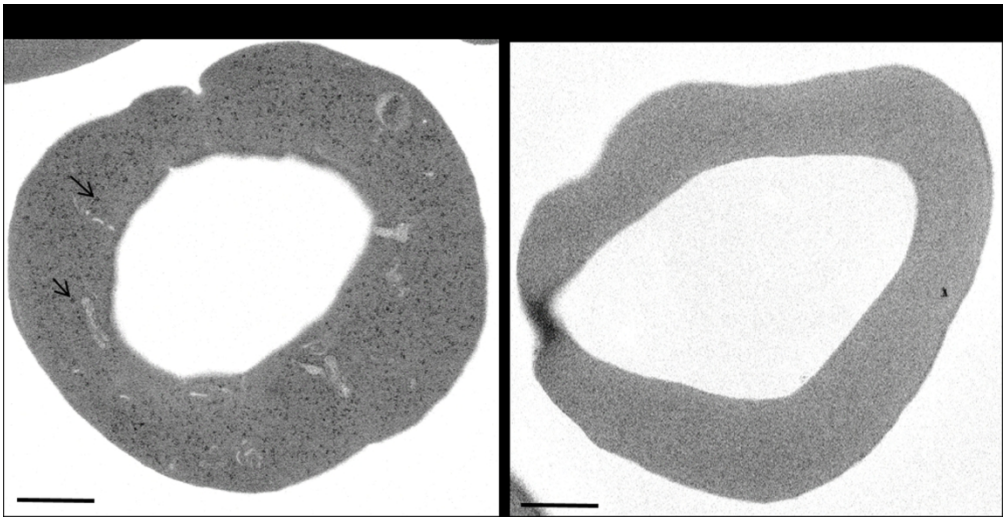

168x86mm (300 x 300 DPI)

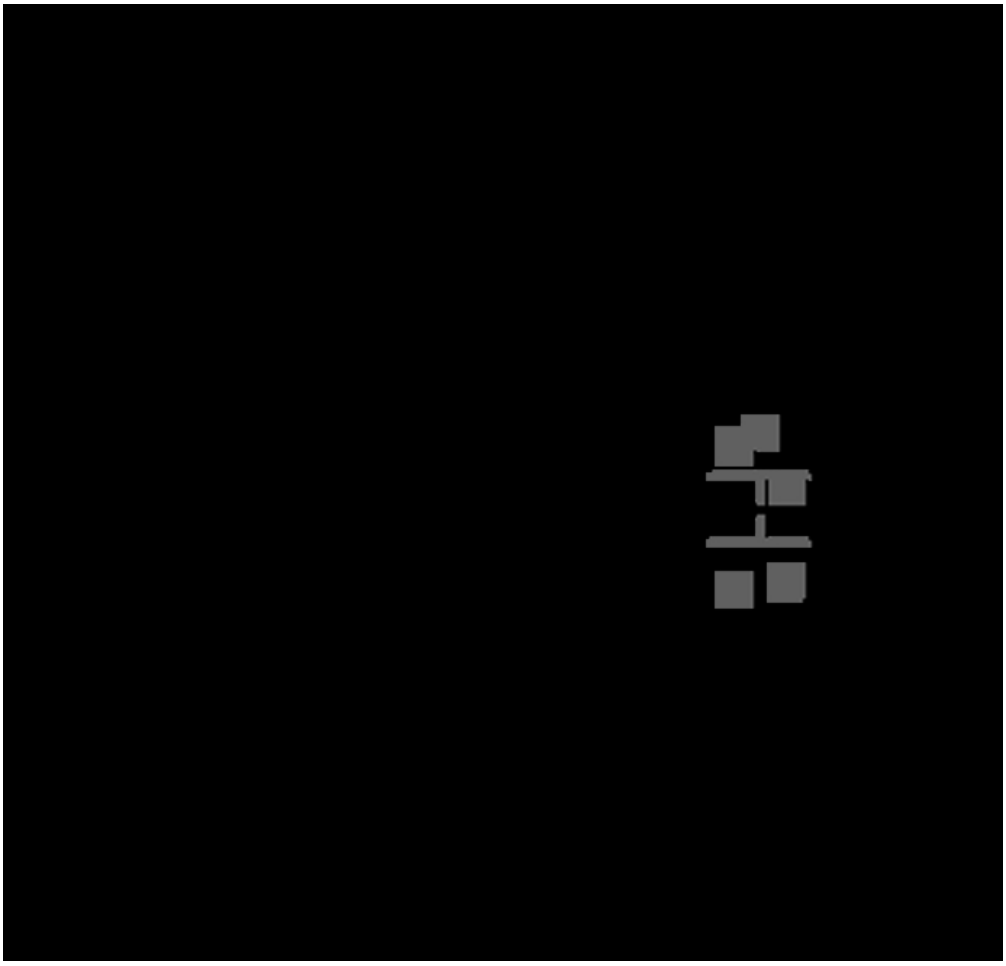

58x55mm (300 x 300 DPI)

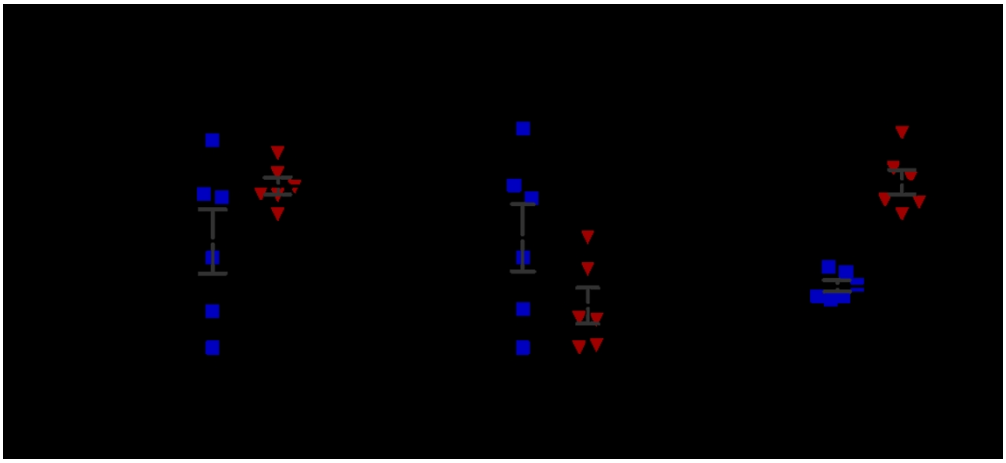

160x72mm (300 x 300 DPI)

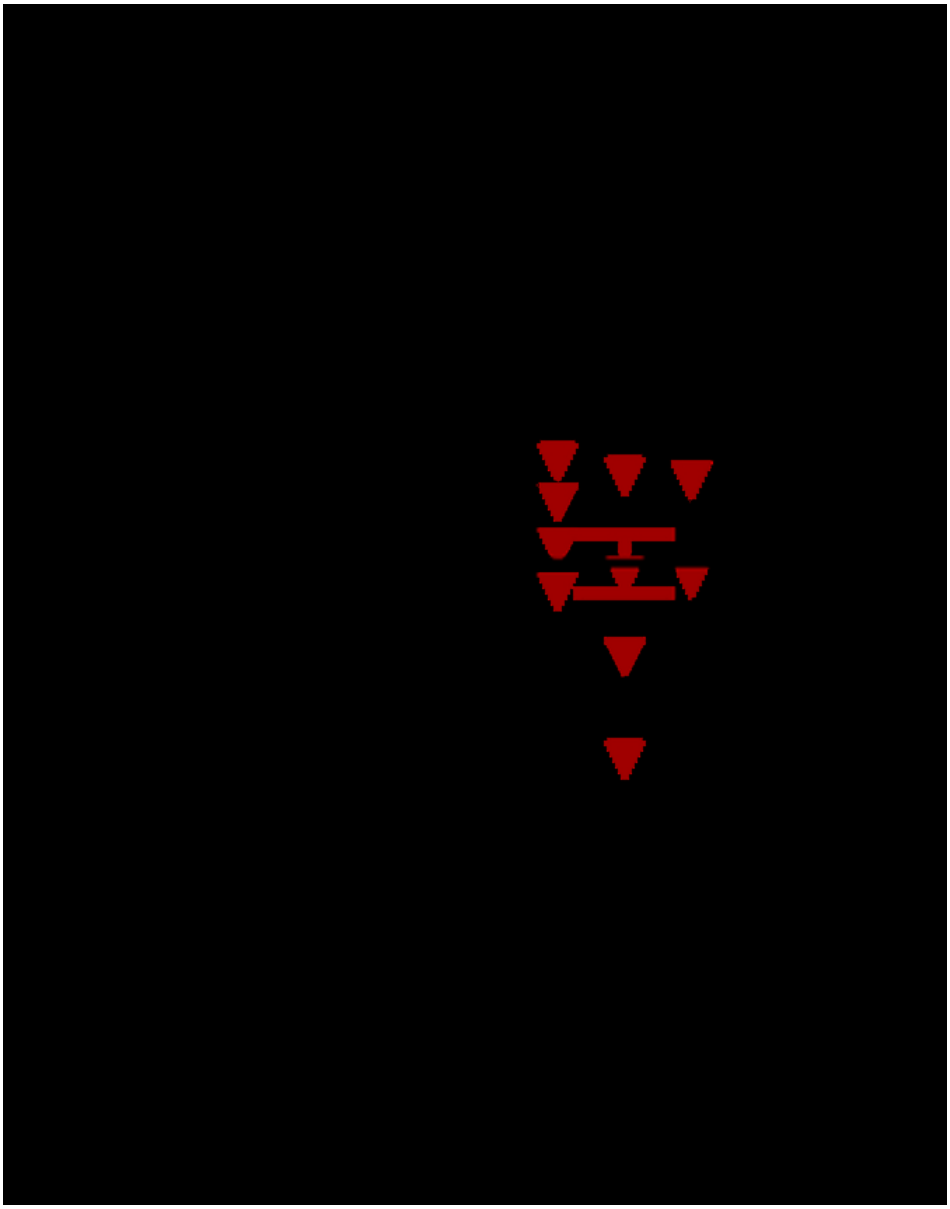

57x72mm (300 x 300 DPI)

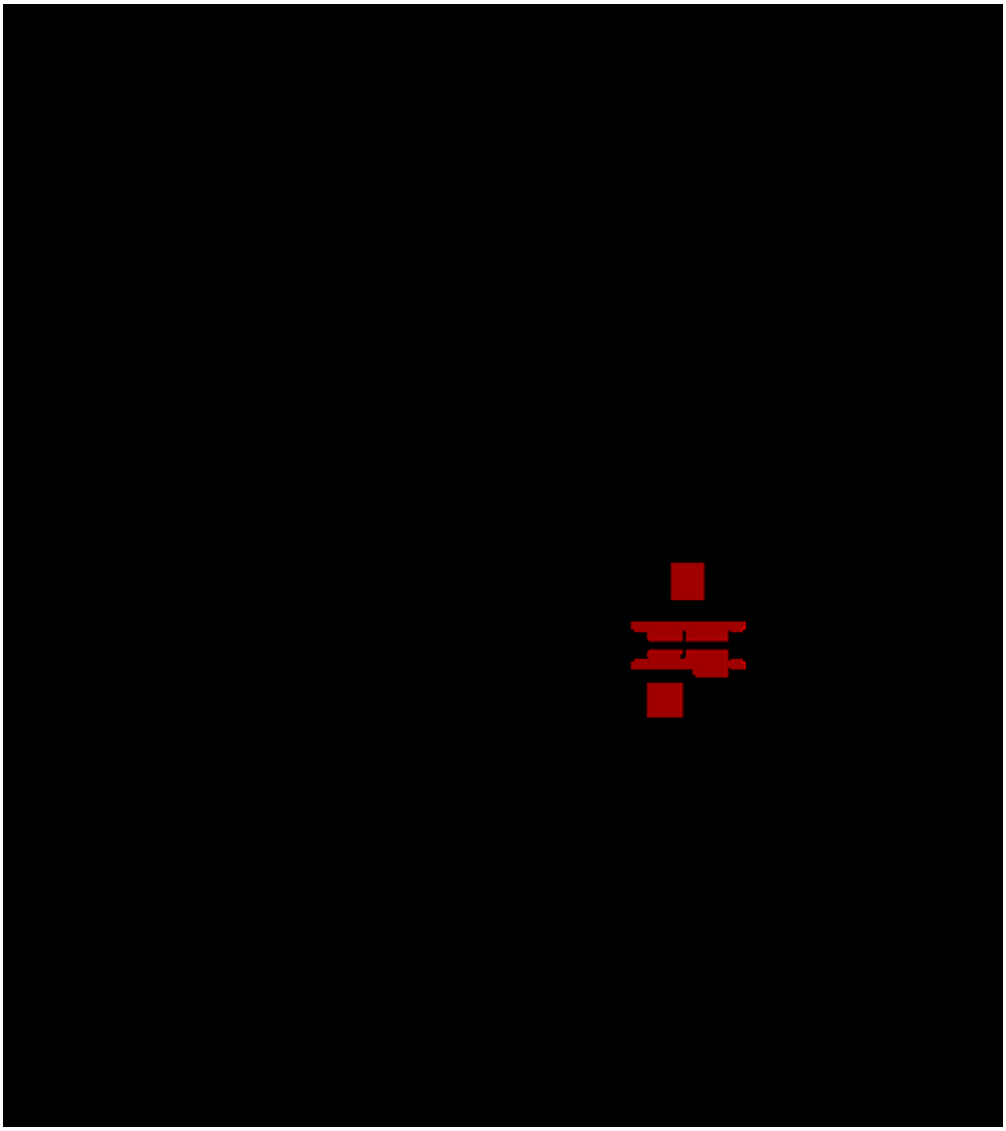

63x71mm (300 x 300 DPI)

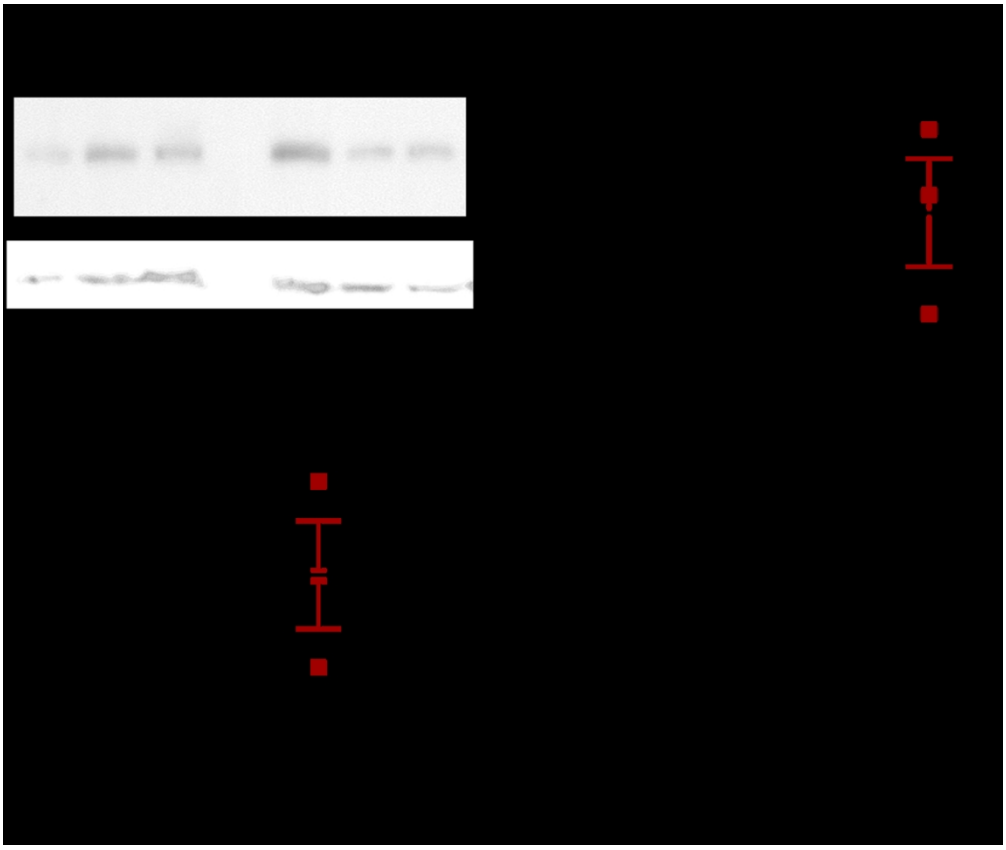

139x117mm (300 x 300 DPI)

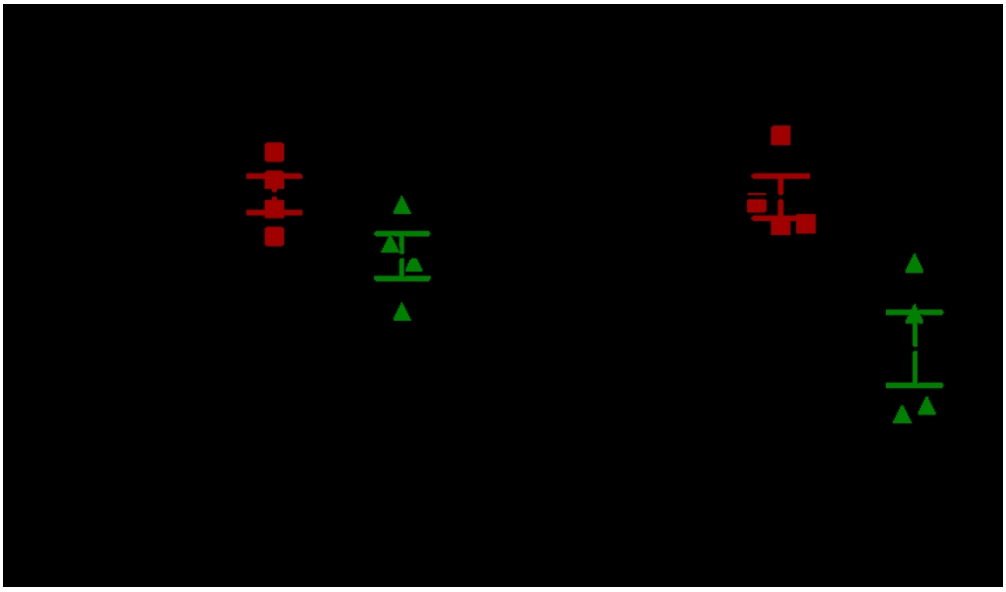

120x70mm (300 x 300 DPI)